STUDIES ON THE PROTEIN DYNAMICS OF PHOTODISSOCIATED CARBONMONOXY MYOGLOBIN AND HEMOGLOBIN BY TIME-RESOLVED RESONANCE RAMAN SPECTROSCOPY

Yoshinao Sakan

Doctor of Philosophy

Department of Functional Molecular Science
School of Mathematical and Physical Science
The Graduate University for Advanced Studies

1992

Contents

Acknowledgments

The author acknowledges helpful discussions and supports with many people on the occasion of writing this doctor's thesis. Especially, the author specially thanks Professor Teizo Kitagawa for many helpful suggestions, Professor Masao Ikeda-Saito and his staffs in Case Western Reserve University Medical School for kind offer of human mutant Myoglobins and some important suggestions, and Professor Masako Nagai in Kanazawa University School of Allied Medical Professions for kind offer of human abnormal Hemoglobins, "Boston" and "Saskatoon", and interesting discussions. Furthermore, the author thanks Dr. Takashi Ogura, Research Associate, Dr. Shyoji Kaminaka, J.S.P.S. fellow, and Assistant Professor Masashi Nakagawa in Himeji Institute of Technology for teaching techniques of Raman spectroscopy and many information of hemoproteins. And finally, the author also thanks Dr. Keiji Kamogawa, Research Associate, for interesting discussions, Dr. Philip J. Jewsbury, J.S.P.S. fellow, for interesting discussions and for correcting English of paper, Shin-ichiro Sato, Technical Associate, for use of his pulse delay-time measuring system with photodiode, and Dr. Satoshi Takahashi, J.S.P.S. fellow, and Dr. Yasuhisa Mizutani, J.S.P.S fellow, for their kindness and friendships.

Abbreviations

Mb	:	myoglobin
Hb	:	hemoglobin
MbO_2	:	oxy complex of myoglobin
HbO_2	:	oxy complex of hemoglobin
MbCO	:	carbonmonoxy complex of myoglobin
HbCO	:	carbonmonoxy complex of hemoglobin
deoxyMb	:	myoglobin with ferrous heme iron and no ligand
metMb	:	myoglobin with ferric heme iron
Gly, G	:	glicine
Ala, A	:	alanine
Val, V	:	valine
Ile, I	:	isoleusine
Leu, L	:	leusine
Lys, K	:	lysine
Arg, R	:	arginine
Gln, Q	:	glutamine
His, H	:	histidine
Trp, W	:	tryptophan
Tyr, Y	:	tyrosine
H64H	:	wild type myoglobin
H64Q	:	mutant myoglobin in which distal histidine substituted with glutamine
H64G	:	mutant myoglobin in which distal histidine substituted with glycine
H64L	:	mutant myoglobin in which distal histidine substituted with leusine
H64V	:	mutant myoglobin in which distal histidine substituted with valine
H64A	:	mutant myoglobin in which distal histidine substituted with alanine
H64I	:	mutant myoglobin in which distal histidine substituted with isoleusine
RR	:	resonance Raman
TR^3	:	time-resolved resonance Raman

Chapter I

General Introduction

I-1. Structures of Myoglobin and Hemoglobin[1]

Proteins can accomplish their original physiological functions by partially modifying their conformations. It is one of the most basic and the most important subject to elucidate the relationship between the conformational change of the protein and its own physiological functions. In order to solve this difficult problem, myoglobin (Mb) and hemoglobin (Hb) were selected in this study. Myoglobin and Hemoglobin are heme proteins whose three dimensional structures and the physiological functions were thoroughly investigated[1].

Myoglobin is a typical and the simplest monomer hemoprotein, while Hb is a tetramer hemoprotein. The physiological role of Mb is storage of oxygen in muscle and that of Hb is to carry oxygen in blood. In 1960, the three dimensional structure of the met form of sperm whale Mb was revealed by Kendrew et al.[2] Since then, the structures of a number of Mb species in various states were analyzed by X-ray[3] and neutron diffraction techniques[4]. Figure I-1 illustrates the three dimensional structure of Mb from ref. 1a. A whole molecule of Mb assumes a spheroid, with the principal axes of $44 \times 44 \times 25$ Å^3. Myoglobin consists of an iron protoporphyrin IX (Figure I-2), called heme, and a single poly-peptide chain, and its molecular weight is ca. 17,000 (it varies with species of organisms). The poly-peptide chain of sperm whale Mb is composed of 153 amino acid residues, which are folded in eight pieces of α-helix. These residues are numbered in order from the N-terminal to the C-terminal. The pieces of α-helix are named "A" - "H" also from the N-terminal to the C-terminal.

Hemoglobin is composed of two α-subunits and two β-subunits. The α-subunit and the β-subunit consist of 141 and 146 amino acid residues, respectively. One heme group is buried in individual subunits. The three dimensional structures of individual subunits are similar to that of Mb. The residues and the pieces of α-

helix are numbered and named in the same order with Mb. Hemoglobin exhibits the cooperativity about oxygen binding, which is explained as a typical homotropic allostery[5]. The αTyr-42 residue forms a hydrogen bond with the βAsp-99 residue at the α_1-β_2 interface[6] in the T (tensed) state that is of the low affinity, but in the R (relaxed) state that has the high affinity for ligand[7], this hydrogen bond is broken and these residues become free[6d]. This hydrogen bond may serve as a trigger of the reversible transition between T and R states, because the on/off state of this hydrogen bond affected the Fe-His bond strength through the poly-peptide chain[8]. This transition between T and R states occur in the microsecond time scale[9].

Figure I-3 shows the detailed structure around the heme[3a]. The heme is completely surrounded by protein except for the two propionic acid side chains. The iron atom of the heme is coordinated by four nitrogen atoms of pyrrole rings, and the fifth coordination position is occupied by histidine residue (His-F8 or His-93) which is called "proximal histidine". The sixth position is the oxygen binding site. Myoglobin and Hemoglobin have the three stable states under the normal conditions, that is, met-type, deoxy-type, and ligated-type. In met-type Mb (metMb), the iron atom of the heme adopts a ferric high-spin state, and a water molecule is bound to the sixth coordination position of the heme iron[3b]. Furthermore, the iron is out of the mean heme plane by 0.4 Å, and the heme is domed similar to that in deoxyMb[14]. The Fe-Nϵ bond of proximal His is 4° away from the normal of the heme plane[1]. In deoxy-type Mb (deoxyMb), the iron atom of the heme adopts a ferrous high-spin state, and the sixth coordination position is vacant. The iron is tugged by proximal His and is displaced from the mean heme plane by 0.55 Å[1]. As a result the heme group is slightly domed toward the proximal His, with the four pyrrole nitrogens at 0.13 Å away from the best mean plane[1a]. The Fe-Nϵ bond makes an angle of 11° with the normal of the heme plane[1a]. In the

ligated-type Mb, O_2, CO, NO and alkylisocyanide can be bound to deoxyMb, that are represented as MbO_2, MbCO, MbNO and MbCNR, respectively. The iron atom lies in the mean heme plane for MbO_2 and MbCO, and the Fe-Nϵ bond is more perpendicular to the heme plane than in deoxyMb and metMb[1a]. The side chain of another histidine (His-E7 or His-64) called "distal histidine" lies over the sixth coordination position as illustrated in the Figure I-3. In MbO_2 and metMb, the distal His contacts with O_2 and H_2O molecules through hydrogen bonding[4b].

When MbO_2 and MbCO change to deoxyMb, in a linked motion with the moving of the iron to proximal His, the F-helix slides approximately 0.15 Å across the heme face in the direction of the FG-corner. This motion is noticed in the F-helix position that pushes the FG-corner away from the heme. These changes are dissipated in the FG-corner and the E-helix, and the rest of the molecule is essentially unchanged in MbO_2, MbCO, and deoxyMb. These movements are the foundation of heme-heme cooperativity of Hb[8].

I-2. Recombination Dynamics of Photodissociated MbCO

Both HbCO and MbCO are reversibly photodissociable upon laser illumination. In HbCO and MbCO, the photodissociation occurs within 350 ± 50 fs after photolysis regardless of pH and partial pressure of CO[10]. Anfinrud et al.[11] estimated that the CO molecule photodissociated at 580 nm could move at most 1 Å in 300 fs from its initial ligated position of the heme. From the crystallographic data[3c, d] and normal van der Waals radii, it is difficult to find a room for a free flight of the CO that is longer than 1 Å but 50% of CO goes out of the protein in 50 ns[11]. The photodissociated Mb relaxes to the deoxyMb with the high-spin iron and the domed heme within 20 - 30 ps[12]. On the other hand, the transient circular dichroism (CD) spectra in the visible and near-UV regions of photodissociated

MbCO shows no differences from the final deoxyMb on the picosecond time scale. Therefore the intermediate must have a similar protein structure not only the heme group but as a whole[13].

The photodissociated CO quickly finds some locations in the protein that are not more than a few angstroms from the iron. The photodissociated CO does not recover on the time scale of a few picosecond but about 4% of the photodissociated CO rebinds to the heme within 1 ns[24]. This rebinding process is called "geminate recombination". While the 85 ±10% of this CO remains in the protein at 1 ns[11], it becomes 50% at 50 ns[11]. The rebinding process of the photodissociated CO out of the heme pocket is called "bimolecular recombination".

According to the X-ray crystallographic studies, there is no pathway for the ligand entry from the solvent to the heme pocket[3a]. Therefore, when the ligand enters to the heme pocket, some conformational change of protein is necessary to open a pathway. Kuriyan et al.[3a] reported from X-ray diffraction analysis that two distinctly different structures equally exist in MbCO. One is a "closed" form which has no pathway for ligand entry, and another one is an "open" form which has an open channel for ligand entry. The distal His of the "open" form swings out 15° and moves 1.4 Å toward the solvent[3a]. If the ligand binds to the "open" form and subsequently the protein relaxes to the "closed" form, the transient Raman spectra of photodissociated MbCO should be different from the spectrum of equilibrium MbCO.

I-3. Relationships between the Fe-CO or C-O Stretching Vibrational Frequencies and Fe-C-O Configuration

In hemoproteins, steric hindrance by bulky amino acid residues near the binding site is believed to lower the affinity ratio of CO versus O_2[15]. X-ray crystal-

lographic studies of CO ligated Hbs and Mbs reveal that the CO unit is bent and/or tilted from the heme normal owing to interactions with various distal residues, particularly histidine, valine, leucine, or isoleucine[16]. The Fe-C-O angle for MbCO (120° - 141°)[3h, k] and HbCO (165° - 175°)[3h, j, l] are closer to a linear geometry than that for MbO_2 (115° - 121°)[3e, h, k, m] and HbO_2 (152° - 160°)[3f, g, i]. While, the O-O bonds of MbO_2 and HbO_2 are tilted by 59° away from the normal to the heme plane[1a], the Fe-C bonds of MbCO and HbCO are tilted by 18° - 20° away from the heme normal[17]. These angles indicate that the Fe-O-O geometry in MbO_2 and HbO_2 is mainly bent and Fe-O bond is perpendicular to the heme plane, while the Fe-C-O geometry is tilt and bent.

The Fe-CO stretching vibrational mode ($\nu_{Fe\text{-}CO}$) was first detected by Tsubaki et al.[18] in the resonance Raman spectra of carbonmonoxy human Hb A, carbonmonoxy sperm whale Mb, and carbonmonoxy carp Hb at 507, 512, and 508 cm^{-1}, respectively. The C-O stretching mode ($\nu_{C\text{-}O}$) was observed at 1944 and 1951 cm^{-1} for MbCO and HbCO, respectively. In a heme-CO model compound, CO ligated tetraphenylporphyrin [(TPP)CO] (Figure I-4a)[23], the $\nu_{Fe\text{-}CO}$ and $\nu_{C\text{-}O}$ bands were observed at 484 and 1976 cm^{-1}, respectively[19]. In meso-substituted tetraaryl porphyrin, the so-called "picket-fence" porphyrin (Figure I-4b)[23] that can bind O_2 and CO reversibly at room temperature and serves as an excellent model for Mb, the $\nu_{Fe\text{-}CO}$ appeared at 489 cm^{-1} [20]. According to the X-ray diffraction studies, these CO ligated model compounds contained the linear Fe-C-O geometry (179°) with perpendicular to the heme plane[21]. Thus, it is considered that these differences in the frequencies of $\nu_{Fe\text{-}CO}$ and $\nu_{C\text{-}O}$ between hemoproteins and model compounds arise from the geometry change of Fe-C-O. In other words, it was also confirmed by the frequencies of $\nu_{Fe\text{-}CO}$ and $\nu_{C\text{-}O}$ that the Fe-C-O configurations of MbCO and HbCO were bent and tilted.

In order to establish the relationship between the frequencies of $\nu_{Fe\text{-}CO}$ or $\nu_{C\text{-}O}$ and the Fe-C-O distortions, Yu et al.[22] conducted a systematic investigations into the effects of nonbonded distal steric hindrance on the Fe-CO stretching, the Fe-C-O bending, and the C-O stretching vibrations employing a series of sterically unhindered and hindered synthetic iron porphyrins. One simple porphyrin, heme 5 (Figure I-5a)[23], which has no group to hinder the CO binding, was studied along with three "strapped" hemes (Figure I-5b)[23]. The "strapped" hemes equipped with a chain of 13- (FeSP-13), 14- (FeSP-14), or 15- (FeSP-15) CH_2 groups, which is strapped across one face of the heme and exerts varying degrees of sideway-shearing strain to the CO ligand. As the chain length is decreased, the degree of steric hindrance increases and the CO binding affinity decreases. The ν_4 (at 1372 cm^{-1}) and ν_{11} (at 1586 cm^{-1}) Raman bands which were sensitive to the π-electron density and the spin state of iron of these synthetic heme, respectively, were shown to be unaltered by the chain length. These facts indicate that the electronic structures and heme geometries are not modified by the straps. The $\nu_{Fe\text{-}CO}$ frequency increases as the length of the strap decreases. The $\nu_{Fe\text{-}CO}$ bands of these hemes were observed at 495 cm^{-1} (heme-5), 509 cm^{-1} (FeSP-15), 512 cm^{-1} (FeSP-14), and 514 cm^{-1} (FeSP-13). In contrast, the C-O stretching frequency decreases with the length of the strap, (heme-5; 1945 cm^{-1}, FeSP-15; 1945 cm^{-1}, FeSP-14; 1939 cm^{-1}, and FeSP-13; 1932 cm^{-1}). In general, the $\nu_{Fe\text{-}CO}$ frequency has been found to increase with a decrease in the $\nu_{C\text{-}O}$ frequency and decreasing CO binding affinity. These facts indicate that the $\nu_{Fe\text{-}CO}$ band shifts to a higher frequency and the $\nu_{C\text{-}O}$ band shifts a lower frequency with increasing the distortion of the Fe-C-O bond or the steric hindrance around the binding site. This relation is consistent between hemoproteins and its model compounds which are ligated by CO[23].

I-4. Summary of This Study

As discussed above, there is no pathway for the ligand entry from the solvent to the binding site buried in the heme pocket[3a]. If the ligands bind to the "open" form and subsequently the protein relaxes to the "closed" form, it is expected that the $\nu_{Fe\text{-}CO}$ Raman band appears around 490 cm^{-1} of the "open" form first and subsequently shifts to 507 cm^{-1} of the "closed" form. Time-resolved resonance Raman (TR^3) spectroscopy is a powerful technique to analyze the dynamical features of protein conformation in short time scale. Information obtained by it is very basic and important in studies of the relationship between physiological functions and protein structures. It is the purpose of this study to elucidate the protein dynamics around the distal side of the heme on recombination reaction of MbCO and HbCO by using nanosecond time-resolved resonance Raman spectroscopy.

A nanosecond TR^3 measurement system was set up for this experiment. Since CO is easily photolyzed by probe light, it was quite important to find experimental conditions under which MbCO is photolyzed perfectly by a pump light but not by probe light. After improving the measurement system including the replacement of the grating, MbCO at neutral and acidic pH, were treated. The $\nu_{Fe\text{-}CO}$ band was assigned with the isotopes ($^{13}C^{18}O$). The temporal behavior of the $\nu_{Fe\text{-}CO}$ in the time range from -20 ns to 1 ms was different between the neutral and acidic forms. Implication of the differences as well as details of the measurement system are described in Chapter II.

The TR^3 spectra were obtained for two human abnormal hemoglobins, "Boston" and "Saskatoon" in addition to normal Hb A. The abnormal hemoglobins contain two types subunits in one molecule, that is, normal and abnormal subunits and accordingly, two $\nu_{Fe\text{-}CO}$ bands arise around 490 and 505 cm^{-1}. These two frequencies happen to correspond to those of the "open" and "close" form of Mb.

They are excellent material for the TR^3 studies since the two bands can be monitored simultaneously under the same experimental conditions. The results are described in Chapter III.

Recently, the protein engineering technique has made a remarkable progress. It is becoming easier to prepare some mutant proteins through site directed mutagenesis. Several mutant human MbCO in which distal His were replaced by various amino acids, were provided by Prof. M. Ikeda-Saito. Since it is interesting to investigates the effect of replacement of distal His on the dynamics of protein, the mutants MbCO were examined by TR^3 spectroscopy. The results are explained in Chapter IV.

The photodissociation of MbCO depends on wavelength of the photolyzing light, but it remains to be clarified how it depends. Therefore, the action spectrum for MbCO photodissociation was determined by using the Okazaki Large Spectrograph in NIBB. The action spectra showed that the photodissociation of MbCO occurred with a relatively higher yield even in the UV region where the heme-CO itself did not give an absorption band. This indicated that the UV energy was absorbed by aromatic amino acid residues and then transferred to the heme. Since MbCO can be photolyzed around 500 nm, the protein would have much extra energy when the MbCO was photodissociated by UV light. The extra energy might affect the transient structure as well as the protein dynamics. To clarify the effect of the extra energy, the TR^3 measurement was carried out by using UV-pump/visible-probe technique, the Fe-proximal His stretching vibrational band ($\nu_{Fe\text{-}His}$), that is believed to sensitive to the structure around the heme, pursued for possible photolyzed intermediates. This study has not been completed yet but the results are described in Chapter V.

References

(1) (a) R. E. Dickerson, I. Geis, *Hemoglobin: Structure, Function, Evolution, and Pathology*, (Benjamin/Cummings, California) (1983).
(b) M. F. Perutz, G. Fermi, *Atlas of Molecular Structures in Biology*, Vol. 2, (Oxford University Press, New York) (1981).

(2) J. C. Kendrew, R. E. Dickerson, B. E. Strandberg, R. G. Hart, D. R. Davies, D. C. Phillips, V. C. Shore, Nature, **185**, 422 (1960).

(3) (a) J. Kuriyan, S. Wilz, M. Karplus, G. A. Petsko, J. Mol. Biol., **192**, 133 (1986).
(b) L. Stryer, J. C. Kendrew, H. C. Watson, J. Mol. Biol., **8**, 96 (1964).
(c) T. Takano, J. Mol. Biol., **110**, 537 (1977).
(d) T. Takano, J. Mol. Biol., **110**, 569 (1977).
(e) S. E. V. Phillips, J. Mol. Biol., **142**, 531 (1980).
(f) B. Shaanan, Nature, **296**, 683 (1982).
(g) B. Shaanan, J. Mol. Biol., **171**, 31 (1983).
(h) A. Bianconi, A. Congiu-Castellano, P. J. Durham, S. S. Hasnain, S. Phillips, Nature, **318**, 685 (1985).
(i) A. Brzozowski, Z. Derewenda, E. Dodson, G. Dodson, M. Grabowski, R. Liddington, T. Skarzynski, D. Valley, Nature, **307**, 74 (1984).
(j) E. J. Heidner, R. C. Landner, M. F. Perutz, J. Mol. Biol., **104**, 707 (1976).
(k) A. Congiu-Castellano, A. Bianconi, M. Dell'Ariccia, S. Della Longa, A. Giovannelli, E. Burattini, M. Castagnola, Biochem. Biophys. Res. Commun., **147**, 31 (1987).
(l) J. M. Baldwin, J. Mol. Biol., **136**, 103 (1980).
(m) S. E. V. Phillips, Nature, **273**, 247 (1978).

(4) (a) J. C. Hanson, B. P. Schoenborn, J. Mol. Biol., **153**, 117 (1981).
(b) S. E. V. Phillips, B. P. Schoenborn, Nature, **292**, 81 (1981).

(5) J. Monod, J. Wyman, J. P. Changeux, J. Mol. Biol., **12**, 88 (1985).

(6) (a) M. F. Perutz, Nature, **228**, 726 (1970).
(b) M. F. Perutz, Annu. Rev. Biochem., **48**, 327 (1979).
(c) J. Baldwin, C. Chothia, J. Mol. Biol., **129**, 175 (1979).
(d) L. W.-M. Fung, C. Ho, Biochemistry, **14**, 2526 (1975).

(7) R. G. Shulman, J. J. Hopfield, S. Ogura, Q. Rev. Biophys., **8**, 325 (1975).

(8) (a) M. J. Irwin, G. H. Atkinson, Nature, **293**, 317 (1981).

(b) K. Nagai, T. Kitagawa, H. Morimoto, J. Mol. Biol., **136**, 271 (1980).
(c) K. Nagai, T. Kitagawa, Proc. Natl. Acad. Sci. U.S.A., **77**, 2033 (1980).
(d) M. R. Ondrias, D. L. Rousseau, T. Kitagawa, M. Ikeda-Saito, T. Inubushi, T. Yonetani, J. Biol. Chem., **257**, 8766 (1980).
(e) S. Matsukawa, K. Mawatari, Y. Yoneyama, T. Kitagawa, J. Am. Chem. Soc., **107**, 1108 (1985).
(f) T. Kitagawa, Pure Appl. Chem., **59**, 1285 (1987).

(9) (a) S. Kaminaka, T. Ogura, K. Kitagishi, T. Yonetani, T. Kitagawa, J. Am. Chem. Soc., **111**, 3787 (1989).
(b) S. Kaminaka, T. Ogura, T. Kitagawa, J. Am. Chem. Soc., **112**, 23 (1990).

(10) J. L. Martin, A. Migus, C. Poyart, Y. Lecarpentier, R. Astier, A. Antonetti, Proc. Natl. Acad. Sci. U.S.A., **80**, 173 (1983).

(11) P. A. Anfinrud, C. Han, R. M. Hochstrasser, Proc. Natl. Acad. Sci. U.S.A., **86**, 8387 (1989).

(12) E. W. Findsen, T. W. Scott, M. R. Chance, J. W. Friedman, M. R. Ondrias, J. Am. Chem. Soc., **107**, 3355 (1985).

(13) S. J. Milder, S. C. Bjorling, I. D. Kuntz, D. S. Kliger, Biophys. J., **53**, 659 (1988).

(14) (a) R. C. Ladner, E. J. Heidner, M. F. Perutz, J. Mol. Biol., **114**, 385 (1977).
(b) T. Takano, J. Mol. Biol., **110**, 533 (1977).

(15) (a) K. Moffat, J. F. Deatherage, D. W. Seybert, Science, **206**, 1035 (1979).
(b) A. Szabo, Proc. Natl. Acad. Sci. U.S.A., **75**, 2108 (1978).

(16) (a) R. Huber, O. Epp, H. Formanek, J. Mol. Biol., **52**, 349 (1970).
(b) E. J. Heidner, R. C. Ladner, M. F. Perutz, J. Mol. Biol., **104**, 707 (1976).
(c) J. M. Baldwin, J. Mol. Biol., **136**, 103 (1980).
(d) J. C. Norvell, A. C. Nunes, B. P. Schoenborn, Science, **190**, 568 (1975).
(e) W. Steigemann, E. Weber, J. Mol. Biol., **127**, 309 (1979).

(17) J. N. Moore, P. A. Hansen, R. M. Hochstrasser, Proc. Natl. Acad. Sci. U.S.A., **85**, 5062 (1988).

(18) M. Tsubaki, R. B. Srivastava, N.-T. Yu, Biochemistry, **21**, 1132 (1982).

(19) E. A. Kerr, N.-T. Yu, D. E. Bartnicki, H. Mizukami, J. Biol. Chem., **260**, 8360 (1985).

(20) E. A. Kerr, H. C. Mackin, N.-T. Yu, Biochemistry, **22**, 4373 (1983).

(21) S.-M. Peng, J. A. Ibers, J. Am. Chem. Soc., **98**, 8032 (1976).

(22) N.-T. Yu, E. A. Kerr, B. Ward, C. K. Chang, Biochemistry, **22**, 4534 (1983).

(23) N.-T. Yu, E. A. Kerr, "Vibrational Modes of Coordinated CO, CN^-, O_2, and NO", in *Biological Applications of Raman Spectroscopy*, Vol. 3, ed. T. G. Spiro, (John Wiley, Canada), pp. 39 - 95 (1988).

(24) E. R. Henry, J. H. Sommer, J. Hofrichter, W. A. Eaton, J. Mol. Biol., **166**, 443 (1983).

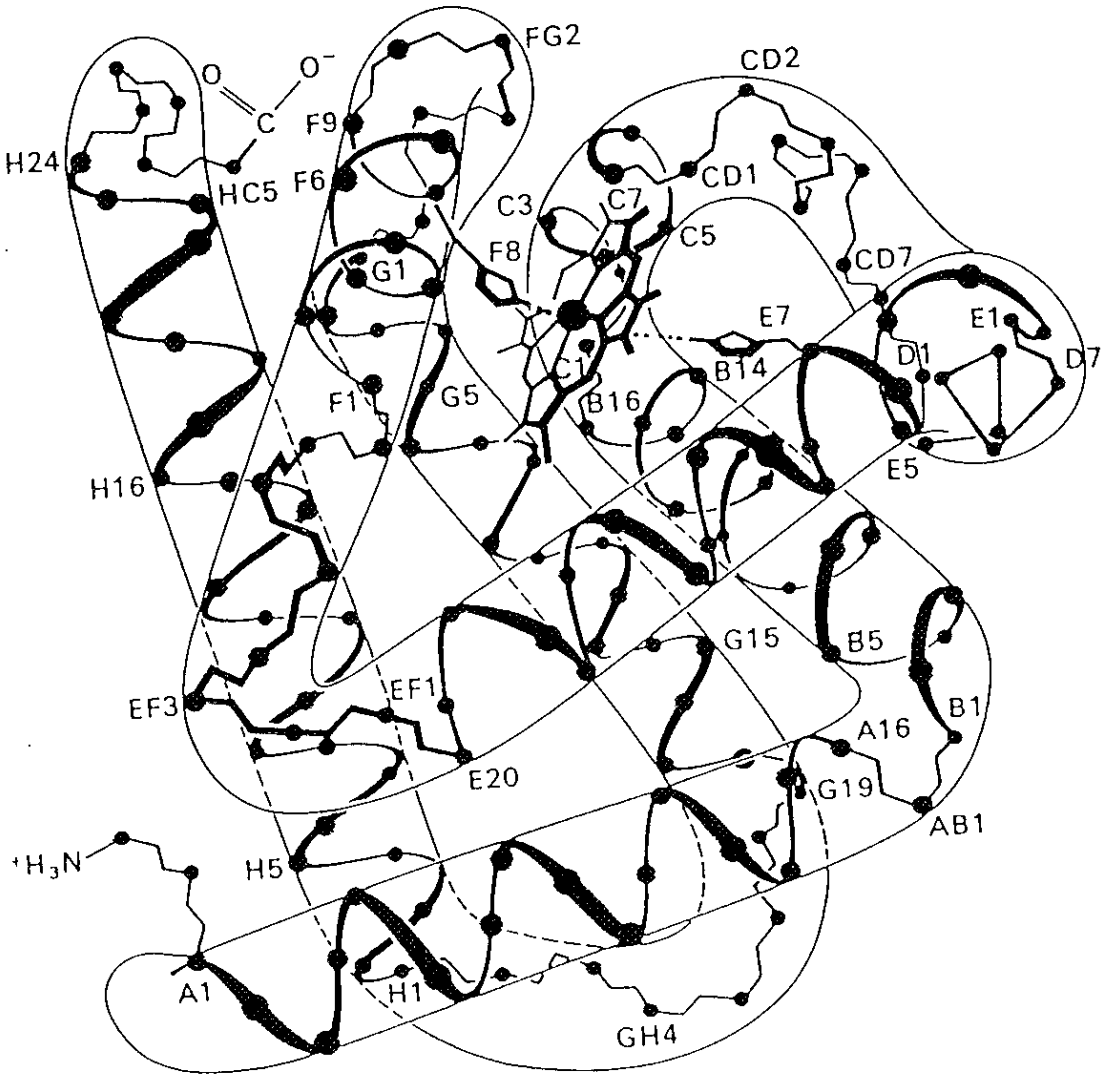

Figure I-1.
The illustration of three dimensional Structure of deoxyMb from ref. 1a.

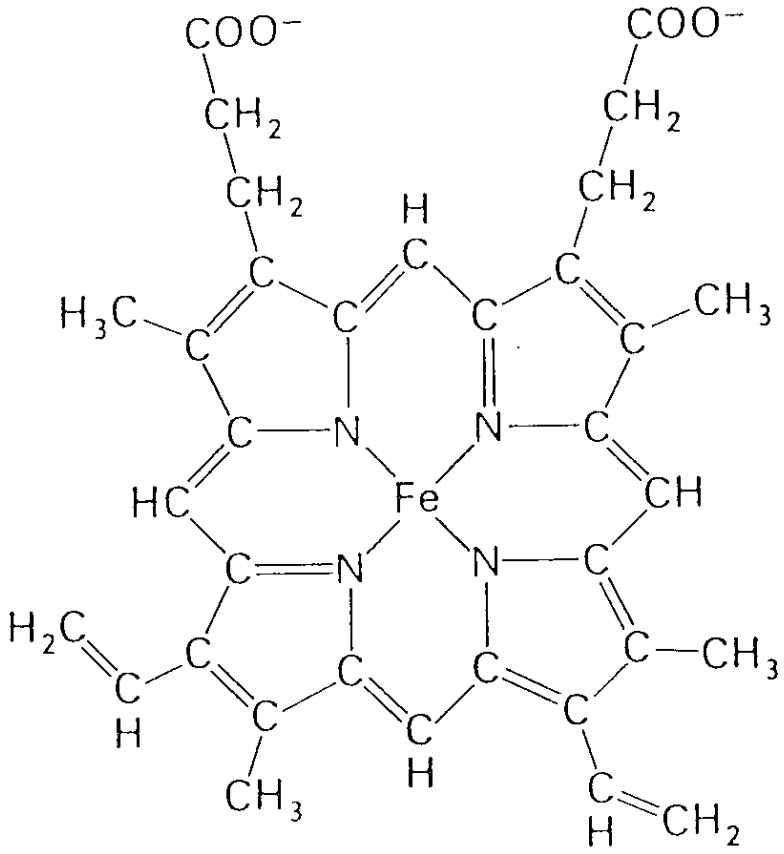

Figure I-2.
The chemical structure of the "heme", iron protoporphyrin IX.

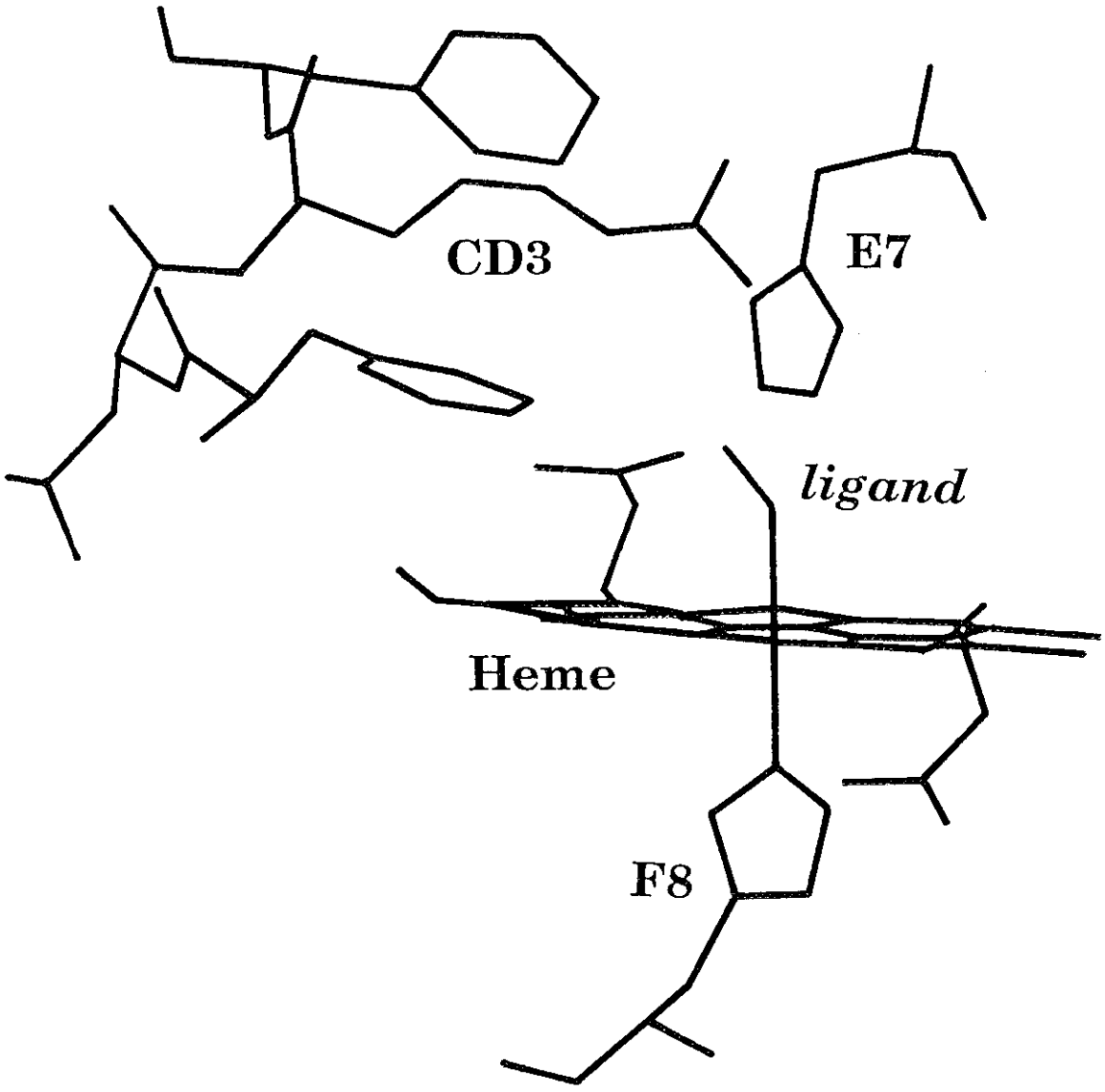

Figure I-3.
The detail structure and conformations of protein amino acid residues around the heme (from ref. 3a).

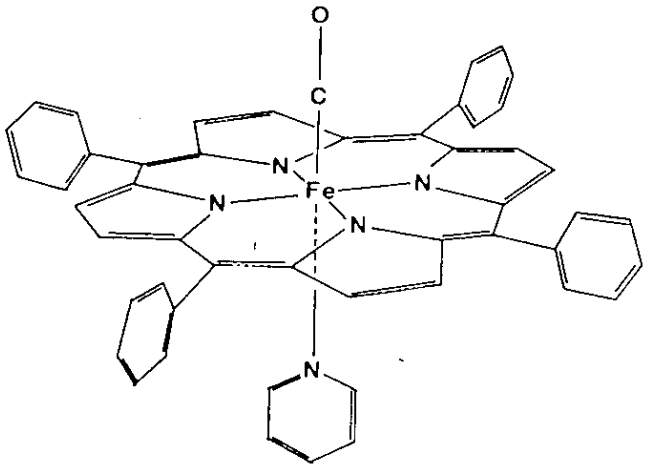

Figure I-4a.
The chemical structure of tetraphenyl porphyrin (from ref. 23).

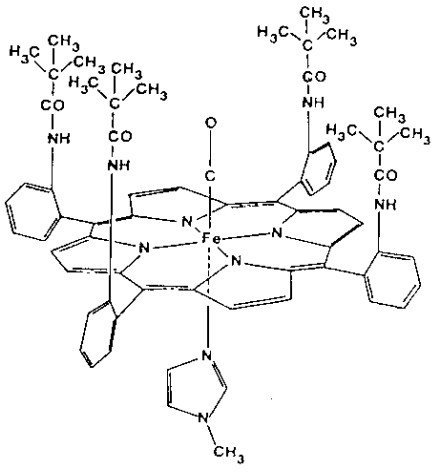

Figure I-4b.
The chemical structure of tetraaryl porphyrin, "picket fence" porphyrin (from ref. 23).

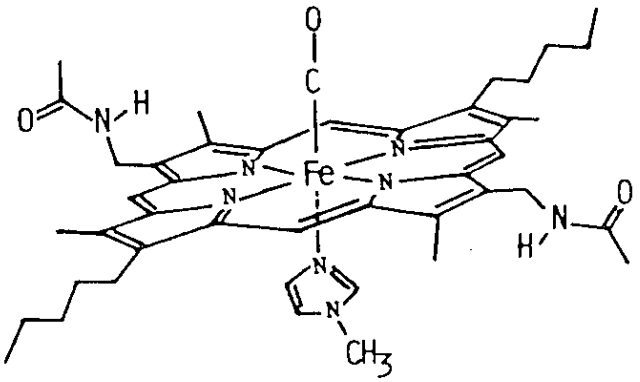

Figure I-5a.
The chemical structure of heme-5 (from ref. 23).

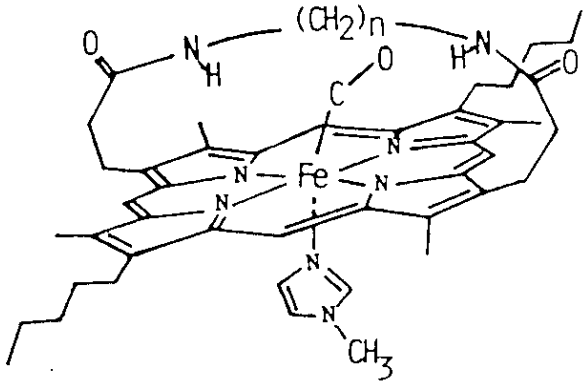

Figure I-5b.
The chemical structure of "strapped" porphyrin (from ref. 23).
n = 5: FeSP-13, n = 6: FeSP-14, n = 7: FeSP-15

Chapter II

Detection of the Transient Fe-CO Stretching Vibrational Modes of Acidic and Neutral Carbonmonoxy Myoglobin

Abstract

The Fe-CO stretching ($\nu_{Fe\text{-}CO}$) Raman band was observed for recombined transient species of photodissociated carbonmonoxy myoglobin (MbCO) at room temperature by using the pump/probe time-resolved technique. The recovery of the equilibrium $\nu_{Fe\text{-}CO}$ band was significantly faster for the acidic form with $\nu_{Fe\text{-}CO}$ at 492 cm^{-1} than the neutral form with $\nu_{Fe\text{-}CO}$ at 511 cm^{-1} when they were coexistent in the solution near pK_a of distal histidine. This is consistent with the proposed assignments of the 511 cm^{-1} and 492 cm^{-1} bands to the "closed" and "open" forms of the protein structure, respectively. However, the transient species present in neutral solution 500 μs - 1 ms after photolysis gave a broad $\nu_{Fe\text{-}CO}$ band around 511 cm^{-1}, but no band around 490 cm^{-1}, suggesting that the CO binding at neutral pH does not go by way of so-called "open" form.

II-1. Introduction

The X-ray crystallographic analysis of deoxy-myoglobin (deoxyMb) and its CO adduct (MbCO)[1] indicated the absence of a pathway for the migration of CO from the solvent to the buried binding site in the heme pocket. There should be rapid rearrangements of the protein structure accompanying the ligand binding. The X-ray studies of ethylisocyanide complex of deoxyMb[2] revealed the opening of a pathway for ligand entry and accordingly, its structure has been regarded as a model of "open" form. Ringe et al.[3] pointed out that the side chains of His-64, Arg-45, and Val-68 were also important residues to form an open channel to the surface.

The Fe-CO stretching ($\nu_{Fe\text{-}CO}$) frequency of the heme-CO complexes is known to be sensitive to the CO geometry in the heme pocket[4, 18]. The CO ligand in MbCO is forced to adopt bent structures, presumably due to steric hindrance from the distal histidine (His-64)[5]. From ab initio MO studies, Augspurger et al.[6] have demonstrated that the CO stretching frequency is affected by the electric field at the CO, which for MbCO is generated by the surrounding amino acid residues and would cause an electronic polarization of the C-O bond. Whatever the mechanism, the $\nu_{Fe\text{-}CO}$ frequency of sperm whale MbCO was, in fact, altered by replacement of His-64 with other residue[7] (it will be discussed in Chapter IV).

Shimada et al.[8] found the four discrete conformations of MbCO at low pH by monitoring the C-O stretching IR band. They also assumed that these conformational changes related to the C-O stretching vibration were arisen from the protonation of distal histidine (His-64). Recently the $\nu_{Fe\text{-}CO}$ resonance Raman (RR) band of acidified MbCO was found at distinctly lower frequencies and the low frequency shift was ascribed to protonation of His-64[9]. It was proposed that the protonated imidazole ring of His-64 swings out of the heme pocket due to

electric repulsion and the CO ligand can then adopt an upright geometry[9]. This conformational change of His-64 results in the opening of a pathway for a ligand entry[1], as found from X-ray crystallographic studies of the ethylisocyanide complex of deoxyMb[2]. Accordingly, the $\nu_{Fe\text{-}CO}$ frequencies of neutral (507 cm^{-1}) and acidic MbCO (488 cm^{-1}) were considered to represent the "closed" and "open" forms of the heme pocket, respectively[7].

Photodissociation of MbCO followed by relaxation to the stable high-spin heme is reported to take place in 350 fs[10]. IR studies on the CO stretching mode indicated that 85% of photodissociated CO remains in the globin 1 ns after photolysis, and 50% after 50 ns[11], although there is no return of CO to the heme in 200-8000 ps range[12]. Since the visible absorption spectrum of the photolysis product of MbCO is reported to be the same as that of the equilibrium deoxyMb for all times greater than 3 ns[13], recombination of photodissociated CO in the 10 ns - 1 ms range is expected to reflect a process of thermal binding. If CO binds to the heme in the so-called "open" form and relaxes to the "closed" form at neutral pH, the $\nu_{Fe\text{-}CO}$ frequency is expected to exhibit a frequency shift from 488 to 507 cm^{-1} during the recombination process of photodissociated CO. In this investigation, the TR^3 spectra of MbCO at neutral and acidic pH were observed, and the $\nu_{Fe\text{-}CO}$ band frequencies and intensities were monitored in order to catch the intemediate species of recombination process after photodissociation.

§II-2. Experimental Procedures

Experimental Apparatus Figure II-1 displays the block diagram of the time-resolved resonance Raman measurement system used in this study. The probe beam (416.0 nm) was obtained as the induced Raman line of H_2 gas (1st Stokes line) excited by the 3rd harmonic of a pulsed Nd:YAG laser (354.7 nm). In prac-

tice, the harmonic was separated by two dichroic mirrors, and passed through the H_2 gas Raman shifter, and the output beam was separated by two pellin broca prisms to remove other higher order Stokes or anti-Stokes lines. The power of the probe beam was made as low as possible (100 - 125 μJ/pulse at the sample point) to avoid detection of photodissociated species by the probe beam. The pump beam (532.0 nm) for the photodissociation was obtained from 2nd harmonic of another pulsed Nd:YAG laser (Quanta-Ray, GCR-11), separated by prism separator (Quanta-Ray, PHS-1), and its power was adjusted to 4.4 mJ/pulse at the sample point. Figure II-2 displays the absorption spectra of MbCO and deoxyMb. The 416.0 nm line is more resonant with MbCO (absorption maximum is 424 nm) rather than with deoxyMb (absorption maximum is 435 nm). The 532.0 nm line is able to photodissociate MbCO in relatively high quantum yield (see Figure V-4 in Chapter V). The pump and probe beams were strictly put upon each other by a dichroic mirror and the colinearly superimposed beams were line focused on the sample point by using two cylindrical lenses made from synthetic quartz. The two pulsed Nd:YAG lasers (7 ns width) were operated in 10 Hz repetition, and the delay time (Δt_d) between pump and probe pulses including the firing of flash lamps and the timing of the Q-switches of individual lasers were controlled by a pulse generator (Stanford Research System, DG-535). The delay time was confirmed by detecting the two pulses with a photodiode (Hamamatsu, S1722-02) and monitoring on the oscilloscope (Tektronix, 2445B). The uncertainty of Δt_d is ± 2 ns.

Scattered light at right angle was collected and focused by two synthetic quartz lenses onto an entrance slit of a triple polychromator (Spex, 1877) equipped with a non-blazed holographic grating (Milton-Roy, 2400 grooves/mm) and an intensified photodiode array (PAR, OMA-III 1421B) which was composed of 1024 pixels. The wavenumber resolution of the present spectra (around 430 nm) was ca.

0.9 cm^{-1}/pixel. The data of each spectra were accumulated for ca. 70 min. on the interface of the OMA-III system (PAR, 1461 and 1463) and transmitted to a personal computer (NEC, PC-9801DA) through a GPIB interface for further calculation.

Materials Horse skeletal muscle Mb (Sigma, type M630) was further purified accordingly to Yamazaki et al.[14] and dissolved in 50 mM Tris-HCl buffer at pH 8.0, which is the most stable pH condition for Mb against autoxidation[14]. Concentrated metMb solution was reduced by sodium dithionite ($Na_2S_2O_4$), subjected by gel filtration through Sephadex G-25M (Pharmacia), and passed through a DEAE-cellulose (Wako Pure Chemical Industry) column for excluding unreduced metMb. Since oxygen molecule in the atmosphere naturally combines with reduced Mb (deoxyMb), the Mb eluted from the column is MbO_2. MbO_2 obtained was flushed by CO gas for a few minutes and made to MbCO. Since deoxyMb has higher affinity against CO molecule than O_2 molecule, MbO_2 easily converted to MbCO by only flushing CO gas. The concentration of MbCO was determined from absorbance at α-band (579 nm, extinction coefficient is 13.9[15]) and β-band (540 nm, extinction coefficient is 15.4[15]).

Concentrated MbCO was diluted to 25 μM with the 50mM pH 8.0 Tris-HCl buffer which was saturated by CO gas, and 1.5 ml of the diluted solution was transferred to an airtight spinning cell (diameter = 20 mm) made of synthetic quartz. The internal gas of the spinning cell containing the MbCO was exchanged to 1 atm. of CO gas after evacuation to 0.1 atm. The pump/fill procedure was repeated three times at least and finally, for complete removal of oxygen, a small amount of degassed dithionite solution was added so that its final concentration was 10 mM. With this concentration, non-resonance Raman bands of dithionite around 460 and 580 cm^{-1} did not disturb the resonance Raman spectra of MbCO.

The acidic MbCO samples were similarly prepared in the spinning cell. 1.5 ml of the CO gas saturated citrate-phosphate (100/200 mM, pH4.5) buffer was put into the airtight spinning cell, and the pump/fill procedure was repeated several times with CO gas. In this spinning cell, the concentrated MbCO was added by using airtight syringe so that the final concentration of MbCO could be 25 μM. These procedures were carried out carefully, because even if a small amount of oxygen remained in the cell, MbCO is autoxidazed to metMb. Since, addition of dithionite into the MbCO caused aggregation of the protein at low pH, dithionite was never used to remove the residual oxygen in the cell.

Measurement Procedures The cell was rotated slowly by stepping motor (Oriental Motor, PX535MH-A, 0.36 degree/step, 25 rpm) in order to avoid the irradiation of two successive probe pulses to the same volume of the sample, and also to reproduce MbCO from the photodissociated state in one turn (2.4 sec) of the spinning cell. The widths of the focused laser beams were about 100 μm at the sample point, thus the transit time of a given molecule across the laser beam is about 3.8 ms. Therefore, even if Δt_d is 1 ms, the 74% of the same photodissociated sample remains at the irradiation area.

Time-resolved spectra were recorded at Δt_d = -20, 0, 20, 100, 500 ns, 1, 10, 100, 500 and 1000 μs in that order and for each samples under the same instrumental conditions. After the last measurement (Δt_d = 1 ms) appearance of the first spectrum (Δt_d = -20 ns) was always confirmed. The whole series of experiments were carried out twice for independent preparations and thus the reproducibility of the present results was confirmed. In the case of low pH solution, since the lifetime of the MbCO at pH 4.5 was only several hours, one sample was used for only measurements of two different Δt_d the sample integrity was confirmed by the probe-only spectra before and after the pump/probe measurements. Cold N_2 gas

was flushed against the spinning cell to maintain it at 10 °C. The dark current data of the photodiode array obtained under the same accumulation times were subtracted from each observed spectra and furthermore, the resultant spectra were divided by white light spectra observed in the same frequency region for correcting sensitivity difference among individual pixels of the photodiode array. The Raman shifts were calibrated with indene and determined with the accuracy of ± 1 cm^{-1} for well defined peaks.

II-3. Results and Discussion

Figure II-3 shows the TR^3 spectra of horse MbCO at pH 8.0. Since the probe wavelength (416.0 nm) is closer to the absorption maximum of MbCO (424 nm) than to that of deoxyMb (435 nm) (see Figure II-2), Raman bands of MbCO are much more strongly resonance enhanced than those of deoxyMb under the present experimental conditions. The ordinate scales of spectra (A) - (E) are common. Since the instrumental conditions including the laser power, the exposure time of the detector and accumulation time are the same for all measurements except for variation of Δt_d, the intensity of Raman bands delineated in the Figure reflects the practical population of MbCO present at each Δt_d. The spectrum for Δt_d = -20 ns was the same as that observed without the pump beam (see Figure II-4) and thus corresponds to a two probe photon photodissociation with a delay time, Δt_d = 2.4 sec, equal to the time separation between pulses. The Raman band at 511 cm^{-1} was confirmed to exhibit an isotopic frequency shift upon $^{13}C^{18}O$ substitution (see Figure II-5), and is therefore assigned to the $\nu_{Fe\text{-}CO}$ mode[16], while an intense band at 674 cm^{-1} is assigned to the ν_7 mode of the porphyrin macrocycle of the CO-bound form (mode number is based on ref. 17). The $\nu_{Fe\text{-}CO}$ band relative intensity in Figure II-3(A) was rather stronger than that observed

with a fast spinning cell (1800 rpm) and CW Kr^+ laser excitation at 406.7 nm (see Figure II-4). This demonstrates that the CO-bound form can be monitored by the pulse excitation when the laser power is reduced, although there may be an appreciable amount of photodissociated species present.

In these neutral pH spectra, the $\nu_{Fe\text{-}CO}$ band almost disappears for Δt_d = 0 ns, although 4% of MbCO from the geminate recombination contributes to the remaining intensity[13]. The $\nu_{Fe\text{-}CO}$ band starts to recover from Δt_d = 500 μs, but its intensity is not restored even at Δt_d = 1 ms, that is at the longest Δt_d available with the present apparatus. In the spectrum for Δt_d = 500 μs, the intensity of a side band around 480 cm^{-1} is comparable to that of the 511 cm^{-1} band and therefore the composite band appears broad. However, the side band is of similar intensity in each spectrum and does not exhibit an $^{13}C^{18}O$ isotopic frequency shift: consequently, it is not evidence of an "open" structural configuration (see Figure II-5, where the TR^3 spectra of $Mb^{12}C^{16}O$ and $Mb^{13}C^{18}O$ are compared for Δt_d = -20 ns, 500 μs, and 1 ms). These spectra were obtained under the same experimental conditions but separately from those shown in Figure II-3, and therefore can serve as a measure of reproducibility. The transient species in the Δt_d = 500 μs range therefore have $\nu_{Fe\text{-}CO}$ around 511 cm^{-1} and exhibit an isotopic frequency shift of 12 cm^{-1}.

Figure II-6 shows the TR^3 spectra of MbCO at pH 4.5 which is reported to be the midpoint pH between the acidic and neutral forms[7, 9a]. Two $\nu_{Fe\text{-}CO}$ bands corresponding to the acidic (492 cm^{-1}) and neutral forms (507 cm^{-1}) are discernible in the spectrum for Δt_d = -20 ns as well as in the probe-only spectrum, in agreement with the reported results[9]. In the spectrum for Δt_d = 0 ns, a weak band remained at 494 cm^{-1}. It cannot be determined exclusively from the present experiment whether the remaining band arisen from non-photodissociable species or rapidly recombined species. However, judging from the facts that the band center

is not coincident with the 492 cm^{-1} band for Δt_d = -20 ns and that the CO complex of the abnormal subunit of Hb M "Boston" with $\nu_{Fe\text{-}CO}$ at 490 cm^{-1}, which is apparently nonphotodissociable by CW laser excitation[17], exhibited photodissociation in picosecond experiments[18] (it will be discussed in Chapter III), it is more likely that the remaining band has arisen from a rapidly recombined species. In contrast with the results at neutral pH, a band is clearly restored at 494 cm^{-1} in the spectrum for Δt_d = 100 ns, while the other band becomes recognizable at 504 cm^{-1} only after Δt_d = 10 μs. The original band-shape is restored at Δt_d = 1 ms, although again the intensity has not fully recovered.

It is evident that the 492 cm^{-1} band recovers significantly faster than the 507 cm^{-1} band at pH 4.5. In Chapters III and IV, human abnormal Hb and various His-64 mutants of human MbCO are also examined. Similarly a faster recovery of the 490 cm^{-1} $\nu_{Fe\text{-}CO}$ band compared to the band around 507 cm^{-1} was found. This trend is consistent with the assumption that the 490 cm^{-1} species corresponds to an "open" structure in which a pathway for ligand entry is available. Since a band at 492 cm^{-1} would have been identified with the present spectral pH, its absence in the spectra of neutral Hb at Δt_d = 100 ns - 100 μs might suggest that the structural change of the globin from the "open" to "closed" form is so fast at neutral pH that the population of the high energy "open" form is too low for rapid recombination to be detected. However, in such a case, the significantly faster recovery of the "open" band at low pH would require strongly pH dependent protein dynamics. Furthermore, this slower recovery of the 507 cm^{-1} species has also been observed at neutral pH for human recombinant mutant Mbs (in Chapter IV), which therefore do not demonstrate such a pH dependence in their dynamics. Therefore, it is more reasonable to conclude that for horse Mb at neutral pH, CO does not bind to the heme iron in the so-called "open" form.

References

(1) J. Kuriyan, S. Wilz, M. Karplus, G. A. Petsko, J. Mol. Biol., **192**, 133 (1986).

(2) K. A. Johnson, J. S. Olson, G. N. Phillips Jr, J. Mol. Biol., **207**, 459 (1989).

(3) D. Ringe, G. A. Petsko, D. E. Kerr, P. R. Ortiz de Montellano, Biochemistry, **23**, 2 (1984).

(4) (a) N. T. Yu, E. A. Kerr, B. Ward, C. K. Chang, Biochemistry, **22**, 4534 (1983).
(b) X-Y. Li, T. G. Spiro, J. Am. Chem. Soc., **110**, 6024 (1988).

(5) J. P. Collman, J. I. Brauman, B. L. Iverson, J. L. Sessler, R. M. Morris, Q. H. Gibson, J. Am. Chem. Soc., **105**, 3052 (1983).

(6) J. D. Augspurger, C. E. Dykstra, E. Oldfield, J. Am. Chem. Soc., **113**, 2447 (1991).

(7) D. Morikis, P. M. Champion, B. A. Springer, S. G. Sliger, Biochemistry, **28**, 4791 (1989).

(8) H. Shimada, W. S. Caughey, J. Biol. Chem., **257**, 11893 (1982).

(9) (a) J. Ramsden, T. G. Spiro, Biochemistry, **28**, 3125 (1989).
(b) S. Han, D. L. Rousseau, G. Giacometti, M. Brunori, Proc. Natl. Acad. Sci. U.S.A., **87**, 205 (1990).

(10) J. L. Martin, A. Migus, C. Poyart, Y. Lecarpentier, R. Astier, A. Antonetti, Proc. Natl. Acad. Sci. U.S.A., **80**, 173 (1983).

(11) P. A. Anfinrud, C. Han, R. M. Hochstrasser, Proc. Natl. Acad. Sci. U.S.A., **86**, 8387 (1989).

(12) T. G. Traylor, D. Magde, D. J. Taube, K. A. Jongeward, D. Bandyopadhyay, J. Luo, K. N. Walda, J. Am. Chem. Soc., **114**, 417 (1992).

(13) E. R. Henry, J. H. Sommer, J. Hofrichter, W. A. Eaton, J. Mol. Biol., **166**, 443 (1983).

(14) I. Yamazaki, K. Yokota, K. Shikama, J. Biol. Chem., **239**, 4151 (1964).

(15) E. Antonini, Physiol. Rev., **45**, 123 (1965).

(16) M. Tsubaki, R. B. Srivasta, N.-T. Yu, Biochemistry, **21**, 1132 (1982).

(17) M. Abe, T. Kitagawa, Y. Kyogoku, J. Chem. Phys., **69**, 4526 (1978).

(18) M. Nagai, Y. Yoneyama, T. Kitagawa, Biochemistry, **30**, 6495 (1991).

(19) R. M. Hochstrasser, private communication.

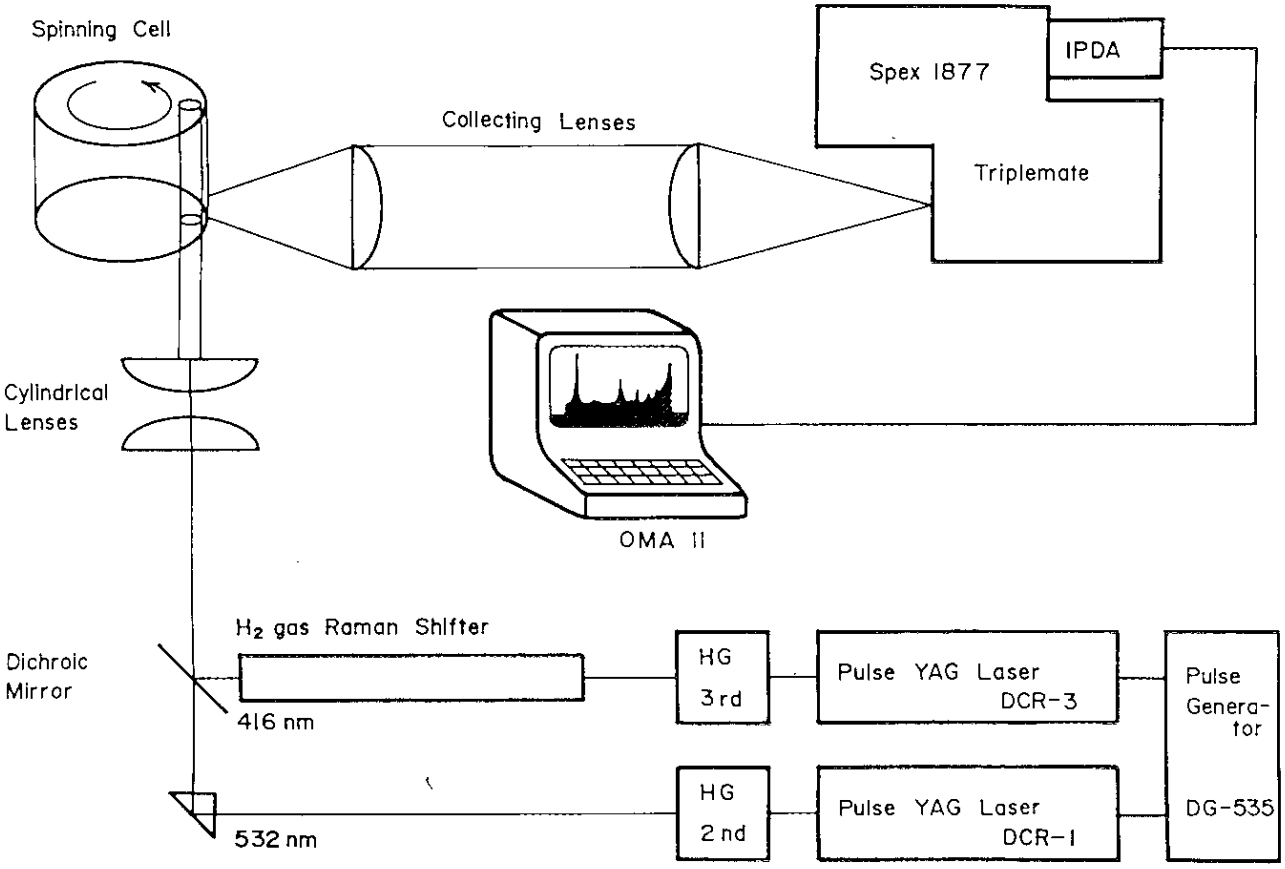

Figure II-1.
Block diagram of the measurement apparatus for the time-resolved resonance Raman spectroscopy in this investigation.

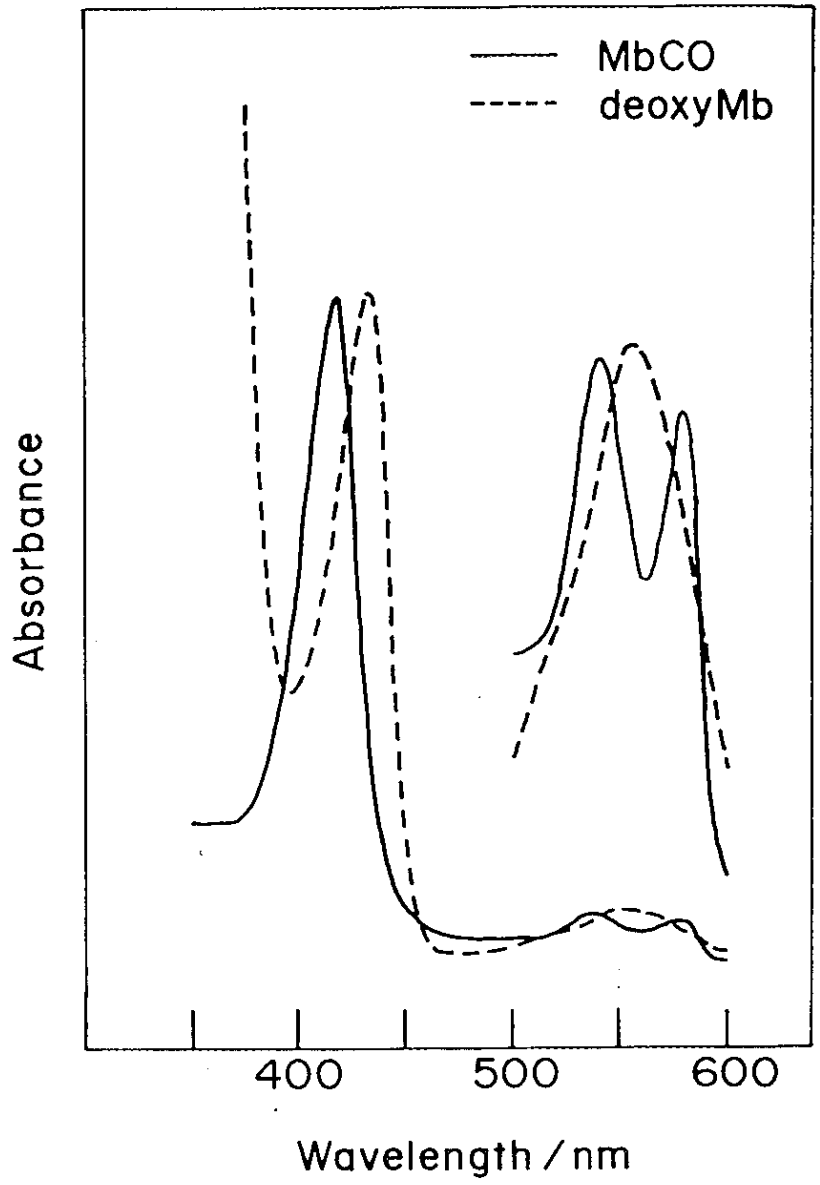

Figure II-2.

Absorption spectra of MbCO and deoxyMb, obtained by spectrometer (Hitachi, 220) with quartz cell (pass length = 10 mm). Absorption maximum of MbCO is 424 nm, and α- and β-bands are 579 and 540 nm, respectively. While, absorption maximum of deoxyMb is 435 nm.

Solid line: MbCO, Broken line: deoxyMb

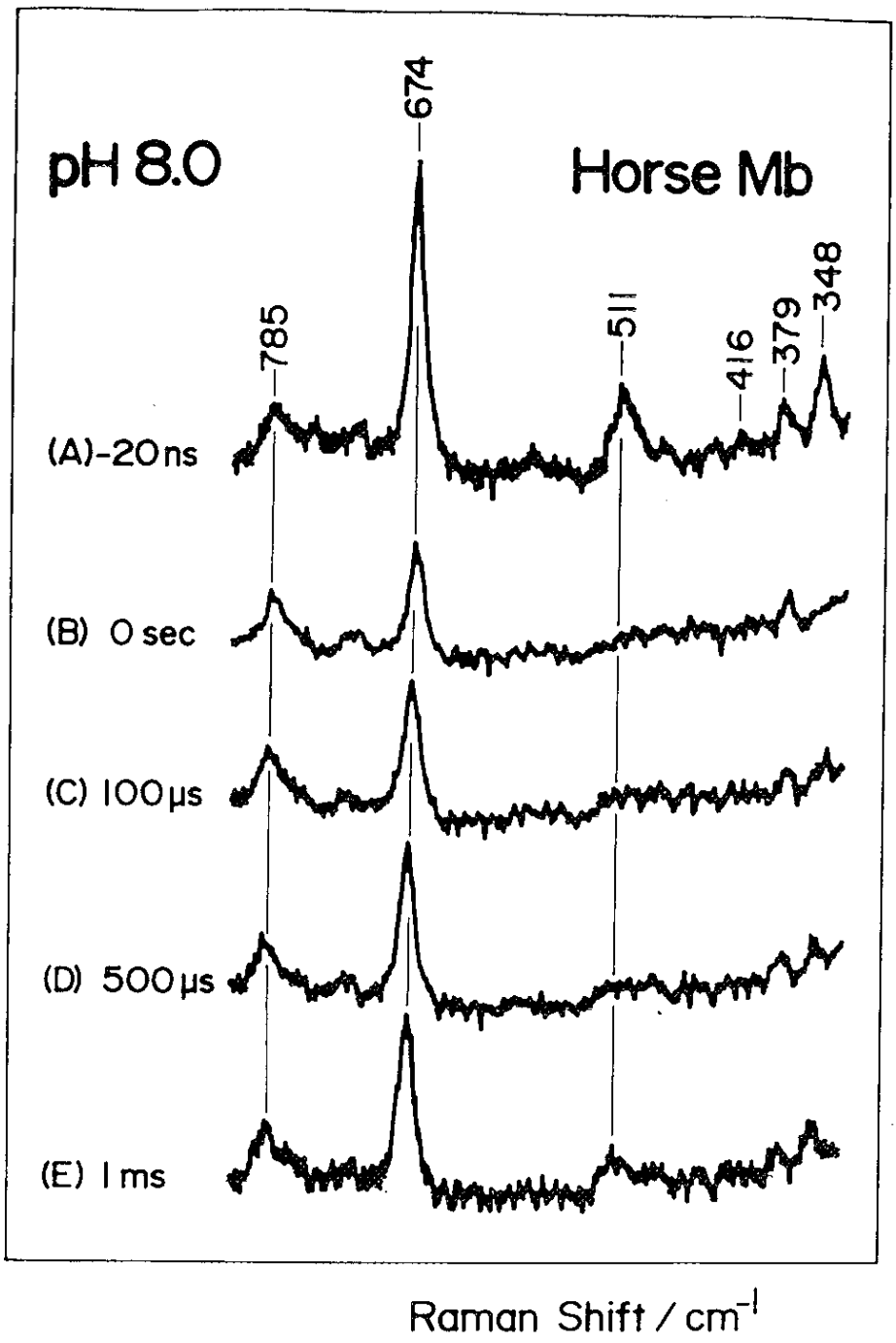

Figure II-3.
Time-resolved resonance Raman spectra of horse MbCO at pH 8.0 under 1 atm. of CO. Delay-time Δt_d is specified at the left side of each spectrum.
Pump beam: 532.0 nm, Probe beam: 416.0 nm

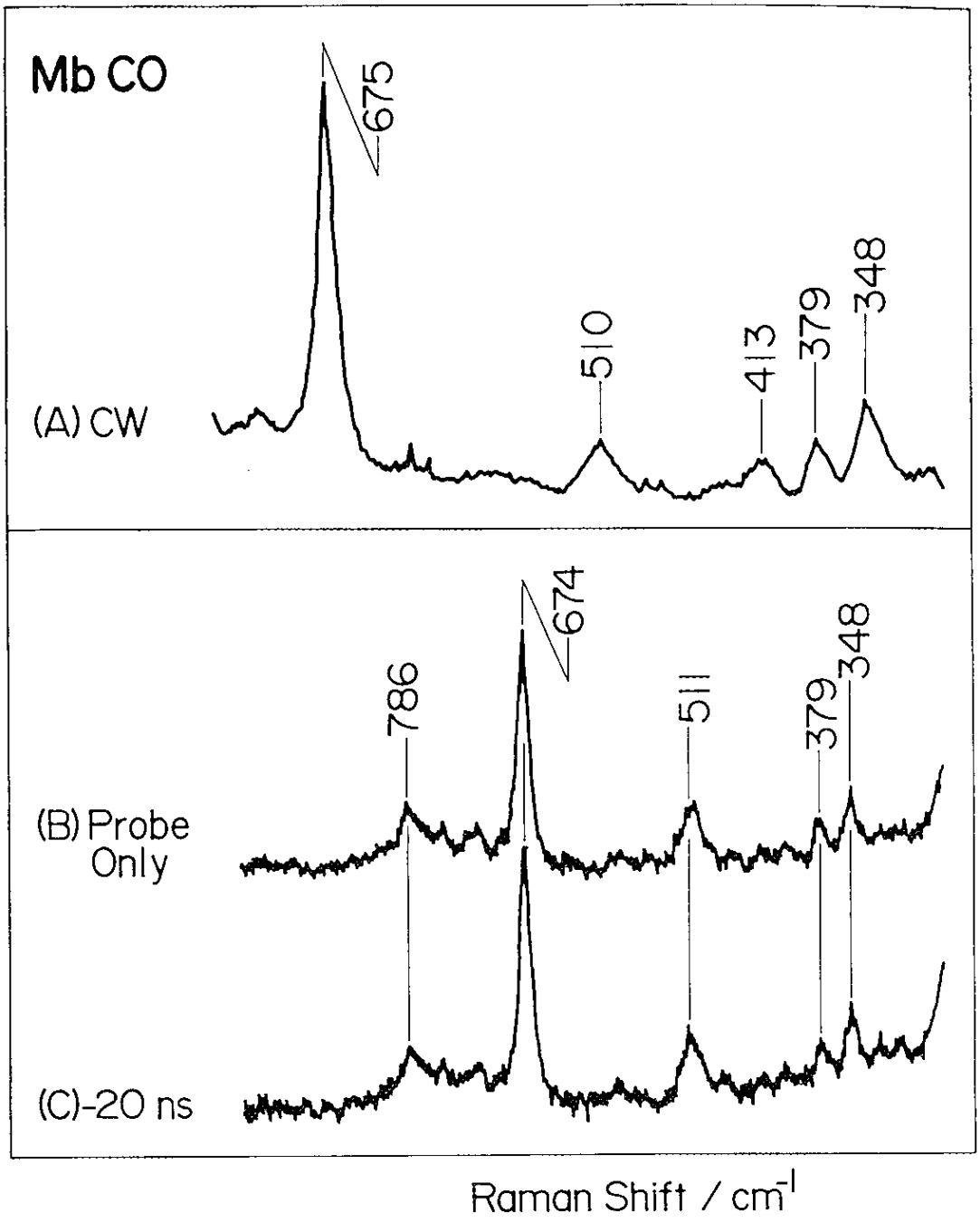

Figure II-4.

Comparison of the spectra of MbCO around the $\nu_{Fe\text{-}CO}$ region under the various conditions. (A) excited by CW Kr^+ 406.7 nm and obtained by using JRS-400D spectrometer (JEOL) with photomultiplier (Hamamatsu, R943-02), (B) without pump beam, (C) Δt_d = -20 ns. The ordinate scales of (A) and (B) are the same, but that of (C) is different.

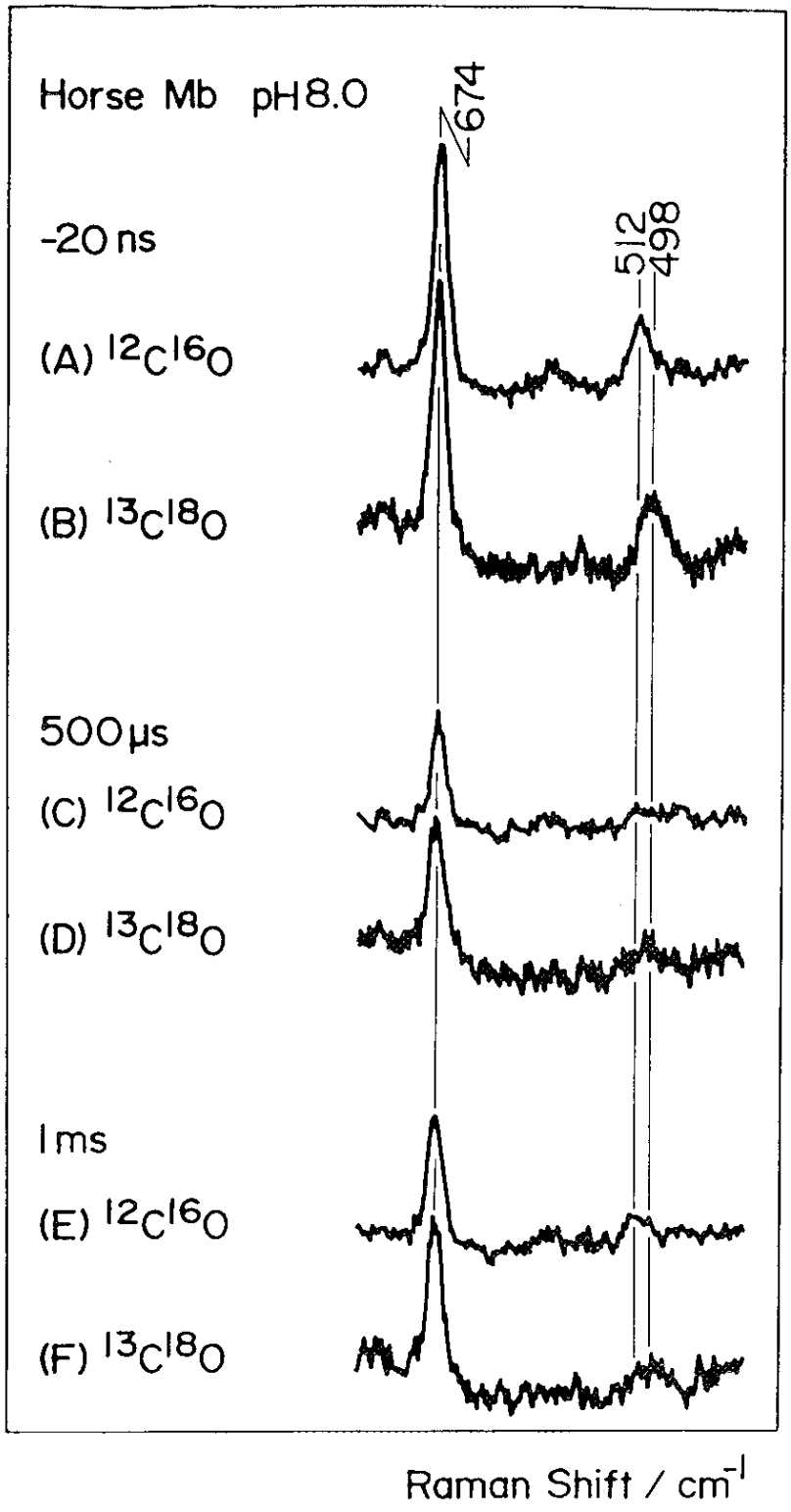

Figure II-5.

Comparison of the time-resolved resonance Raman spectra of $Mb^{12}C^{16}O$ with those of $Mb^{13}C^{18}O$ for Δt_d = -20 ns, 500 μs, and 1 ms.

Pump beam: 532.0 nm, Probe beam: 416.0 nm

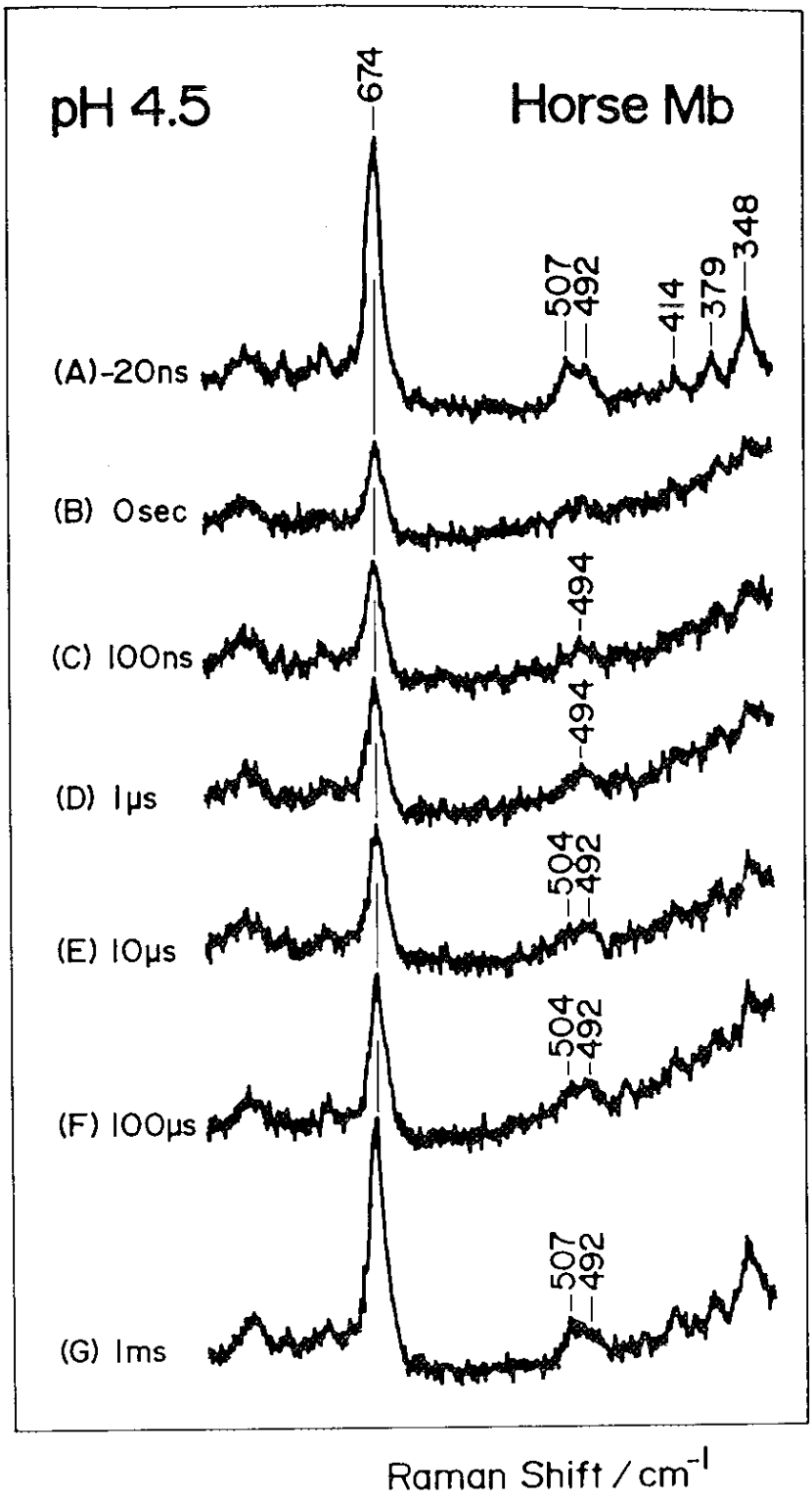

Figure II-6.

Time-resolved resonance Raman spectra of horse MbCO at pH 4.5 under 1 atm. of CO. Δt_d is specified at the left side of each spectrum.

Pump beam: 532.0 nm, Probe beam: 416.0 nm

Chapter III

Relationship between the Fe-C-O Geometry and Temporal Phenomena of the Fe-CO Stretching Vibrational Band of Human Abnormal Hemoglobin

Abstract

The two kinds of human abnormal hemoglobins M, "Boston" and "Saskatoon", and the human normal hemoglobin A were examined with time-resolved resonance Raman technique. These abnormal Hbs M consist of two abnormal and two normal subunits. The distal His (E7-His) of the abnormal chain of both Hbs M are replaced by tyrosine residue. The $\nu_{Fe\text{-}CO}$ Raman bands of the normal and the abnormal chains were observed around 507 and 490 cm^{-1}, respectively. Thus, the normal and the abnormal chains can be regarded as a model of the "closed" and "open" forms, respectively. The TR^3 spectra of these Hbs M showed that while the two $\nu_{Fe\text{-}CO}$ bands exhibit no frequency shift in the transient state, the lower frequency band has recovered faster than the higher frequency band. In contrast to the case of Mb, both of two bands almost fully recovered within 1 ms. On the basis of these observations, it was concluded that the "closed" form did not go by way of the so-called "open" form during the recombination process, but the photodissociated CO entered to the heme pocket through the pathway constructed by the conformational change of the protein in the vicinity of the distal side of the heme.

III-1. Introduction

As discussed in Chapter II, the recombination rate of "open" form was faster than that of "closed" form. However, those results were obtained at low pH condition. The recombination rate might be affected by pH and therefore, it is necessary to measure the TR^3 spectra of both of "open" and "closed" forms under the same conditions. Human abnormal hemoglobins M, "Boston" and "Saskatoon", are excellent models for this purpose. These abnormal Hbs consist of two types subunits in one molecule, that is, normal and abnormal chains[1]. The abnormal chain of Hb M, in which an amino acid residue in the vicinity of the heme is substituted by other amino acid, is stabilized in the ferric state (metHb). In "Boston", the distal His (His-64) of the α-subunits are replaced by tyrosine, while in "Saskatoon", the distal His of the β-subunits are substituted by tyrosine. Tyrosine (Tyr) has a structure similar to His, but the differences lie in the volume and hydrophobicity.

The absorption spectra in the visible region of these Hbs M are similar to that of normal Hb A in the fully reduced state (deoxyHb) and CO bound state (HbCO), but in the ferric state (metHb), the spectra of Hb M are different from that of normal Hb A[2]. According to the X-ray diffraction data of Hb M "Boston", its proximal His (His-87) did not bind to the heme iron but the distal substituted Tyr (Tyr-58) is bound to the iron atom in the met form[3]. However, in the reduced state of the abnormal subunits, the iron atoms were in the pentacoordinate structure and bound with the proximal F8 His like deoxyHb A[2]. In the partially reduced type (the normal chain was reduced while the abnormal chain was in ferric state), Hb M "Boston" exhibits neither present the cooperativity nor the Bohr effect and remains in the low affinity quarternary state[4, 5], while "Saskatoon" represents an appreciable cooperativities, the Bohr effect, and the normal affinity for oxygen[6]. In the fully reduced type, however, both Hbs M exhibit higher affinity for ligands

than Hb A and also the Bohr effect and the cooperativity in a similar magnitude to those of Hb A[7]. The $\nu_{Fe\text{-}CO}$ Raman band of these abnormal Hbs M appeared as two distinguishable peaks at 490 and 505 cm^{-1} [2] corresponding to the abnormal and normal chains, respectively. These two frequencies happen to be the same as those of the "open" and "closed" forms, respectively[8]. The Fe-C-O bond angles of the abnormal subunit of both of Hb M CO "Boston" and "Saskatoon" were estimated to be 176° from the isotopic frequency shifts and normal coordination calculations, while that of normal Hb A CO was 156° [2]. Nagai et al.[2] pointed out that the lower frequency band did not disappear under the laser illumination condition where the higher frequency band disappeared. To study this difference in details, the TR[3] spectra of CO adduct of these Hbs M and Hb A in the $\nu_{Fe\text{-}CO}$ region were examined. The temporal behaviors of the $\nu_{Fe\text{-}CO}$ bands of two Hbs M are described in this Chapter.

III-2. Experimental Procedures

The human abnormal Hbs M and normal Hb A were purified from patients' hemolysate and human blood, respectively by Prof. M. Nagai, Kanzawa University School of Allied Medical Professions[2, 9]. Purity of the isolated Hbs M were examined by analytical electrofocusing on an ampholine plate gel (pH range 3.5 - 9), and contamination of Hb A in each Hbs M preparation was confirmed to be less than 1%. The Hb concentration was determined after conversion to the pyridine hemochrome by assuming the extinction coefficient ϵ_{mM} (557 nm) = 34.

"Boston" was reduced by adding dithionite (10 mM) and leaving it for an over night in the airtight spinning cell filled with CO gas. In the abnormal subunits of both Hbs M, ferric state is more stabilized than ferrous state, and therefore it is hardly changed from met-type to full reduced-type[9b, c]. However, "Saskatoon" was

reduced relatively rapidly by dithionite. For the Raman measurements the concentration of these samples were adjusted to 30 μM in terms of hemes by 10 mM bis-Tris HCl buffer at pH 7.0 involving 0.1 M NaCl, as in most of Hb investigations. In this concentration (30 μM), the tetramer of Hb is not separated to monomers or dimmers (the dissociation constant of Hb A CO between tetramer and dimmer is 2 $\times$ 10^{-6} M)[10].

The measurement system of Raman spectra were as same as that described in Chapter II. Because of the high concentrations of hemes compared with that for Mb (in Chapters II and IV), the power of the pump pulse (532.0 nm) was raised to 6.3 mJ/pulse, so that the photodissociation could be complete as in the case of MbCO. Since, the higher frequency species of $\nu_{Fe\text{-}CO}$ of both Hbs were apt to be photolyzed, so the power of probe pulse was lowered to 38 - 63 μJ/pulse, to reduce the photodissociation by probe beam itself. The accumulation time was ca. 150 min. for each spectrum, which is as twice as longer than that adopted for Mbs, in order to obtain the TR^3 spectra of HbCO with the same S/N ratio as those in Chapter II or IV. The other procedures for measurements are the same as those described in Chapter II.

III-3. Results and Discussions

Figure III-1 displays the TR^3 spectra of human normal Hb A CO. The ordinate scales of each spectra (A) - (F) are common. The spectrum at -20 ns was in agreement with the probe only spectrum obtained before and after the pump/probe measurements. This fact indicates that the Hb A CO in the spinning cell was not injured by pump and/or probe pulses during the measurements, although it takes about 30 hours for one systematic measurement, and that the photodissociated CO fully recovered within one turn of spinning cell (2.4 sec).

This was also confirmed with "Boston" and "Saskatoon". In Figure III-1 (A), the $\nu_{Fe\text{-}CO}$ band appears at 506 cm^{-1}. This $\nu_{Fe\text{-}CO}$ band seems to be a single peak and very sharp, suggesting that the environments around the Fe-C-O is the same among the four subunits, including the α- and β-chains. At Δt_d = 0 and 20 ns, the $\nu_{Fe\text{-}CO}$ band perfectly disappeared. The intensity of the ν_7 band at 677 cm^{-1} in the spectrum for Δt_d = 20 ns is much weaker than that for Δt_d = -20 ns. This is due to stronger resonance to HbCO than to deoxyHb, since the probe beam (416.0 nm) is closer to the absorption maximum of HbCO (419 nm) than to that of the photolyzed species (430 nm). At longer times than Δt_d = 100 ns, the intensities of the $\nu_{Fe\text{-}CO}$ recovered gradually but even at Δt_d = 1 ms, the intensity did not fully recovered. Note that any transient bands did not appear around 490 cm^{-1} corresponding to the "open" form and that the transient $\nu_{Fe\text{-}CO}$ band did not shift to a higher or a lower frequency.

The TR^3 spectra of Hb M CO "Boston" are shown in Figure III-2. The ordinate scale of each spectra is also common. At Δt_d = -20 ns, two distinct peaks were observed at 507 cm^{-1} and 490 cm^{-1}, corresponding to the "closed" and "open" form, respectively. The frequencies of the two $\nu_{Fe\text{-}CO}$ band were consistent with the statical spectrum obtained by Nagai et al.[2] At Δt_d = 0 sec, the intensities of both of $\nu_{Fe\text{-}CO}$ bands almost vanished, but very weak and broad band seemed to remain around 490 cm^{-1}. This weak and broad band at Δt_d = 0 sec indicates that the recombination rate of the "open" form was so fast that a part of the photodissociated CO recovered within 7 ns, or that the minimal unphotodissociated CO remained. However, the time-resolved IR spectrum on the picosecond time scale showed that both of these bands exactly disappeared in the short time[11], and additionally, according to the examinations by CW Kr^+ laser (406.7 nm) the intensity of the lower frequency band remained under the condition in which the higher

frequency band perfectly vanished[2]. From these facts, it is inferred that the remained band in the spectrum for Δt_d = 0 sec arises from a small amount of the photodissociated CO bound "open" form restored within 7 ns. This behavior that the weak and broad band at lower frequency remains even at Δt_d = 0 sec was also detected in Hb M CO "Saskatoon" (in Figure III-4, it will be discussed below) and acidic MbCO at pH 4.5 discussed in Chapter II. At the longer delay time than the Δt_d = 20 ns, both of higher and lower frequency bands recovered, gradually, but the lower frequency band recovered much faster than the higher frequency band. It was attempted to separate the $\nu_{Fe\text{-}CO}$ bands with two Lorentzian functions by dumped least square method[12] in order to discuss quantitatively the difference of recombination rate between the "open" and "closed" form. Figure III-3 shows the results of separation at Δt_d = -20, 20 ns, 500, and 1000 μs. These ordinate scales were normalized with the minimum and maximum intensities of each spectra. At Δt_d = -20 ns (Figure III-3(A)), the $\nu_{Fe\text{-}CO}$ bands were identified as two peaks at 507 and 490 cm^{-1}. The lower frequency band was stronger and broader than the higher frequency band. At Δt_d = 20 ns (Figure III-3(B)), the higher frequency band did not recover, but the lower frequency band has already recovered about 50% of the intensity at -20 ns. At Δt_d = 500 μs (Figure III-3(C)), the higher frequency band slightly recovered, and the band width was much broader than that at -20 ns. At Δt_d = 1 ms (Figure III-3(D)), both of higher and lower frequency bands almost fully recovered, and the band width of higher frequency band became sharp. The peak frequencies have never shifted in the transient state from the equilibrium values of 507 and 490 cm^{-1}.

The TR[3] spectra of Hb M CO "Saskatoon" are shown in Figure III-4. The ordinate scales of all spectra are also common. Figure III-4(A) obviously shows that the two $\nu_{Fe\text{-}CO}$ bands appear at 508 and 493 cm^{-1} in the spectra for Δt_d = -20

ns. This spectrum was also consistent with Nagai et al.[2] Both bands almost disappeared at Δt_d = 0 sec, although a weak and broad feature remained around 490 cm^{-1}. This weak band comes from the fast recovering species of photodissociated CO as discussion above. After Δt_d = 20 ns, the intensity of the $\nu_{Fe\text{-}CO}$ band was restored gradually as increase of Δt_d. Both bands almost fully recovered at the Δt_d = 1 ms.

Figure III-5 shows the $\nu_{Fe\text{-}CO}$ bands spectra decomposed to two component bands of Lorentzian band shape through the dumped least square calculations[12]. These ordinate scales are different, that is, the intensities of the minimum and maximum values of each spectra are normalized. At the Δt_d = 20 ns (Figure III-5(B)), there is only one peak at 496 cm^{-1}. There are two possible interpretations for this. One is that the lower frequency band at 493 cm^{-1} shifts to a higher frequency at 496 cm^{-1} and the higher frequency band at 508 cm^{-1} perfectly disappears or shifts to a lower frequency at 496 cm^{-1}, and the other is that while the higher frequency band makes no contribution, the lower frequency band at 493 cm^{-1} apparently shifts to higher frequency at 496 cm^{-1}. The latter seems more likely, since the transient species of the lower frequency band is not detected at other delay time. These transient spectra show that both peaks do not shift after Δt_d = 100 ns.

According to the TR[3] spectra of two types of human abnormal Hb M CO and normal Hb A CO, it is concluded that the recombination rate of the abnormal subunit, which corresponds to "open" form with the lower $\nu_{Fe\text{-}CO}$ frequency, is much faster than that of the normal subunit, which corresponds to the "closed" form with the higher $\nu_{Fe\text{-}CO}$ frequency. These results indicate that the photodissociated CO enter into the heme pocket from the solvent through the pathway in the distal side, that is prepared or created by the conformational change of the distal E7, CD3,

and E11 residues[13]. Because the "open" form with the pathway for the ligand entry does not require a conformation change for ligand entry, it takes shorter time for the recombination of ligand than in the case of the "closed" form that needs to modify the conformation of protein to the "open" form.

Why is the conformation of the distal side protein reformed by the substitution of only one E7 residue ? In the past time, it had been assumed that the size of amino acid residue of distal side was very important to determine the conformation of protein. However, in the cases of "Boston" and "Saskatoon", although the substituted E7-Tyr residue of abnormal chain has a similar structure to His and a slightly larger volume than that of His, the conformation of abnormal chain is the "open" form. This may indicate that the size of E7 residue is less important for the determination of the protein conformation in the vicinity of the heme. Both His and Tyr have similar structures and volumes each other, but their hydrophobicities are different. The values of hydropathy index that indicate the hydrophobicities of His and Tyr are -3.2 and -1.3, respectively[14]. Since, His is more hydrophilic than Tyr, the E7-Tyr residues of abnormal chain of both Hbs M, "Boston" and "Saskatoon", may swing out to the solvent and form the "open" structure. Therefore, it is proposed that the determination factor of the protein conformation in the vicinity of the heme is mainly the hydrophobicity of distal side amino acid residues. This proposal will be verified and discussed in detail in Chapter IV.

Both of the two $\nu_{Fe\text{-}CO}$ bands originated from the two conformations of the protein corresponding to the "open" and "closed" form in "Boston" and "Saskatoon" almost fully recovered within 1 ms after photolysis. These facts were different from the cases of MbCOs described in Chapter II and IV. It is not clearly why this faster recombination rates of the normal subunits of both Hbs M than those of Mbs were observed in spite of "closed" form. Furthermore, the higher frequency

$\nu_{Fe\text{-}CO}$ bands of both Hbs M CO corresponding to the "closed" form have never shifted to lower frequency, and in the earlier time after the photodissociation, the weak recovered bands were broader than the static band. These facts lead us to conclude that the CO migrated into the heme pocket through the pathway binds to the heme iron at a nearly equilibrium Fe-C-O angle, but in the short time region after the photodissociation the Fe-C-O bond fluctuates around the equilibrium geometry.

References

(1) (a) H. Hörlein, G. Weber, Dtsch. Med. Wochenschr., **73**, 476 (1948).
(b) K. Singer, Am. J. Med., **18**, 633 (1955).

(2) M. Nagai, Y. Yoneyama, T. Kitagawa, Biochemistry, **30**, 6495 (1991).

(3) (a) P. D. Pulsinelli, M. F. Perutz, R. L. Nagel, Proc. Natl. Acad. Sci. U.S.A., **70**, 3800 (1973).
(b) M. Nagai, Y. Yoneyama, T. Kitagawa, Biochemistry, **28**, 2418 (1989).

(4) J. Greer, J. Mol. Biol., **59**, 107 (1971).

(5) (a) N. Hayashi, Y. Motokawa, G. Kikuchi, J. Biol. Chem., **241**, 79 (1966).
(b) T. Suzuki, A. Hayashi, Y. Yamamura, Biochem. Biophys. Res. Commun., **19**, 691 (1965).

(6) H. M. Ranny, R. L. Nagel, P. Heller, L. Uden, Biochim. Biophys. Acta, **160**, 112 (1968).

(7) (a) K. Nishikura, Y. Sugita, M. Nagai, Y. Yoneyama, Nature, **254**, 727 (1975).
(b) K. Nishikura, Y. Sugita, M. Nagai, Y. Yoneyama, J. Biol. Chem., **250**, 6679 (1975).

(8) (a) J. Ramsden, T. G. Spiro, Biochemistry, **28**, 3125 (1989).
(b) D. Morikis, P. M. Champion, B. A. Springer, S. G. Sligar, Biochemistry, **28**, 4791 (1989).

(9) (a) M. Nagai, Acta Haematol. Jpn., **48**, 2015 (1985).
(b) M. Nagai, T. Yubisui, Y. Yoneyama, J. Biol. Chem., **255**, 4599 (1980).
(c) M. Nagai, S. Takama, Y. Yoneyama, Acta Haematol., **78**, 95 (1987).

(10) S. J. Edelstein, M. J. Rehmar, J. S. Olson, Q. H. Gibson, J. Biol. Chem., **245**, 4372 (1970).

(11) R. M. Hochstrasser, private communications.

(12) (a) K. Levenberg, Q. Appl. Math., **2**, 164 (1944).
(b) Y. Senga, S. Minami, Bunko-Kenkyu, **33**, 142 (1986).

(13) J. Kuriyan, S. Wilz, M. Karplus, G. A. Petsko, J. Mol. Biol., **192**, 133 (1986).

(14) J. Kyte, R. F. Doolittle, J. Mol. Biol., **157**, 105 (1982).

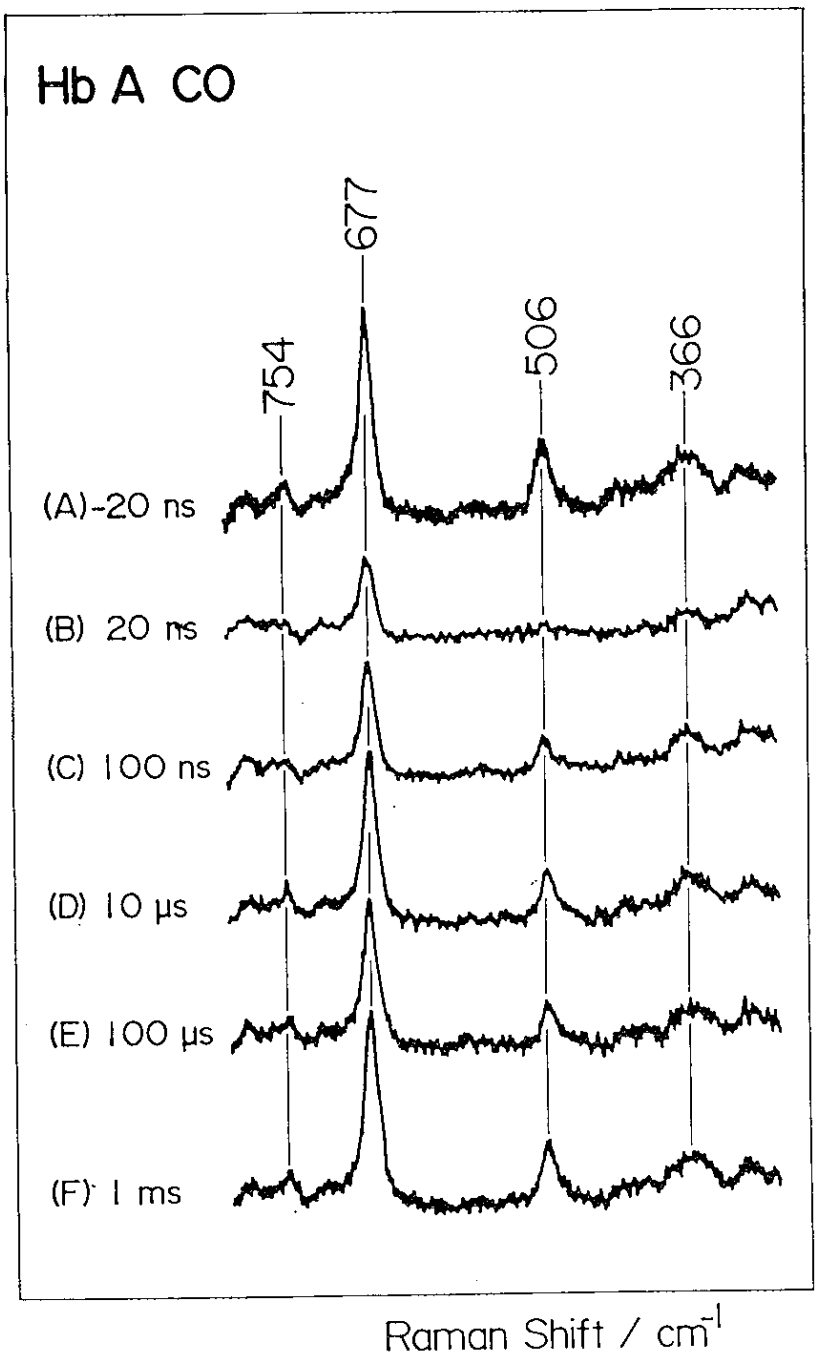

Figure III-1.

The time-resolved resonance Raman spectra of human normal Hb A CO. The pump/probe delay times (Δt_d) are showed in the left side of this Figure.

Pump beam: 532.0 nm, Probe beam: 416.0 nm

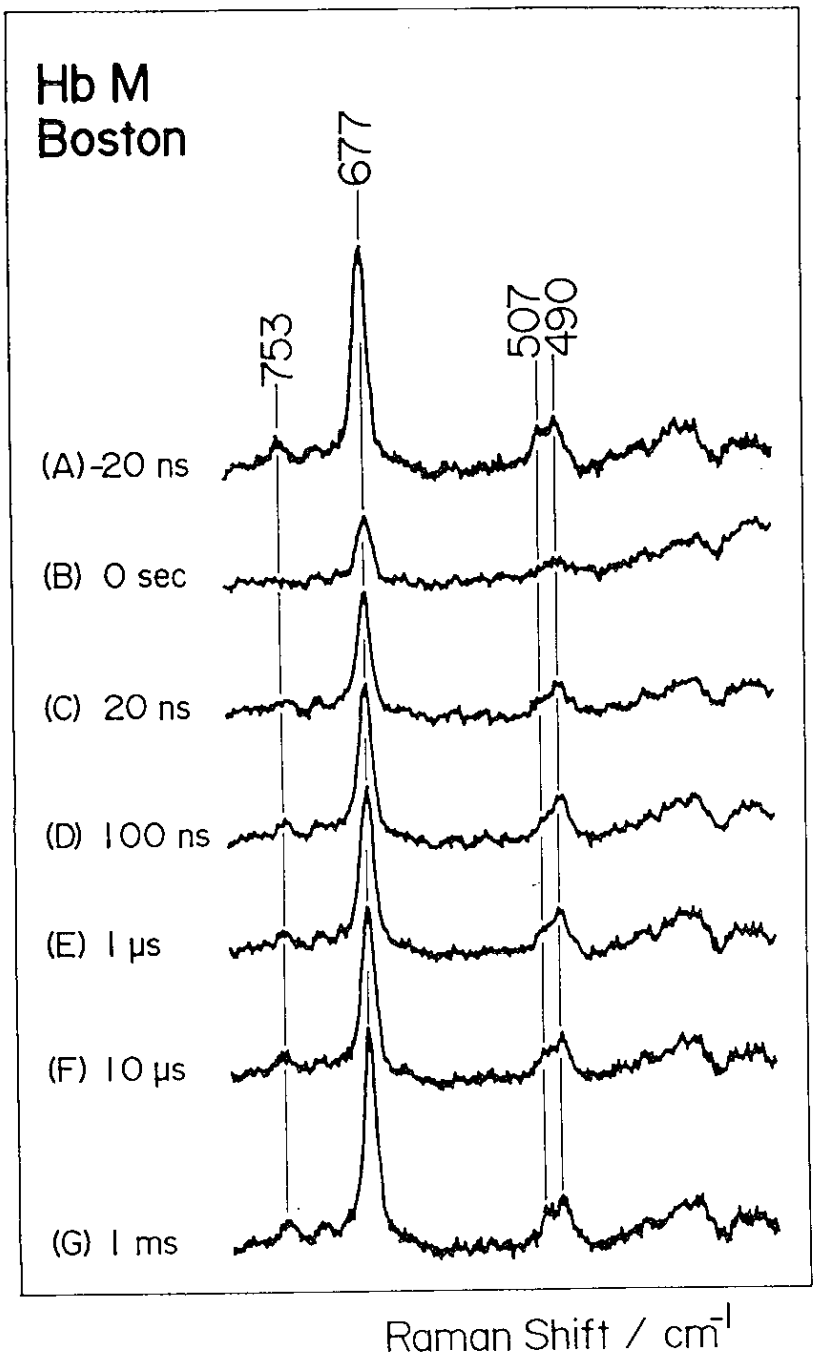

Figure III-2.

The time-resolved resonance Raman spectra of human abnormal Hb M CO, "Boston". The pump/probe delay times (Δt_d) are showed in the left side of this Figure.

Pump beam: 532.0 nm, Probe beam: 416.0 nm

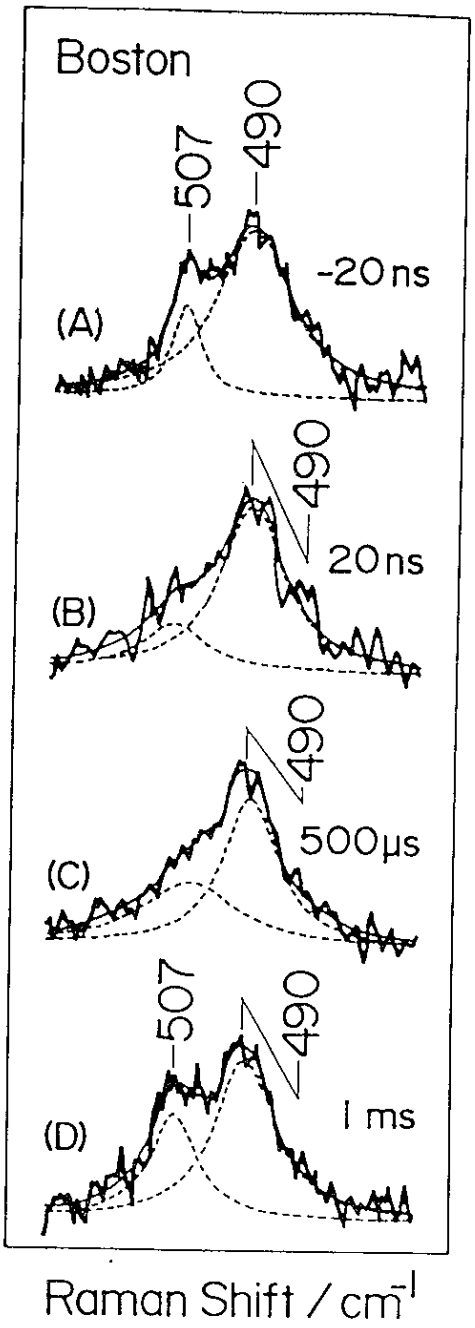

Figure III-3.

The results of the band separations of the transient $\nu_{Fe\text{-}CO}$ bands of Hb M "Boston" with two Lorentzian functions through the dumped least square method. The solid lines denote the sum of the calculated components spectra represented by broken lines.

(A): Δt_d = -20 ns, (B): Δt_d = 20 ns, (C): Δt_d = 500 μs, (D): Δt_d = 1 ms.

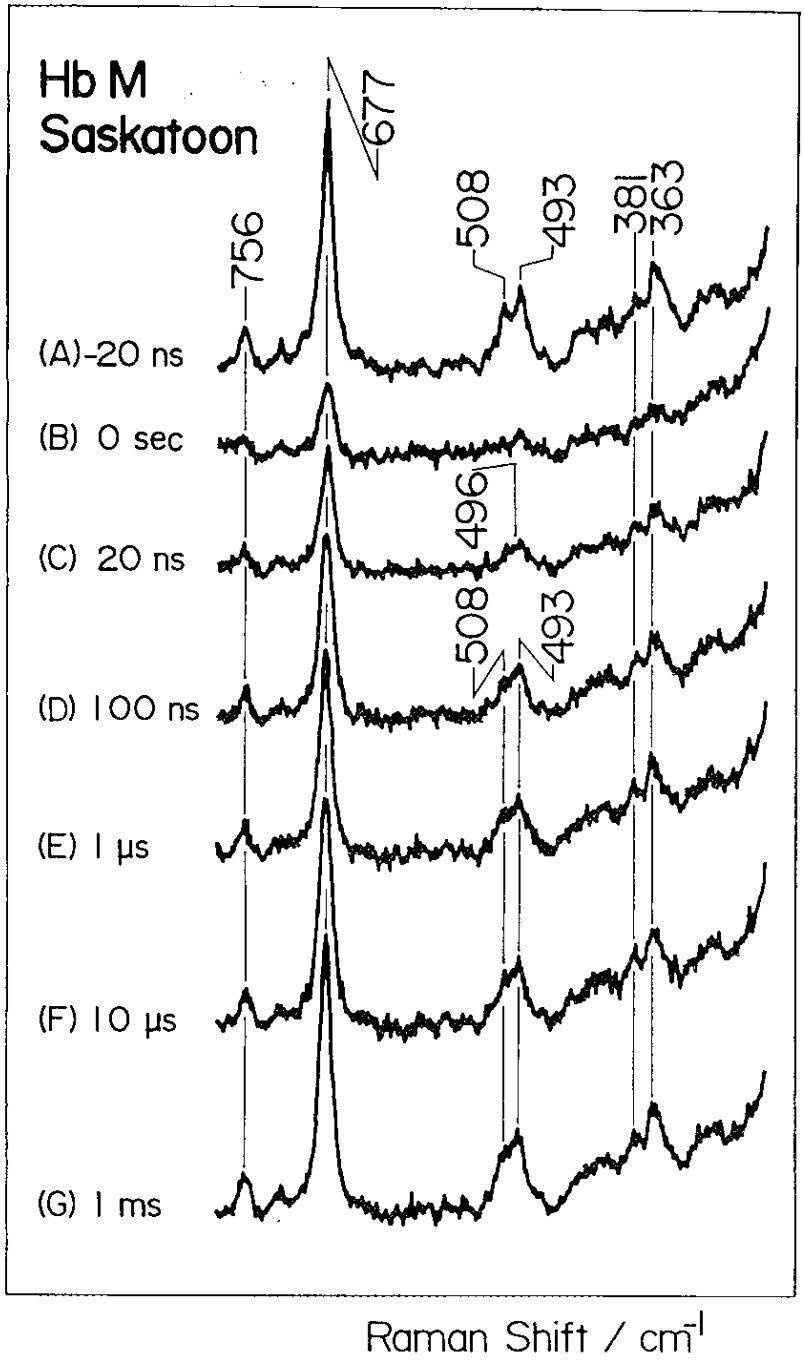

Figure III-4.

The time-resolved resonance Raman spectra of human abnormal Hb M, "Saskatoon". The pump/probe delay times (Δt_d) are showed in the left side of this Figure.

Pump beam: 532.0 nm, Probe beam: 416.0 nm

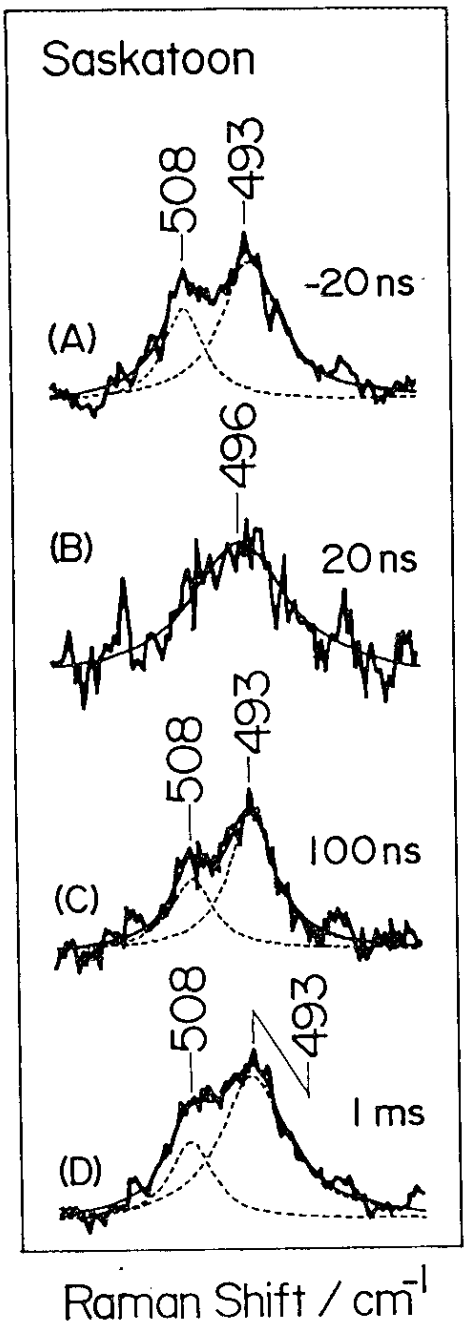

Figure III-5.

The results of the band separations of the transient $\nu_{Fe\text{-}CO}$ bands of Hb M "Saskatoon" with two Lorentzian functions through the dumped least square method. The solid lines denote the sum of the calculated components spectra represented by broken lines.

(A): Δt_d = -20 ns, (B): Δt_d = 20 ns, (C): Δt_d = 100 ns, (D): Δt_d = 1 ms.

Chapter IV

Elucidation of the Protein Dynamics in the Distal Side of Heme Pocket by Using Distal Histidine Mutant Human Carbonmonoxy Myoglobins Obtained through Site-Directed Mutagenesis

Abstract

Time-resolved resonance Raman spectra of the recombined species of photodissociated CO with recombinant human myoglobin and several E7 mutants, in which distal His was replaced by Gly (H64G), Gln (H64Q), Ala (H64A), Ile (H64I), Val (H64V), and Leu (H64L) through site-directed mutagenesis, were observed in the time range -20 ns and 1 ms following photolysis. The Fe-CO stretching ($\nu_{Fe\text{-}CO}$) RR band was observed successfully with pulse excitation when the laser power was greatly reduced. H64H, H64G, and H64Q gave the $\nu_{Fe\text{-}CO}$ band at 505 - 510 cm^{-1} in their stationary state. In their recovery process 1 - 100 μs after photodissociation, a broad transient band was observed at slightly lower frequencies than in their equilibrium structures for H64G and H64Q, but a transient $\nu_{Fe\text{-}CO}$ band corresponding to the so-called "open" form was not identified around 490 cm^{-1} for any of the three species. A second group, H64A, H64I, H64V, and H64L gave the main $\nu_{Fe\text{-}CO}$ band at 490 - 495 cm^{-1} with a shoulder around 510 cm^{-1} (except for H64L) in the stationary state, and exhibited a much faster recovery than the first. These latter four species gave a broad transient band around 492 - 500 cm^{-1} in the time range of 100 - 1000 ns, while the ~510 cm^{-1} shoulder appeared much later. The equilibrium relative intensity of the two bands was attained at 500 μs, suggesting that the interconversion between the two forms is slower than 100 μs. For all MbCO examined here, the recovery, determined from the area intensity of the $\nu_{Fe\text{-}CO}$ band, exhibited two phases irrespective of the presence of one or two $\nu_{Fe\text{-}CO}$ bands. The $\nu_{Fe\text{-}CO}$ frequencies could be correlated with hydropathy index of the E7 residue but not with its size. It is inferred that the more hydrophobic environments around CO reduces polarization of CO and lowers the $\nu_{Fe\text{-}CO}$ frequency to ~490 cm^{-1} in one hand and more stabilizes the protein separated CO, resulting in faster recombination of CO on the other.

IV-1. Introduction

Molecular structures of myoglobin (Mb) and its CO complex (MbCO) have been determined by X-ray crystallography at a level of 1.5 Å resolution and it has been noted that there is no pathway for the migration of a ligand from solvent to the buried binding site in the heme pocket[1]. It is of fundamental importance in the study of the structure-function relationships of these proteins to elucidate the rapid rearrangements of the globin structure accompanying the ligand entry. While the O_2 complex of Mb (MbO_2) adopts a "closed" structure[2] similar to MbCO, the X-ray studies of ethylisocyanide complex ($MbCNC_2H_5$) revealed the opening of a pathway for ligand entry[3], presumably due to steric repulsion between the bulky ethyl group and distal residues, and accordingly its structure has been regarded as a model of an "open" form. Champion and co-workers[4] have investigated the pH dependent change of the "open"/"closed" equilibrium, but there has been no direct time-resolved measurement for the protein structural change upon ligand entry.

Photodissociation of CO from Mb and hemoglobin (Hb) has been extensively investigated to understand the dynamical features of proteins[5 - 14]. Photodissociation of MbCO followed by relaxation to the stable high spin heme is reported to take place in 350 fs[6]. IR studies on the CO stretching ($\nu_{C\text{-}O}$) mode indicated that 85% of photodissociated CO remains in the globin 1 ns after photolysis and 50% after 50 ns[8b], although there is no return of CO to the heme in the 200 - 8000 ps range[13]. The visible absorption spectrum of the photolysis product of MbCO is reported to be the same as that of the equilibrium deoxyMb for all times greater than 3 ns[14], although the recent transient absorption study[45] revealed that the geminate recombination of photodissociated CO was nonexponential and thus that the distal pocket relaxation might be nonequilibrium. However, the bimolecular process in the 10 ns - 1 ms range is expected to reflect the thermal binding.

In most of these kinetic studies transient absorption spectroscopy was used, which did not allow for a detailed discussion of the molecular structure. In contrast, resonance Raman (RR) spectroscopy, which reveals a vibrational spectrum of the protein chromophore, is capable of providing detailed structural information[15]. The Fe-CO stretching ($\nu_{Fe\text{-}CO}$) frequency of the heme-CO complexes is known to be sensitive to the CO geometry in the heme pocket[16 - 18], and the differences in the $\nu_{Fe\text{-}CO}$ frequency between heme proteins and model heme-CO complexes are ascribed to tilting or bending of the Fe-C-O linkage in the protein[16]. The $\nu_{Fe\text{-}CO}$ frequencies are known to have linear inverse correlation with the $\nu_{C\text{-}O}$ frequencies[16, 17, 19]. From ab initio MO calculations, Augspurger et al.[20] have also demonstrated that the $\nu_{C\text{-}O}$ frequency is correlated with ^{13}C NMR shift of the ^{13}CO ligand and affected by the electric field at the CO ligand, which for MbCO is generated by the surrounding amino acid residues and would cause an electronic polarization of the C-O bond. Whatever the origin, the $\nu_{Fe\text{-}CO}$ frequency is expected to reflect the protein structure around the CO ligand.

On the other hand, a role of the highly conserved distal histidine (E7-His or His-64), which forms a hydrogen bond to bound O_2 to stabilize the oxy form[21 - 23], and is deduced to destabilize the CO form through steric hindrance[24], has been a matter of physico-chemical concern. Recent kinetic studies suggested that CO entered into the binding site through a channel between the E7-His and distal valine (Val-68)[10], and therefore the orientation of the side chain of E7-His, whose mobility depends on the position of the Arg-45 side chain, would determine the opening/closing of the gate for the ligand entry[1] as well as the equilibrium CO-heme geometry[24]. In fact, the $\nu_{Fe\text{-}CO}$ frequency was reported to be altered by replacement of distal His for sperm whale Mb[4a] and human Hb[25]. The X-ray study demonstrated the positional uncertainty only for Arg-45 of sperm whale MbCO;

two positions with 50% occupancy. The abnormal subunit of M-type Hbs, in which E7-His is replaced by Tyr, gave the $\nu_{Fe\text{-}CO}$ RR band at a distinctly lower frequency (490 cm^{-1}) and the heme-CO was apparently not photodissociated by the weak laser illumination known to dissociate the normal subunit[18].

The $\nu_{Fe\text{-}CO}$ RR band of acidified sperm whale MbCO was also found at a lower frequency (488 - 489 cm^{-1})[26, 27] than that of neutral MbCO (507 cm^{-1}), and the low frequency shift was ascribed to a structural change of the CO-heme to an upright geometry following the swinging out of the His-64 side chain from the heme pocket upon its protonation and thus removing the steric hindrance to CO[26, 27]. This conformational change of His-64 results in the opening of a pathway for ligand entry and accordingly, the two $\nu_{Fe\text{-}CO}$ frequencies of the neutral (507 cm^{-1}) and acidic MbCO (~488 cm^{-1}) were considered to represent the "closed" and "open" forms of the heme pocket[4].

If CO binds to the heme in the so-called "open" form and relaxes to the "closed" form at neutral pH and this relaxation is relatively slow as seen for MbCO crystal and frozen solutions[46], the $\nu_{Fe\text{-}CO}$ RR band is expected to exhibit a temporal shift from 488 to 507 cm^{-1} during the recombination process of the photodissociated CO. In fact for acidified horse MbCO, two $\nu_{Fe\text{-}CO}$ RR bands were resolved for transient species and their recovery rates appeared distinctly different (see Chapter II). In some mutant MbCOs the corresponding two structures may be in an equilibrium at neutral pH, and if the interconversion between the two structures is sufficiently fast in contrast with the acidified horse MbCO, the two bands are expected to grow simultaneously with the intensity ratio of the equilibrium state. When a mutant has predominantly an upright geometry corresponding to the "open" form, the structural relaxation would be unnecessary and consequently recombination of CO would be fast.

To examine the "open"/"closed" model from these points of view, time-resolved resonance Raman (TR^3) experiments were carried out for recombinant human MbCO and several E7 mutants, in which distal His was replaced by Gly (H64G), Gln (H64Q), Ala (H64A), Ile (H64I), Val (H64V), and Leu (H64L) through site-directed mutagenesis. Our results indicate that the mutants with ν_{Fe-CO} around 490 cm^{-1} generally recover faster than those with ν_{Fe-CO} around 507 cm^{-1}. Although this is apparently consistent with the assignments of the ~490 and ~507 cm^{-1} bands to the "open" and "closed" forms, respectively, the ν_{Fe-CO} frequency becomes lower as the E64 residue becomes more hydrophobic, having no relation with its physical size. We also note that for the mutants with ν_{Fe-CO} around 507 cm^{-1}, the ~490 cm^{-1} band does not appear before the appearance of the ~507 cm^{-1} band that the transient state around 500 ns after photolysis under 1 atm. of CO is not always the same as the equilibrium state whether of the ~490 or ~507 cm^{-1} type. These results are in agreement with those from our previous TR^3 studies on neutral and acidified horse MbCO (see Chapter II).

IV-2. Experimental Procedures

The human Mb expression system[28] was a kind gift from Dr. S. G. Boxer of Stanford University. The introduction of fusion proteins in AR68, and purification of Mb were carried out as reported by Varadarajan et al[29]. and Ikeda-Saito et al.[30] The reference protein used here, H64H, was originally designated as C110A[29], in which Cys 110 was replaced by Ala for ease of purification. The spectroscopic and functional properties of this mutants were indistinguishable from those of the wild type Mb[2], and therefore C110A was designated as the wild-type (H64H).

The expression and purification of then mutant Mbs were carried out by Prof. Ikeda-Saito and co-workers in Case Western Reserve University, and these

sample were stored by ammonium sulfate precipitation. Just before the measurements, the stored samples were dialyzed against tris-HCl buffer at pH 8.0 for an overnight. The concentrations of MbCO were determined with the extinction coefficients of α- and β-bands for horse normal Mb ($\epsilon_{mM}(\alpha) = 13.9, \epsilon_{mM}(\beta) = 15.4$)[47]. The experimental apparatus and procedures were as same as those in Chapter II.

The integrated intensity of a Raman band was obtained with either of two methods after assuming a linear base line between both ends of integration. An example of the baseline is drawn by a broken line in the spectrum of H64H (Figure IV-2). One method for evaluation of band intensity is a computer summation of the areas of individual channels within the band. In this case the spike noise may affect the results. The second method is to weigh the cut papers of the smoothed spectra. In the latter case the intensity was determined to be an average of 10 cut papers. The two methods yielded qualitatively the same results. Band fitting calculations were carried out with Lorentzian functions by using the damped least squares method[31, 32] as same as in Chapter III.

IV-3. Results and Discussions

Static Spectra The RR spectra of the mutant MbCOs in the 1200 - 1700 cm^{-1} region were similar to those of wild type MbCO (see Figure IV-1). Morikis et al.[33] also reported that Raman spectra in the high frequency region (1300 - 1700 cm^{-1}) of the met-type native Mb, H64G and H64V were alike and all have high spin heme iron and bound water molecule at the sixth coordination position. Figure IV-2 shows the stationary state RR spectra in the $\nu_{Fe\text{-}CO}$ region of the seven MbCO species observed without the pump beam. These spectra are in agreement with those observed with a high-speed (1800 rpm) spinning cell and CW Kr^+ laser

excitation at 406.7 nm. Although there may be an appreciable amount of photo-dissociated species present, Figure IV-2 demonstrates that the remaining CO-bound form can be monitored by pulse excitation when the laser power is greatly reduced.

The maximum intensity of the $\nu_{Fe\text{-}CO}$ band is seen at 510 - 505 cm^{-1} for H64H, H64G and H64Q, whereas at 495 - 490 cm^{-1} for H64V, H64I, H64A and H64L, while the porphyrin ν_7 mode (the mode number is based on ref. 34) remains unshifted at 675 $\pm$1 cm^{-1} (only H64G gives it at 677 cm^{-1}) by E7-mutation. The assignments of the $\nu_{Fe\text{-}CO}$ band was confirmed by the observation of isotopic frequency shifts for $^{13}C^{16}O$ (-4 cm^{-1} for H64Q and -4.5 cm^{-1} for H64L). The Fe-C-O bending band was too weak to be identified for all samples. H64H and H64L seem to yield a single $\nu_{Fe\text{-}CO}$ band but others give unresolved multiple bands. Judging from the main $\nu_{Fe\text{-}CO}$ frequencies, H64H (510 cm^{-1}), H64G (505 cm^{-1}), and H64Q (508 cm^{-1}) are of normal type but H64V (493 cm^{-1}), H64I (492 cm^{-1}), H64A (495 cm^{-1}), and H64L (490 cm^{-1}) are of acidified MbCO type[4, 26, 27] or distal-His mutant Hb M CO type[18]. It is apparent that the $\nu_{Fe\text{-}CO}$ frequencies cannot be classified solely on bulkiness of the E7 residue as first pointed out by Nagai et al.[35]

Time-resolved RR Spectra of H64H, H64G and H64Q The TR^3 spectra for H64H and H64G are displayed in Figures IV-3 and IV-4, respectively. The ordinate scales of each spectra (A) - (F) in each Figure are common. Since the instrumental conditions including the laser power, the exposure time of the diode-array detector and the accumulation time, are the same for all measurements expect for variation of Δt_d, the intensity of Raman bands delineated in the Figures reflect practical populations of MbCO present at each Δt_d, although we failed to incorporated an internal intensity standard (sodium cacodylate as an intensity standard photoreacted with dithionite during the measurements). The spectra for Δt_d = -20

ns, and which correspond to the pump/probe spectra for a delay time, Δt_d = 2.4 sec, equal to the period for one turn of the spinning cell, are in agreement with the spectra observed without the pump beam (Figure IV-2). This indicates that recombination of CO to photodissociated species is completed in one turn of the spinning cell. Disappearance of the $\nu_{Fe\text{-}CO}$ band for Δt_d = 0 ns means that photodissociation is achieved by the pump beam. Since the excitation wavelength (416 nm) is closer to the Soret maximum of MbCO (424 nm) than to that of deoxyMb (435 nm), the RR spectrum of the CO-bound form is expected to be more enhanced than that of deoxyMb.

The $\nu_{Fe\text{-}CO}$ band of H64H at 510 cm^{-1} starts to increase in intensity from 100 μs, but it has still not fully recovered at Δt_d = 1 ms. The band shapes at 500 μs and 1 ms are similar and it is hard to assume the presence of a transient band around 490 cm^{-1} in the spectra for Δt_d = 10 - 500 μs. For H64G the $\nu_{Fe\text{-}CO}$ band is discernible in an earlier time range (Δt_d = 1 - 100 μs), despite the fact that the equilibrium $\nu_{Fe\text{-}CO}$ frequency is higher than 500 cm^{-1}. The center of the transient band is shifted slightly to a lower frequency and its band width is broader. If the 490 cm^{-1} species were present and the conversion from the "open" to "closed" form is slow, the 490 cm^{-1} band should have been separately observed in the present spectral resolution as was confirmed for acidified horse MbCO (see Chapter II). This means that a species present at Δt_d = 1 - 100 μs is different from the 490 cm^{-1} species. The band center returns to the original position at Δt_d = 1 ms.

A similar but more conspicuous feature was observed for H64Q as shown in Figure IV-5. The TR^3 spectra for Δt_d = 1 μs (C) and 100 μs (D) give rise to a weak and broad band at 497 and 501 cm^{-1}, respectively, but their frequencies are not as low as the 490 cm^{-1} as expected for the "open" form. The transient band with heterogeneous broadening returns gradually to the original position (508 cm^{-1}) as

the recombination proceeds, suggesting the presence of an intermediate species distinct from either the equilibrium ~510 or ~490 cm^{-1} species.

Time-resolved RR spectra of H64L, H64V, H64A and H64I The TR^3 spectra of H64L are presented in Figure IV-6. The $\nu_{Fe\text{-}CO}$ band is completely absent for Δt_d = 0 - 20 ns but is definitely present for Δt_d = 100 ns. The original spectrum is almost restored at Δt_d = 100 μs and the band center does not exhibit any shift during the recombination. Figure IV-7 shows the TR^3 spectra of H64V. Two $\nu_{Fe\text{-}CO}$ bands are present in the spectrum for Δt_d = -20 ns and both bands disappear in the spectrum for Δt_d = 0 ns. If CO binds to the "open" form and is rapidly ($< 10^{-5}$ s) converted to the "closed" form, the TR^3 spectrum for Δt_d = 100 μs is expected to exhibit two bands at 509 and 492 cm^{-1} with the same relative intensity as that for Δt_d = -20 ns. In practice, a single broad band appeared between the two bands (500 cm^{-1}) for Δt_d = 100 ns and the band center gradually shifted to lower frequencies as Δt_d became longer. The two bands were not resolved in the spectra for Δt_d = 100 μs as will be discussed later, but the original pattern was nearly restored for Δt_d = 1ms.

The TR^3 spectra of H64A and H64I are shown in Figures IV-8 and IV-9, respectively. In the static spectra of these mutants (Δt_d = -20 ns) the presence of a side band at 510 cm^{-1} besides the main band at 492 - 496 cm^{-1} is prominent. Both bands disappeared in the spectra for Δt_d = 0 - 20 ns. For H64A the low frequency component is recognizable in the spectrum for Δt_d = 1 μs. The high frequency component is discernible in the spectra for Δt_d > 100 μs. The relative intensity of the two bands appears to be restored after Δt_d = 500 μs. The corresponding two bands for H64I are not resolved in the spectrum for Δt_d = 10 μs, giving the appearance of a broad symmetric band at 495 cm^{-1}, i.e. between the two static frequencies.

In order to investigate the temporal behavior of these $\nu_{Fe\text{-}CO}$ bands in more detail, the observed bands of H64V, H64I, and H64A were fitted with two Lorentzian functions. Figure IV-10 illustrates the observed and calculated spectra of H64V, H64I, and H64A for Δt_d = -20 ns (A), 100 μs (B) and 1 ms (C). Since the S/N ratios of the observed spectra are not high enough, the deduced component spectra may contain significant errors. However, the peak frequencies of the component bands for the Δt_d = -20 ns spectra are in agreement with those for the Δt_d = 1 ms spectra for each of the species H64I and H64A. It is noted from this calculation that the spectra of H64V and H64I at Δt_d = 100 μs were reproduced with a single Lorentzian function but could not be uniquely fitted by assuming the presence of two bands. It is only after 100 μs that the high frequency component becomes recognizable. For H64A the spectrum for Δt_d = 100 μs was fitted with two bands, but is dominated by a band at 496 cm^{-1}.

Analysis of Data A kinetic description of ligand binding to Mb has been proposed out by Gibson et al.[36] The most practical model is to assume two intermediate states between MbCO and Mb + CO, that is,

$$\text{MbCO} \Leftrightarrow \text{contact pair} \Leftrightarrow \text{protein separated pair} \Leftrightarrow \text{deoxyMb} + \text{CO} \quad \text{(IV-1)}$$

In earlier days, the bimolecular rebinding of photodissociated CO to deoxyMb has been treated using a single exponential function[14], but the present results could not be reproduced with such a model despite of no inhomogeneity present in the sample as described in Experimental Procedures. This was also true with horse MbCO at pH 8.0 (see Chapter II). Therefore, it was assumed that the recovery of MbCO followed a biexponential growth, that is

$$[\text{MbCO}] = A_1\{1\text{-}\exp(-k_1 t)\} + A_2\{1\text{-}\exp(-k_2 t)\} \quad \text{(IV-2)}$$

The phenomenological parameters can be related to the rate constants of the individual elementary processes of Eq. (IV-1) under specified conditions[36]. The

recombination from the contact pair is called the geminate process and reflects the rate of bond formation, which has been determined as 10^9 s^{-1}.[13] Recently the geminate recombination is represented by a stretched exponential or biexponential functions[45]. Since the flash photolysis experiments by Eaton and co-workers[14] indicated that the geminate rebinding occurs with a relaxation time of 180 ns and its contribution over the first 180 ns is less than 4% of the total for MbCO, it does not contribute significantly to the spectra observed in this study. Here for convenience sake, we describe that the k_1 and k_2 processes as the fast and slow phases, respectively, which are approximately composed of the recombination of a protein separated pair, and the bimolecular reaction, respectively.

The integrated intensities of the $\nu_{Fe\text{-}CO}$ bands have been determined for all spectra. When a given band consisted of two components, their sum was taken as the integrated intensity. Relative values with regard to the intensity at Δt_d = -20 ns for each species are plotted against the delay time in Figures IV-11 and IV-12. The broken lines represent the values calculated with Eq. (IV-2) and the parameters listed in Table IV-1. Note that these rate constants correspond to the values for a CO pressure of 1 atm.

Figure IV-11 contains the plots for H64H, H64G and H64Q. All of them have the equilibrium $\nu_{Fe\text{-}CO}$ band in the frequency region of the "closed" form, but their recovery behaviors differ. H64H and H64G have similar fast phases whose rate constants are 2×10^4 s^{-1} which dominant over the first 30% of the recovery, but their slow phases are different; a larger k_2 for H64G leads to a faster recovery at 1 ms. H64Q exhibit a 5 times faster rate of recovery than H64H for the fast phase, while their slow phases are alike.

Figure IV-12 plots the results of H64L, H64V, H64I and H64A. H64I and H64A (Figure IV-12A) involve a dominant fast phase over the first 20% of recov-

ery whose rate constants are ~10 times larger than that of H64H. H64I is different from H64A with regard to the slow phase. In contrast, H64L and H64V (Figure IV-12B) have much larger contributions from the fast phase whose rate constants are 100 - 200 times larger than that of H64H, while the rate of the slow phase of H64V is similar to those of H64A and H64G. The faster rebinding of CO in H64L compared with that in H64H is qualitatively (but not quantitatively) in agreement with the results of Carver et al[11]. who reported that for sperm whale MbCO the kinetic parameters for rebinding from the protein separated pair is 20 times faster for H64L than for H64H, and the rate of entry to the protein is also 6 times faster (k_1 and k_2 of H64L are 270 and 40 times larger than those of H64H, respectively).

Controlling Factors of the CO Recombination The present experiments demonstrated that MbCO whose $\nu_{Fe\text{-}CO}$ is 490 - 495 cm^{-1} recovers from photodissociation much faster than those whose $\nu_{Fe\text{-}CO}$ is 505 - 510 cm^{-1}. Therefore, a factor which determines the static $\nu_{Fe\text{-}CO}$ frequency is essential to discuss the kinetics of the CO recombination. To date the species with $\nu_{Fe\text{-}CO}$ at 490 - 495 cm^{-1} and 505 - 510 cm^{-1} have been thought to have the upright and distorted structures, respectively, on the basis of the following observations; the protein-free heme-CO complex with imidazole as a trans ligand, which has an upright geometry[38], gives the $\nu_{Fe\text{-}CO}$ band at 495 cm^{-1} in an organic solution[39], while the CO-heme with an intermediate length of "strap", in which the upright geometry is sterically prohibited, gives the $\nu_{Fe\text{-}CO}$ band at 506 cm^{-1} in organic solution[15a]. The distorted structure in native MbCO is considered to be a consequence of a steric hindrance of His-64(E7)[24]. However, the results shown in Figure IV-2. demonstrate that the steric hindrance from the E7 residue is not the main factor for determination of the $\nu_{Fe\text{-}CO}$ frequency as pointed out by Nagai et al.[35], since a small E7-Gly gives $\nu_{Fe\text{-}CO}$ at 504 cm^{-1} while a bulky E7-Ile gives $\nu_{Fe\text{-}CO}$ at 492 cm^{-1}. As far as the frequencies of the main $\nu_{Fe\text{-}CO}$ bands in

Figure IV-2. are concerned with, polar and nonpolar residues at E7 seem to give rise to $\nu_{Fe\text{-}CO}$ at 505 - 510 cm^{-1} and 490 - 495 cm^{-1}, respectively.

A relation between the $\nu_{Fe\text{-}CO}$ frequency and the Fe-C-O valence angle or tilting of the Fe-C bond has been investigated theoretically[16 - 18] and some models have been proposed. In these treatments a set of potential constants, which can reproduce the observed frequencies of the equilibrium structure, are used to predict the frequencies expected for other geometries. Unfortunately the models are not complementary; one calculation predicts that the $\nu_{Fe\text{-}CO}$ frequency becomes lower as the Fe-C-O bending angle becomes smaller[18] but the other predicts the opposite[17]. This discrepancy arises from the different assignments of the Fe-C-O bending RR band[37]; the observed Fe-C-O bending RR band around 580 cm^{-1} was assumed to be a fundamental in the former[17] but an overtone in the latter[18], and in the former the stretching-bending interaction determines the frequency while in the latter only the kinetic coupling influences the frequency. Another problem in these theoretical treatments is the use of the same force constants for different geometrical structures.

Oldfield and co-workers[20] pointed out that the $\nu_{C\text{-}O}$ frequency is also affected by the electronic polarization of the C-O bond and thus in the protein by the electric field at CO generated by surrounding amino acid residues. Based on this idea, CO would be more polarized when the E7 residue is more polar. Generally, polar residues are more hydrophilic. Accordingly, we adopted a parameter representing the hydrophilic character of the E7 residue, that is the hydropathy index[40]. The static $\nu_{Fe\text{-}CO}$ frequencies shown in Figure IV-2 have been plotted against the hydropathy index[40] of substituted E7 residue as shown in Figure IV-13. A good linear correlation is found, and it is empirically evident that the $\nu_{Fe\text{-}CO}$ frequency becomes lower as the environment around CO becomes more hydrophobic. This

may suggest that the surrounding electric field effect causes some change simply in the CO bond polarization without altering the geometry of heme-CO or structural changes of Lys-45 and nearby residues which influence geometrical structure of the Fe-C-O unit.

When this polarization model is correct, the words, "open"/"closed", might be misleading, since the "closed" form also allows entering of CO into the heme pocket without going by way of the "open" form, although multiple conformations are postulated with the polarization model. Here, one would ask why CO binds faster for more hydrophobic environments. There is no definite answer for it, but it is noted that the solubility of CO is significantly higher for hydrophobic than hydrophilic solvents; 0.029 (0.021) ml/ml for H_2O and 0.170 (0.184) ml/ml for benzen at 10°C (25°C) (see Table IV-2), which indicates stabilization of CO by ΔG = 5.4 kJ/mol in benzen than in water. In other words, the photodissociated CO is more stabilized when the heme pocket is more hydrophobic. This would yield some difference in the potential minimum corresponding to the protein separated pair of Eq.(IV-1) as illustrated in Figure IV-14. The lower free energy for it with the hydrophobic heme pocket would raise the probability that CO is trapped in this potential minimum than escaped into the solvent after photodissociation. Accordingly, it is qualitatively understandable that the more hydrophobic heme pocket results in faster recombination[10, 11] as well as the lower $\nu_{Fe\text{-}CO}$ frequency. In this case, interpretation for the presence of two $\nu_{Fe\text{-}CO}$ bands in a single species is somewhat difficult; we have to assume the presence of two protein conformations which yield different polarization effects on the CO bound to the heme.

According to the X-ray crystallographic analysis on sperm whale MbO_2[2], a hydrogen bond is formed between E7-His and CD3-Arg via a water molecule as illustrated in Figure I-3. (in Chapter I). Kuriyan et al.[1] pointed out that the side

chain of CD3-Arg of sperm whale MbCO stays in two equally populated conformations, and that one of the two structure allows the entry of CO into the binding site, since it does not block the motion of the distal His out of the heme pocket. For human Mb, on the other hand, the CD3 residue is replaced by Lys. The replacement of the CD3 residue (Lys-45) with Arg for human Mb (K45R) has yielded a faster bimolecular recombination rate of CO[41]. Carver et al.[42] also observed that the Lys-45 to Arg-45 mutation caused a 2-fold increase in the CO association rate in pig Mb. Although there is no X-ray analysis for wild type human Mb, the CD3 Lys is deduced to interact with E7-His. Such interactions would be facilitated when the E7 residue is hydrophilic similar to the CD3 residue. As a measure of facileness of their interaction, the relative hydropathy values (χ) of the two residues might serve as a parameter. In this idea, as the difference, $\chi_{E7} - \chi_{CD3}$, becomes larger, the two residues would repel with each other. This corresponds to measure the hydrophobicity of the E7 residue relative to that of the CD3 residue. If this idea is accepted, it is possible to interpret qualitatively the difference in the $\nu_{Fe\text{-}CO}$ frequencies of Gly-64 mutant of human MbCO (510 cm^{-1}, Figure IV-2) and sperm whale MbCO (508 cm^{-1})[4]; the CD3 residue of sperm whale Mb is Arg with χ = -4.5 but that of human Mb is Lys with χ = -3.8 (negative values meaning hydrophilic residues), and $\chi_{E7} - \chi_{CD3}$ is positively shifted with sperm whale Mb and the $\nu_{Fe\text{-}CO}$ frequency is therefore expected to be lower for sperm whale Mb than for human Mb.

Recombination Dynamics The photodissociation of MbCO is characterized by a high quantum yield (nearly unity) in contrast with other cases (0.13 for MbO_2 and much smaller for MbNO)[36]. This implies that the escape from the contact pair valley in Figure 14. is the largest for CO among small ligands. On the other hand, the rate limiting step for binding of CO is reported to be the bond formation step

in contrast with that of O_2 for which the rate limiting step is the ligand entry[36, 43].

The present results suggest the CO binding to Mb takes place in two phases but their rate constants cannot be systematically grouped into two. In the case of H64H, the reference species, the $\nu_{Fe\text{-}CO}$ band exhibited no frequency shift, and throughout the recombination process a transient band was not discernible around 490 cm^{-1}. For H64G a transient band was recognizable around 100 μs. Since the interaction time between a molecule and a photon is sufficiently short, two bands corresponding to the "open" and "closed" forms should appear without exhibiting a frequency shift when there is interconversion between the two forms, which occurs presumably in the order of 100 μs. This transient band is significantly broader but its band center is not greatly different from the equilibrium one. Thus it suggests the presence of slight structural disorder of distal residues (or an appreciable distribution of the heme-CO bent angles) in the bond formation process. If the structure with $\nu_{Fe\text{-}CO}$ at ~490 cm^{-1} is a precursor of the "closed" form, the corresponding band should have appeared in the spectra of H64H, H64G, and H64Q for Δt_d = 100 ns - 10 μs. Its absence strongly suggests that CO entry goes by way of a protein rearrangement which is distinct from an "open" structure intermediate, i.e. the swinging out of the His-64 side chain.

H64I and H64A have similar rate constants for the fast phase, although its dominance only spans the first 20% of the recovery for these Mb. Both have two $\nu_{Fe\text{-}CO}$ bands in the equilibrium state, but the frequency of the transient band around 1 - 100 μs is nearly equal to that of the low frequency counterpart. The high frequency counterpart contributes only after 100 μs. The relative intensity of the high and low frequency components is little altered between 500 - 1000 μs. Accordingly it is likely that there are two protein conformations corresponding to $\nu_{Fe\text{-}CO}$ = 492 - 496 cm^{-1} and $\nu_{Fe\text{-}CO}$ = 508 - 512 cm^{-1}, of which the former binds CO

significantly faster than the latter, and that the two conformations are not interconverted within 100 μs.

H64L and H64V have a noticeably large rate constant for the fast phase and its amplitude is large. H64L always exhibit the $\nu_{Fe\text{-}CO}$ band at the equilibrium position (491 cm^{-1}), although the bandwidth is somewhat broader for Δt_d = 100 - 1000 ns. H64V consists of two bands (509 and 492 cm^{-1}), but the earlier transient species gives a broad feature at the frequency between the two bands, and afterwards its band center approaches the frequency of the low frequency component. It is likely that the fast component corresponds to the recombination from the minimum of the protein separated pair, which is deeper for the hydrophobic E7 residues than for hydrophilic E7 residues, and that the frequency shift reflects slight structural relaxation of the distal residues.

H64I and H64A have similar rate constants for the fast phase, although its dominance only spans the first 20% of the recovery for these Mbs. Both have two $\nu_{Fe\text{-}CO}$ bands in the equilibrium state, but the frequency of the transient band around 1 - 100 μs is nearly equal to that of the low frequency counterpart. The high frequency counterpart contributes only after 100 μs. If the interconversion between the "open" and "closed" forms is sufficiently fast, the equilibrium intensity ratio of the high and low frequency components should be attained earlier, but it was attained at 500 - 1000 μs.

In conclusion, we found that MbCO with $\nu_{Fe\text{-}CO}$ around ~510 cm^{-1} is not generated via a ~490 cm^{-1} ("open") precursor. It is evident that there are two protein conformations corresponding to $\nu_{Fe\text{-}CO}$ = 492 - 496 cm^{-1} and $\nu_{Fe\text{-}CO}$ = 508 - 512 cm^{-1}, of which the former binds CO significantly faster than the latter, and that the two conformations are not interconverted within 100 μs. Since the $\nu_{Fe\text{-}CO}$ frequencies seem to depend on the hydrophobicity of the E7 residue and the

photodissociated CO is stabilized more in the hydrophobic than hydrophilic environments, it is likely that the hydrophobicity of the heme pocket and a conformation of a few distal residues are significant for the determination of the CO recombination rate.

References

(1) J. Kuriyan, S. Wilz, M. Karplus, G. A. Petsko, J. Mol. Biol., **192**, 133 (1986).

(2) S. E. V. Phillips, J. Mol. Biol., **142**, 531 (1980).

(3) K. A. Johnson, J. S. Olson, G. N. Phillips Jr., J. Mol. Biol., **207**, 459 (1989).

(4) (a) D. Morikis, P. M. Champion, B. A. Springer, S. G. Sligar, Biochemistry, **28**, 4791 (1989).
(b) J. T. Sage, D. Morikis, P. M. Champion, Biochemistry, **30**, 1227 (1991).

(5) J. Hofrichter, J. H. Sommer, E. R. Henry, W. A. Eaton, Proc. Natl. Acad. Sci. U.S.A., **80**, 2235 (1983).

(6) J. L. Martin, A. Migus, C. Poyart, Y. Lecarpentier, R. Astier, A. Antonetti, Proc. Natl. Acad. Sci. U.S.A., **80**, 173 (1983).

(7) D. Braunstein, A. Ansari, J. Berendzen, B. R. Cowen, K. D. Egeberg, H. Frauenfelder, M. K. Hong, P. Ormos, T. B. Sauke, R. Scholl, A. Schulte, S. G. Sligar, B. A. Springer, P. J. Steinbach, R. D. Young, Proc. Natl. Acad. Sci. U.S.A., **85**, 8497 (1988).

(8) (a) J. N. Moore, P. A. Hansen, R. M. Hochstrasser, Proc. Natl. Acad. Sci. U.S.A., **85**, 5062 (1988).
(b) P. A. Anfinrud, C. Han, R. M. Hochstrasser, Proc. Natl. Acad. Sci. U.S.A., **86**, 8387 (1989).

(9) J. W. Patrich, C. Poyart, J. L. Martin, Biochemistry, **27**, 4049 (1988).

(10) R. J. Rohlfs, A. J. Mathews, T. E. Carver, J. S. Olson, B. A. Springer, K. D. Egeberg, S. G. Sligar, J. Biol. Chem., **265**, 3168 (1990).

(11) T. E. Carver, R. J. Rohlfs, J. S. Olson, Q. H. Gibson, R. S. Blackmore, B. A. Springer, S. G. Sligar, J. Biol. Chem., **265**, 20007 (1990).

(12) V. Srajer, L. Reinisch, P. M. Champion, Biochemistry, **30**, 4886 (1991).

(13) T. G. Traylor, D. Magde, D. J. Taube, K. A. Jongeward, D. Bandyopadhyay, J. Luo, K. N. Walda, J. Am. Chem. Soc., **114**, 417 (1992).

(14) E. R. Henry, J. H. Sommer, J. Hofrichter, W. A. Eaton, J. Mol. Biol., **166**, 443 (1983).

(15) (a) T. G. Spiro ed., *Biological Applications of Raman Spectroscopy*, Vol. 3, (John Wiley, Canada) (1989).
(b) T. Kitagawa, in *Spectroscopy of Biological Systems*, (R. J. H. Clark, R. E. Hester, eds.), (Wiley & Sons), pp. 443 - 481 (1986).

(16) (a) N.-T. Yu, E. A. Kerr, B. Ward, C. K. Chang, Biochemistry, **22**, 4534 (1983).

(b) N.-T. Yu, E. A. Kerr, in *Biological Applications of Raman Spectroscopy* (T. G. Spiro ed.), Vol. 3, pp. 40 - 95, (Wiley-Interscience, New York) (1988).

(17) X-Y. Li, T. G. Spiro, J. Am. Chem. Soc., **110**, 6024 (1988).

(18) M. Nagai, Y. Yoneyama, T. Kitagawa, Biochemistry, **30**, 6495 (1991).

(19) M. Tsubaki, R. B. Srivastava, N.-T. Yu., Biochemistry, **21**, 1132 (1982).

(20) J. D. Augspurger, C. E. Dykstra, E. Oldfield, J. Am. Chem. Soc., **113**, 2447 (1991).

(21) T. Yonetani, H. Yamamoto, T. Iizuka, J. Biol. Chem., **249**, 2168 (1974).

(22) S. E. V. Phillips, B. P. Shoenborn, Nature, **292**, 81 (1981).

(23) T. Kitagawa, M. R. Ondrias, D. L. Rousseau, M. Ikeda-Saito, T. Yonetani, Nature, **298**, 869 (1982).

(24) J. P. Collman, J. I. Brauman, B. L. Iverson, J. L. Sessler, R. M. Morris, Q. H. Gibson, J. Am. Chem. Soc., **105**, 3052 (1983).

(25) S.-H. Lin, N.-T. Yu, J. Tame, D. Shih, J.-P. Renaud, J. Pagnier, K. Nagai, Biochemistry, **29**, 5562 (1990).

(26) J. Ramsden, T. G. Spiro, Biochemistry, **28**, 3125 (1989).

(27) S. Han, D. L. Rousseau, G. Giacometti, M. Brunori, Proc. Natl. Acad. Sci. U.S.A., **87**, 205 (1990).

(28) R. Varadarajan, A. Szabo, S. G. Boxer, Proc. Natl. Acad. Sci. U.S.A., **82**, 5681 (1985).

(29) R. Varadarajan, D. G. Lambright, S. G. Boxer, Biochemistry, **28**, 3771 (1989).

(30) M. Ikeda-Saito, R. S. Lutz, D. A. Shelley, E. J. McKelvey, R. Mattera, H. Hori, J. Biol. Chem., in press (1992).

(31) K. Levenberg, Q. Appl. Math., **2**, 164 (1944).

(32) Y. Senga, S. Minami, Bunko Kenkyu, **33**, 142 (1986).

(33) D. Morikis, P. M. Champion, B. A. Springer, K. D. Egeberg, S. G. Sligar, J. Biol. Chem., **265**, 12143 (1990).

(34) M. Abe, T. Kitagawa, Y. Kyogoku, J. Chem. Phys., **69**, 4526 (1978).

(35) K. Nagai, B. Luisi, D. Shih, G. Miyazaki, K. Imai, C. Poyart, C. DeYoung, L. Kwiatkowsky, R. W. Noble, S.-H. Lin, N.-T. Yu, Nature, **329**, 858 (1987).

(36) Q. H. Gibson, J. S. Olson, R. E. McKinnie, R. J. Rohlfs, J. Biol. Chem., **261**, 10228 (1986).

(37) M. Tsuboi, Indian. J. Pure Appl. Phys., **26**, 188 (1988).

(38) S.-M. Peng, J. A. Ibers, J. Am. Chem. Soc., **98**, 8032 (1976).
(39) R. Evangelista-Kirkup, G. Smulevich, T. G. Spiro, Biochemistry, **25**, 4420 (1986).
(40) J. Kyte, R. F. Doolittle, J. Mol. Biol., **157**, 105 (1982).
(41) D. G. Lambright, S. Balasubramanian, S. G. Boxer, J. Mol. Biol., **207**, 289 (1989).
(42) T. E. Carver, J. S. Olson, S. J. Smerdon, S. Krzywda, A. J. Wilkinson, Q. H. Gibson, R. S. Blackmore, J. D. Ropp, S. G. Sligar, Biochemistry, **30**, 4697 (1991).
(43) S. Adachi, I. Morishima, J. Biol. Chem., **264**, 18896 (1989).
(44)
(45) W. D. Tian, J. T. Sage, V. Srajer, P. M. Champion, Phys. Rev. Lett., **68**, 408 (1992).
(46) L. Zhu, J. T. Sage, A. A. Rigos, D. Morikis, P. M. Champion, J. Mol. Biol., **224**, 207 (1992).
(47) E. Antonini, Physiol. Rev., 45, 123 (1965).

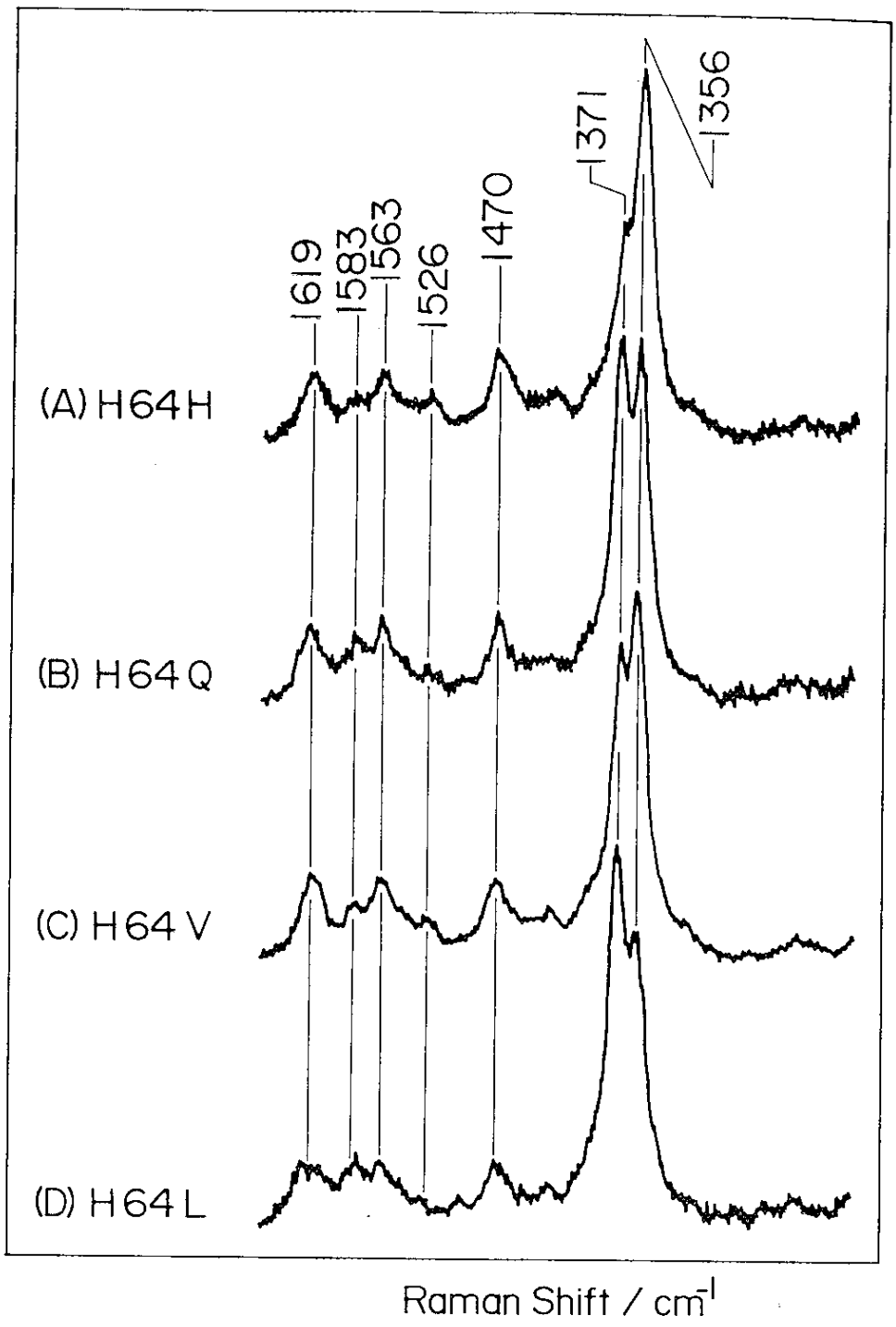

Figure IV-1.

Comparison with the RR spectra of four CO adducted Mbs in the higher frequency (1200 - 1700 cm^{-1}) region. These spectra were obtained by only probe pulse (416.0 nm). The two intense bands at 1356 and 1371 cm^{-1} are assigned to the ν_4 bands of photodissociated species (deoxyMb) and MbCO, respectively.

(A): H64H, (B): H64Q, (C): H64V, (D): H64L

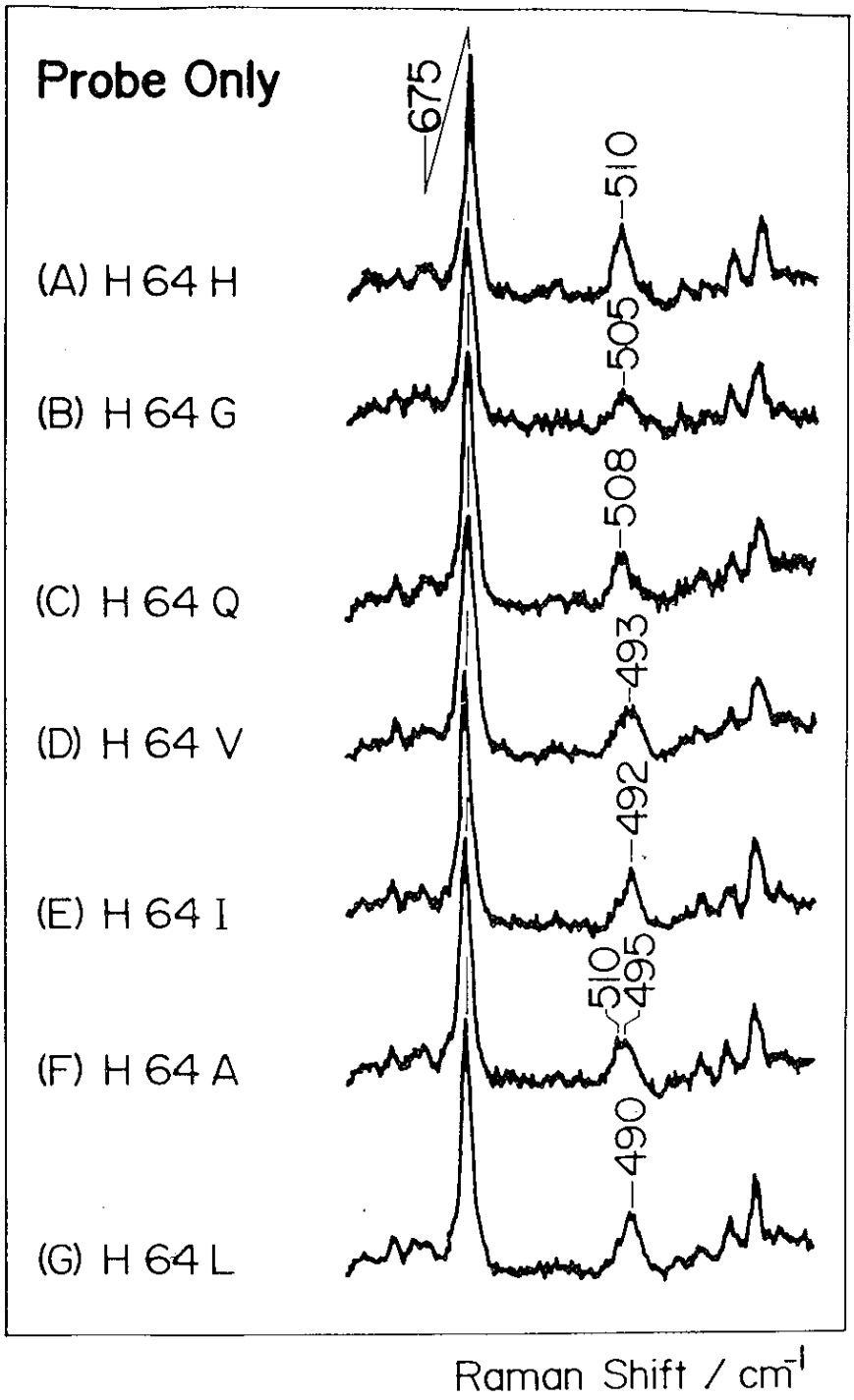

Figure IV-2.

The probe only resonance Raman spectra in the $\nu_{Fe\text{-}CO}$ region of the wild type (H64H) and its E7-Gly (H64G), E7-Gln (H64Q), E7-Val (H64V), E7-Ile (H64I), E7-Ala (H64A), and E7-Leu (H64L) mutants of human MbCO.

Probe beam: 416.0 nm

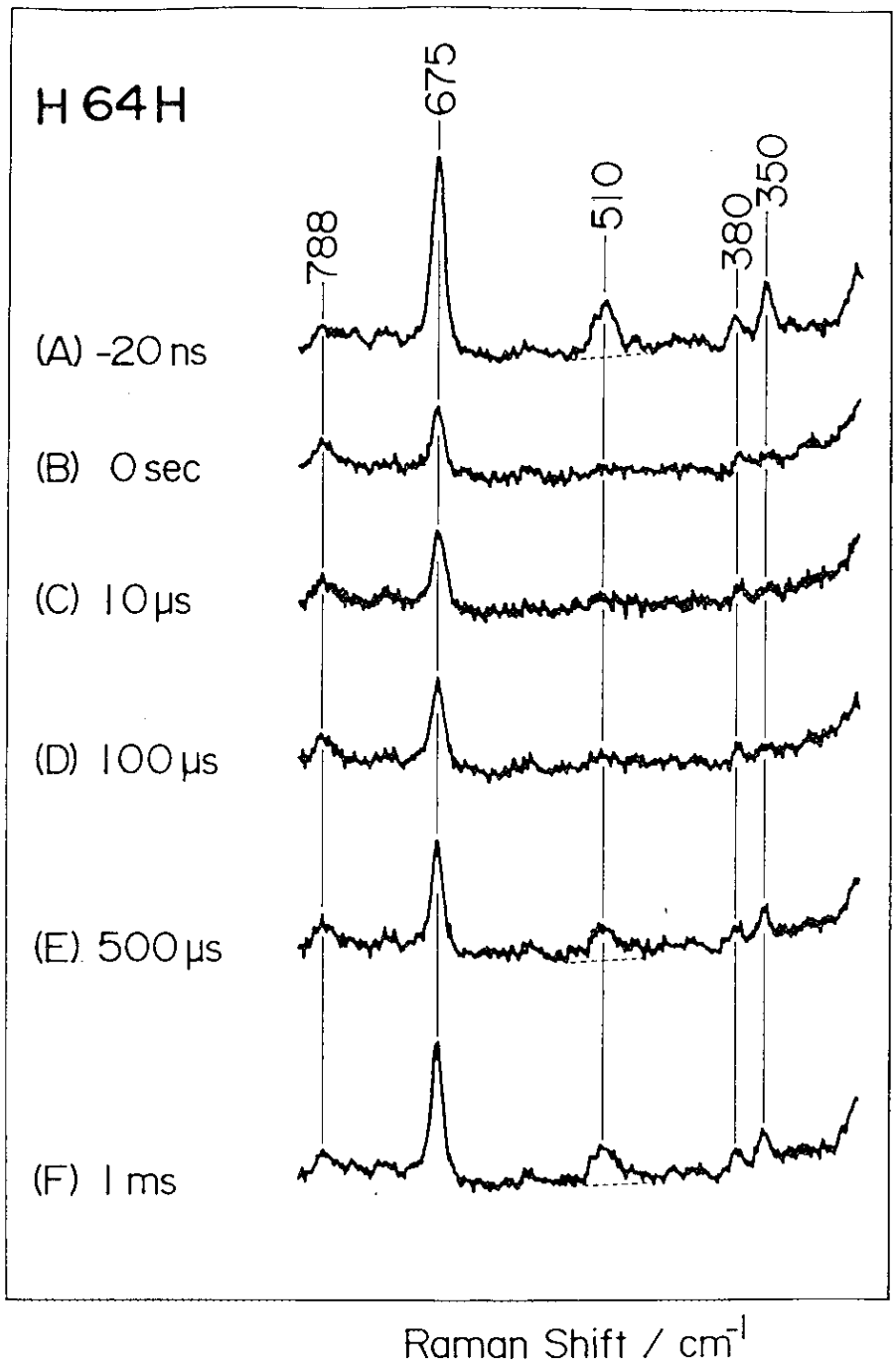

Figure IV-3.

The pump/probe time-resolved resonance Raman spectra in the $\nu_{Fe\text{-}CO}$ region of the wild type (H64H) human MbCO. The delay time (Δt_d) of the probe beam from the pump beam is specified at the left side of each spectrum. Broken lines indicate the assumed base lines to estimate the integrate intensities of $\nu_{Fe\text{-}CO}$.
Pump beam: 532.0 nm, Probe beam: 416.0 nm

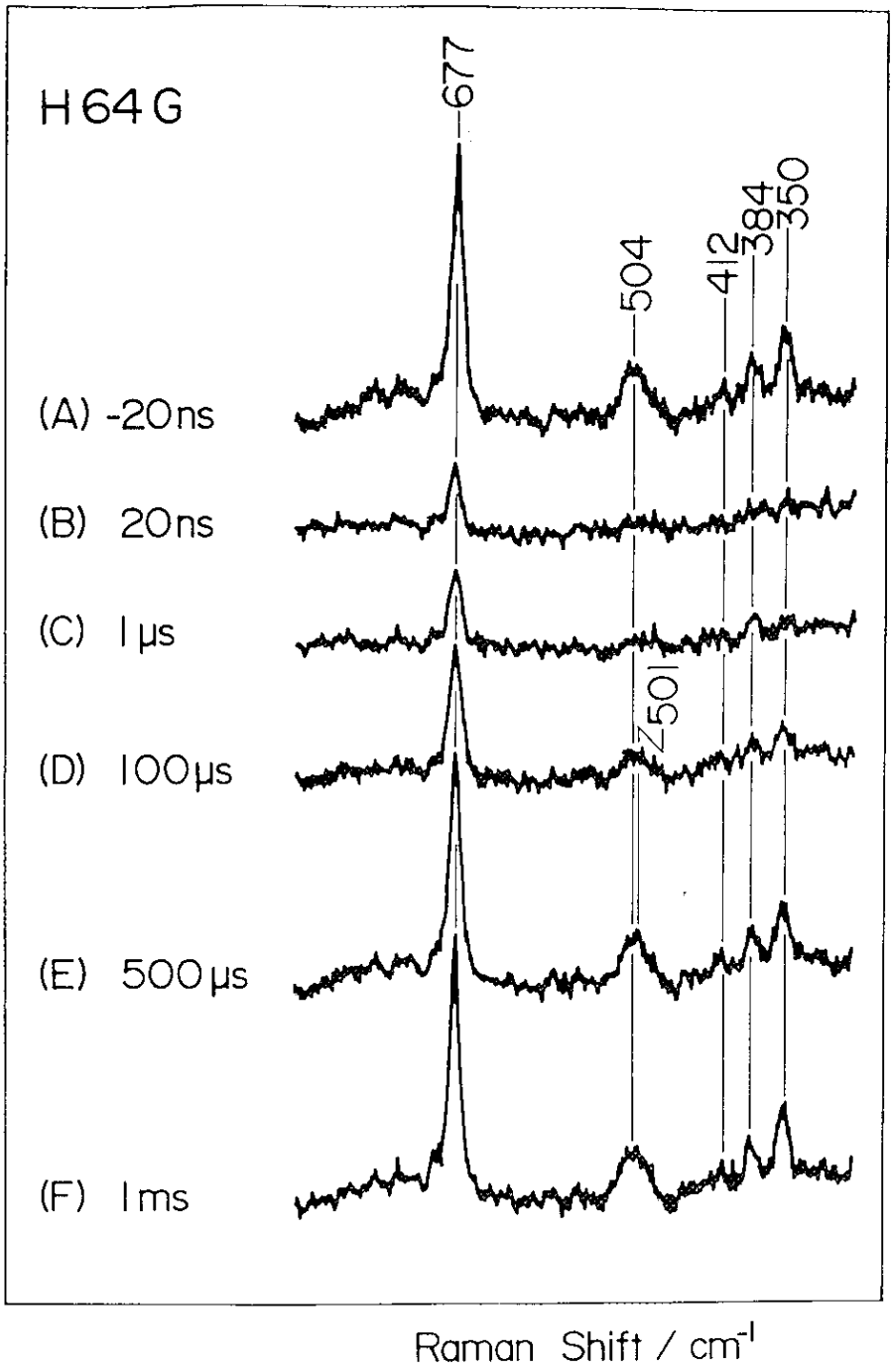

Figure IV-4.

The pump/probe time-resolved resonance Raman spectra of E7-Gly (H64G) mutant MbCO. The delay time (Δt_d) of the probe beam from the pump beam is specified at the left side of each spectrum.

Pump beam: 532.0 nm, Probe beam: 416.0 nm

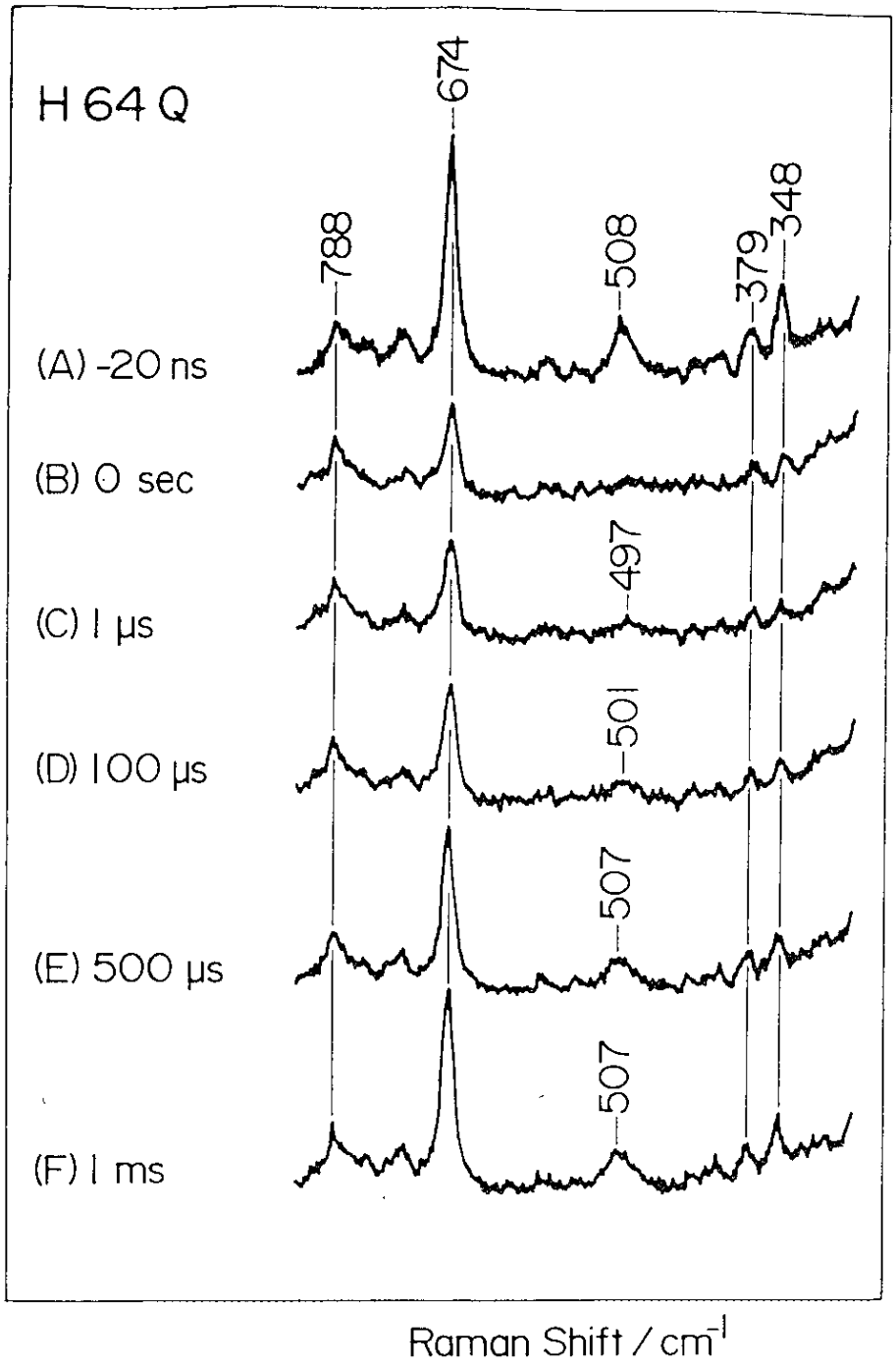

Figure IV-5.

The pump/probe time-resolved resonance Raman spectra of E7-Gln (H64Q) mutant MbCO. The delay time (Δt_d) of the probe beam from the pump beam is specified at the left side of each spectrum.

Pump beam: 532.0 nm, Probe beam: 416.0 nm

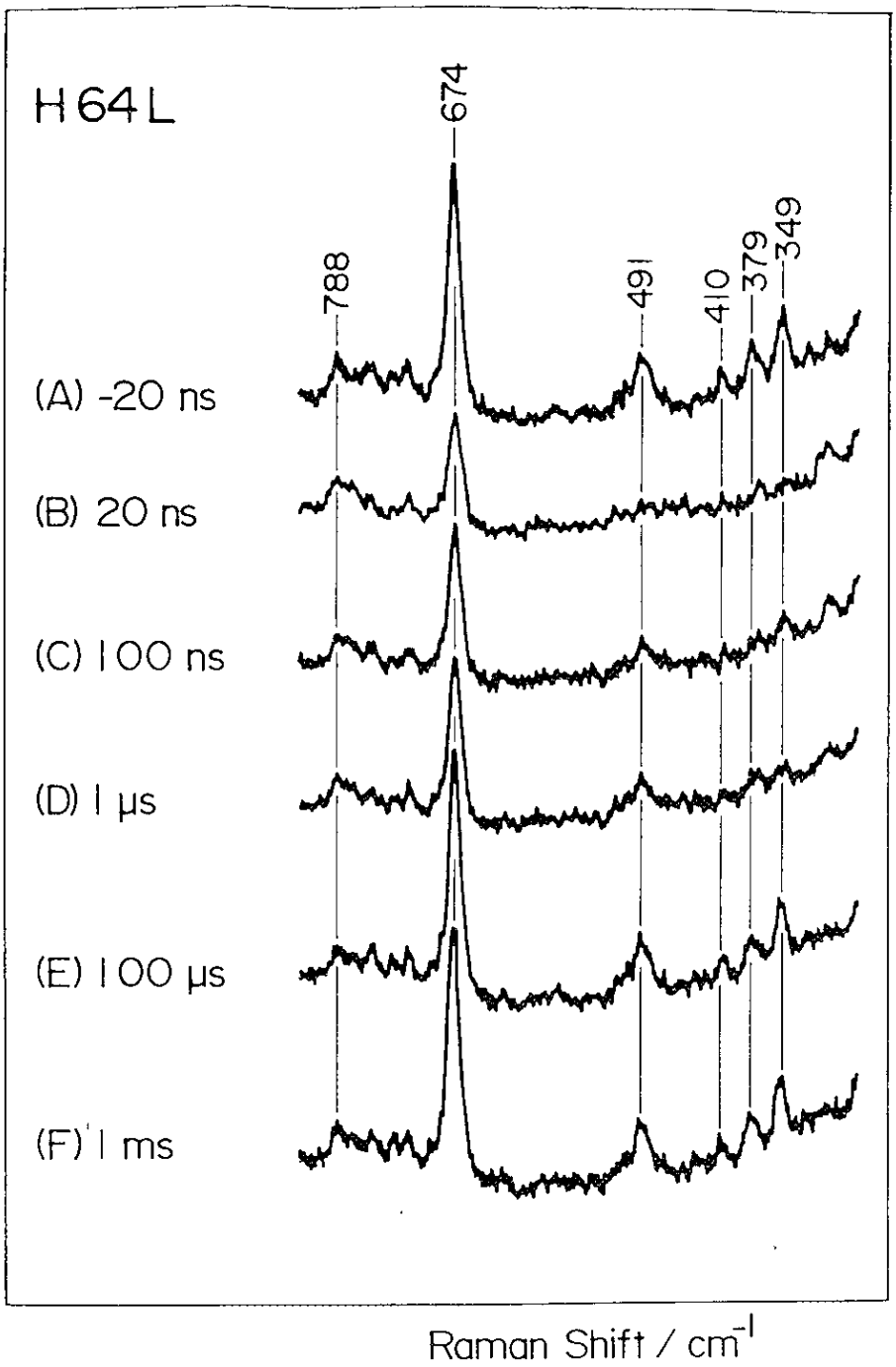

Figure IV-6.

The pump/probe time-resolved resonance Raman spectra of E7-Leu (H64L) mutant MbCO. The delay time (Δt_d) of the probe beam from the pump beam is specified at the left side of each spectrum.

Pump beam: 532.0 nm, Probe beam: 416.0 nm

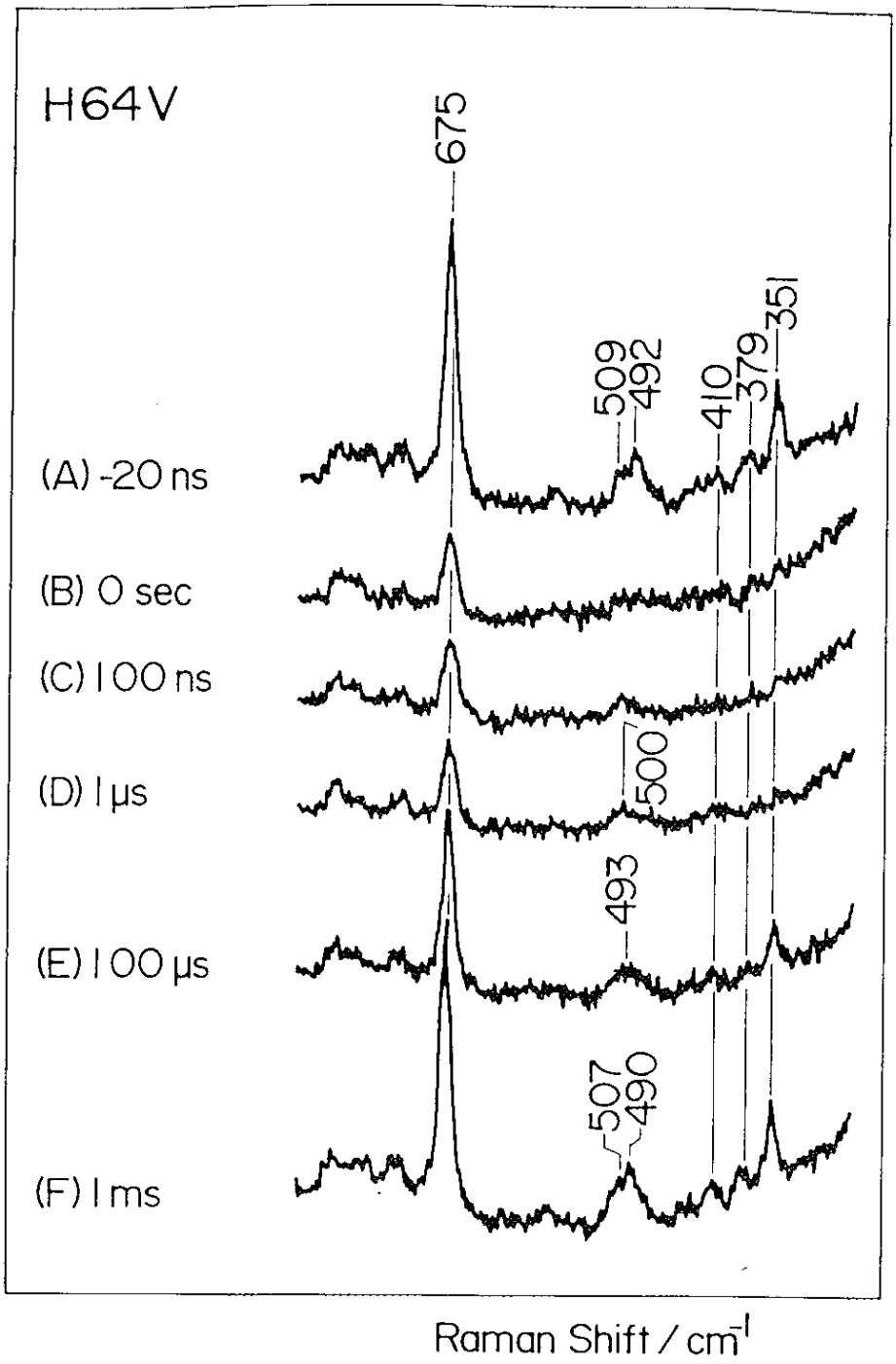

Figure IV-7.

The pump/probe time-resolved resonance Raman spectra of E7-Val (H64V) mutant MbCO. The delay time (Δt_d) of the probe beam from the pump beam is specified at the left side of each spectrum.

Pump beam: 532.0 nm, Probe beam: 416.0 nm

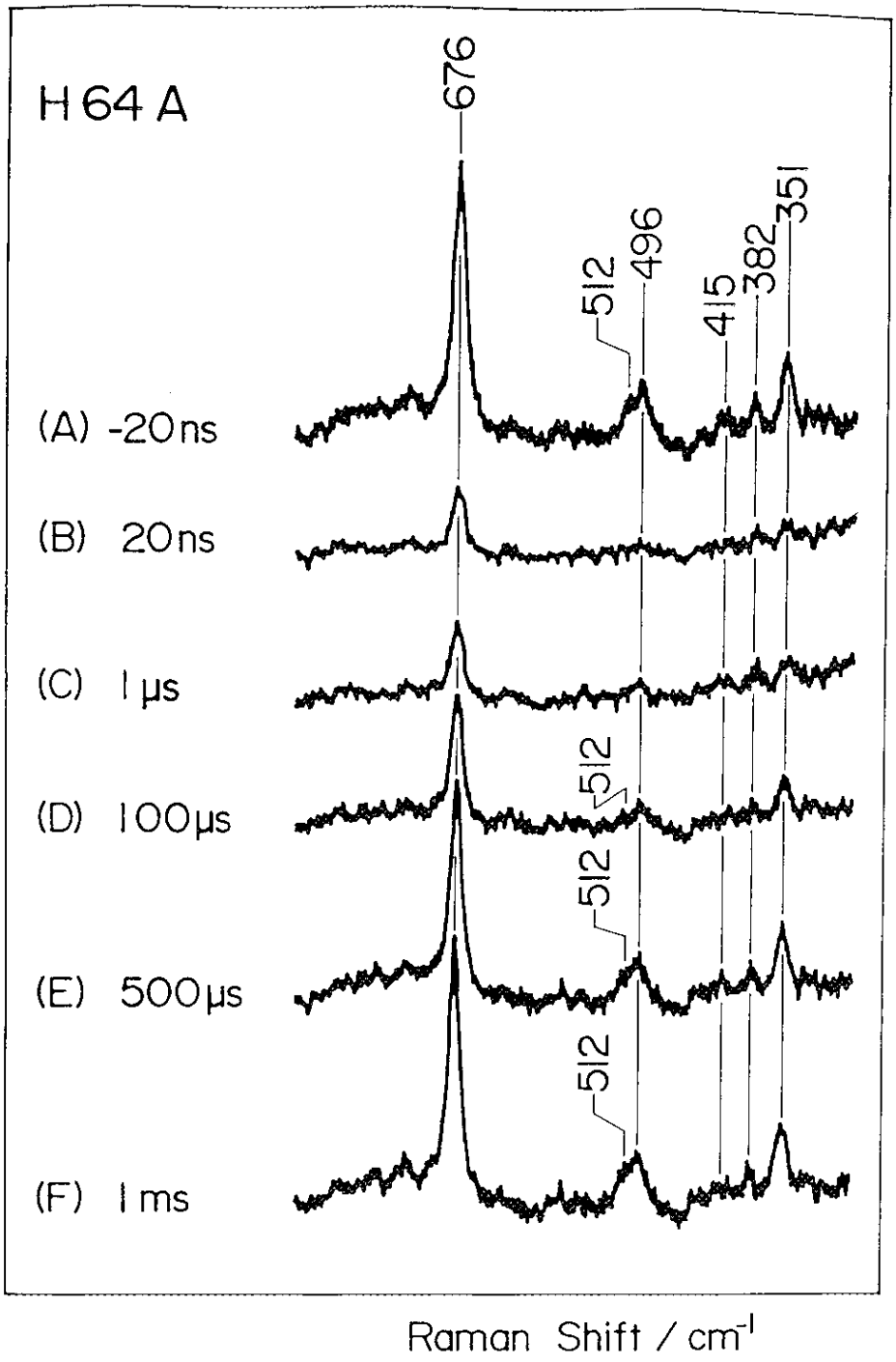

Figure IV-8.

The pump/probe time-resolved resonance Raman spectra of E7-Ala (H64A) mutant MbCO. The delay time (Δt_d) of the probe beam from the pump beam is specified at the left side of each spectrum.

Pump beam: 532.0 nm, Probe beam: 416.0 nm

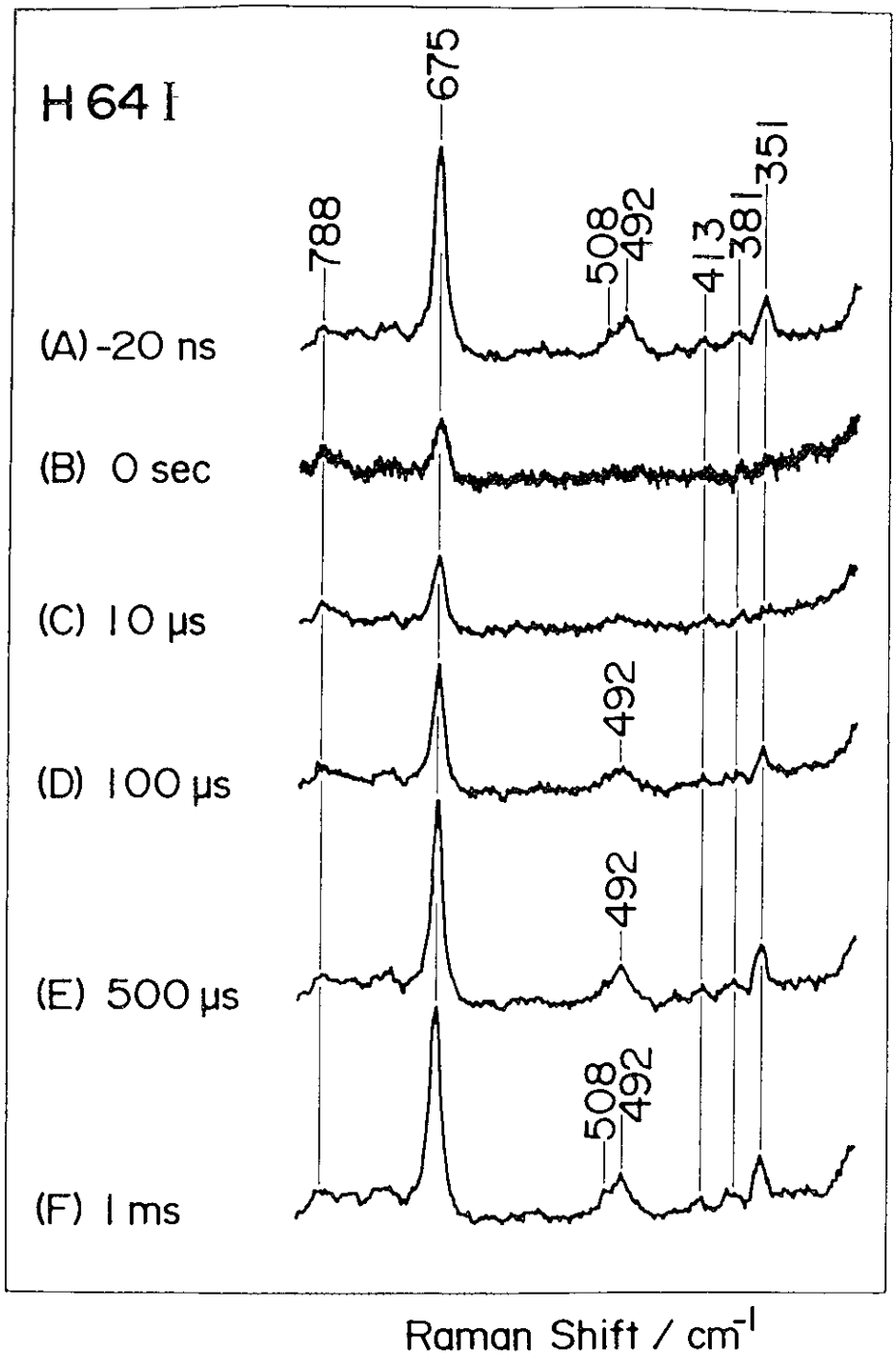

Figure IV-9.

The pump/probe time-resolved resonance Raman spectra of E7-Ile (H64I) mutant MbCO. The delay time (Δt_d) of the probe beam from the pump beam is specified at the left side of each spectrum.

Pump beam: 532.0 nm, Probe beam: 416.0 nm

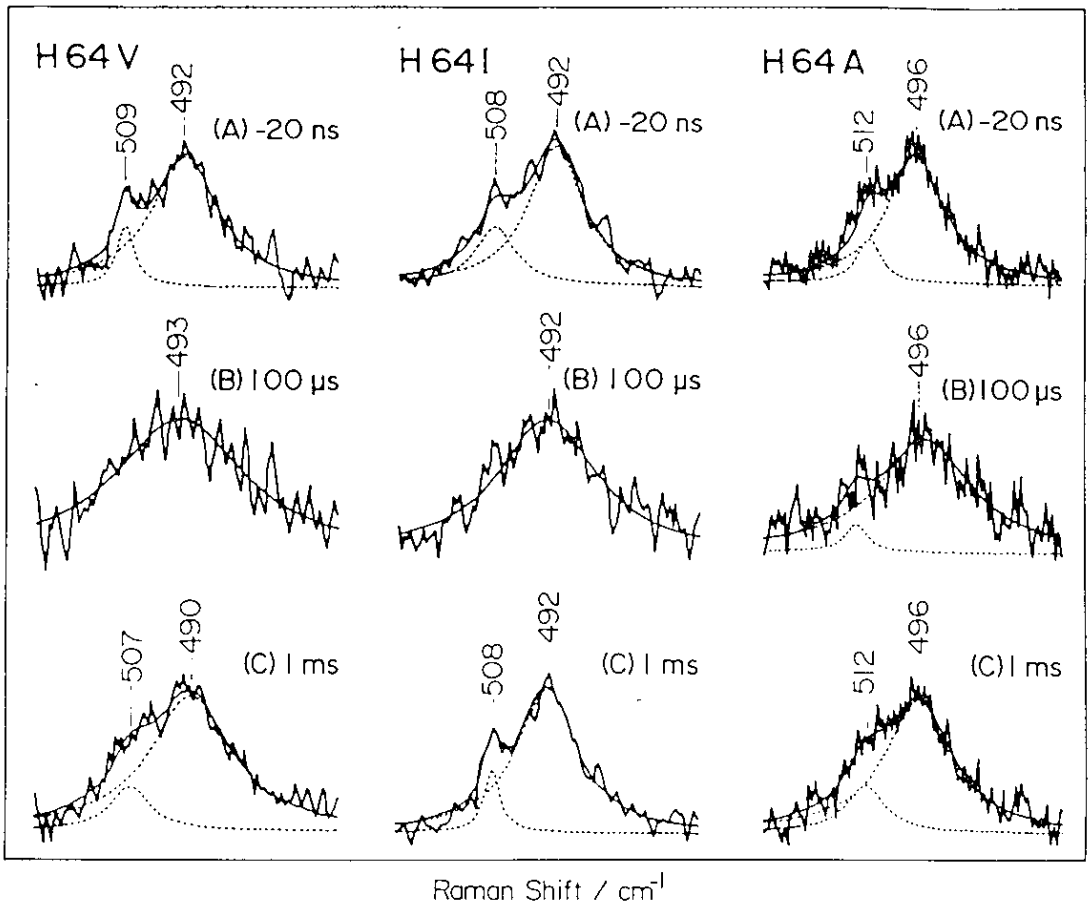

Figure IV-10.

Band fitting calculations for the transient $\nu_{Fe\text{-}CO}$ bands of H64V, H64I, and H64A. The solid lines denote the sum of the calculated components spectra represented by broken lines.

(A): Δt_d = -20 ns, (B): Δt_d = 100 μs, (C): Δt_d = 1 ms.

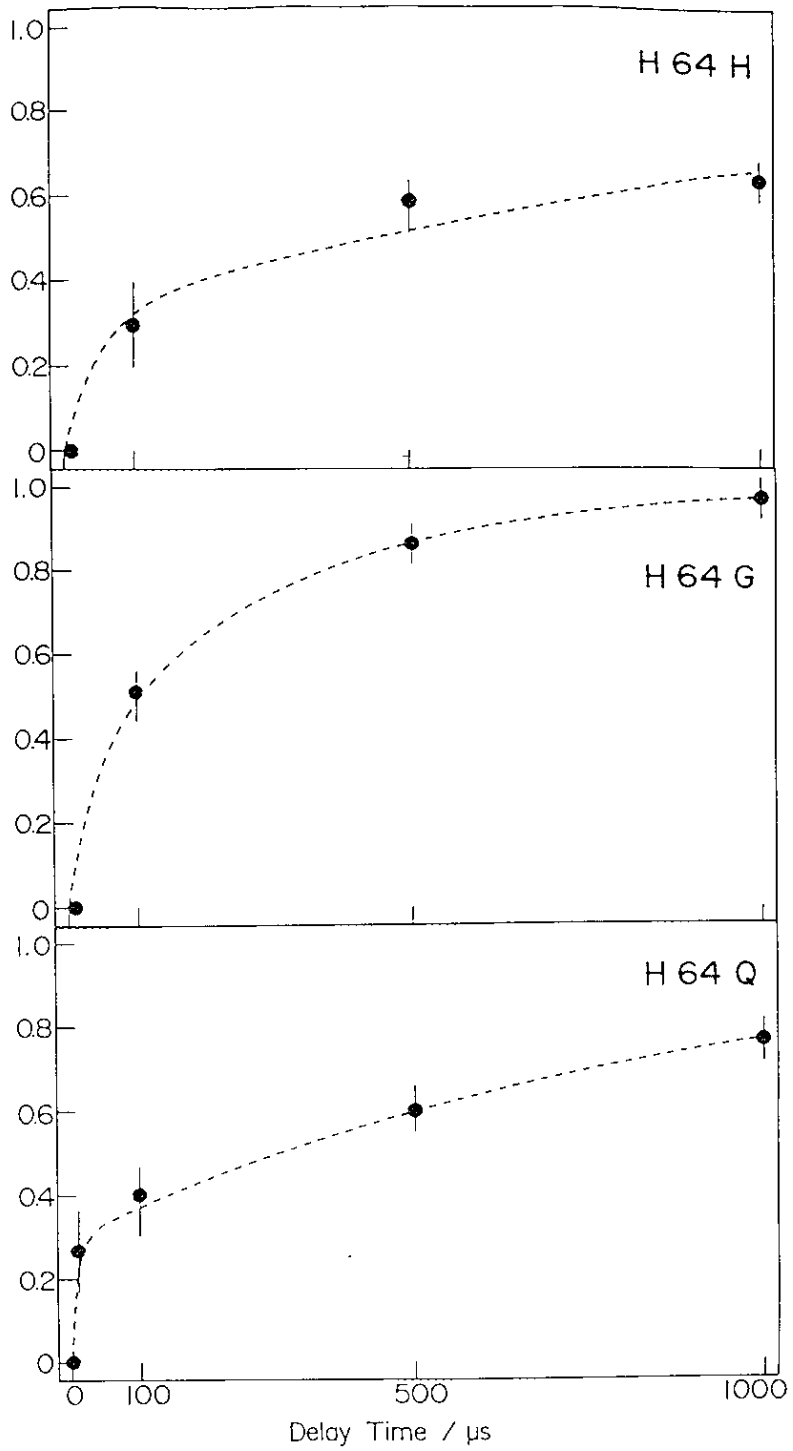

Figure IV-11.

Recovery of CO bound form for H64H, H64G, and H64Q. Experimental points represent the relative area intensity at each Δt_d with regard to that for Δt_d = -20 ns. The broken lines denote the values calculated from Eq. IV-2 and parameters listed in Table IV-1.

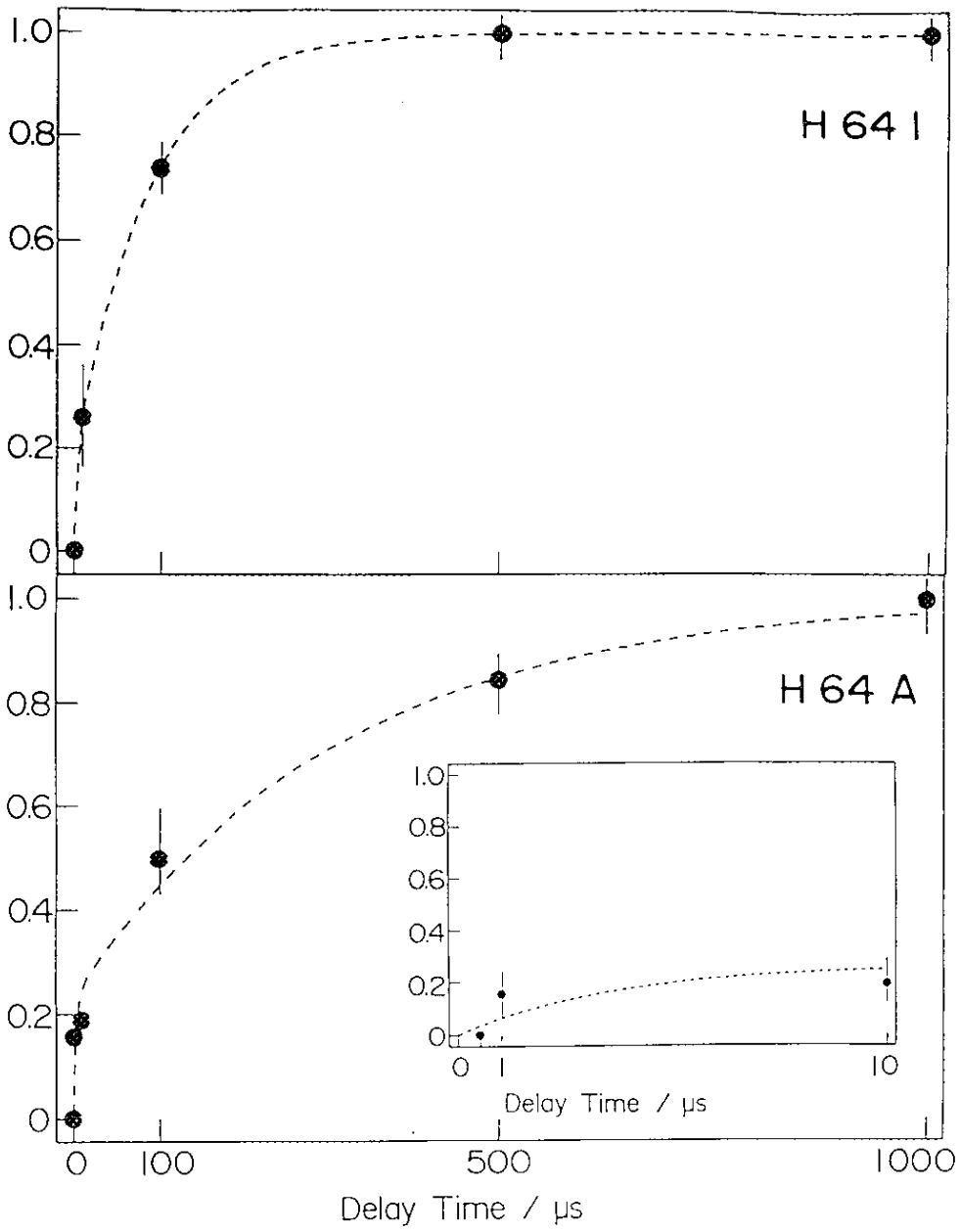

Figure IV-12A.

Recovery of CO bound form of H64I and H64A. Insertion represents the expanded Figure of the same curves for shorter Δt_d region. Otherwise as for Figure IV-11.

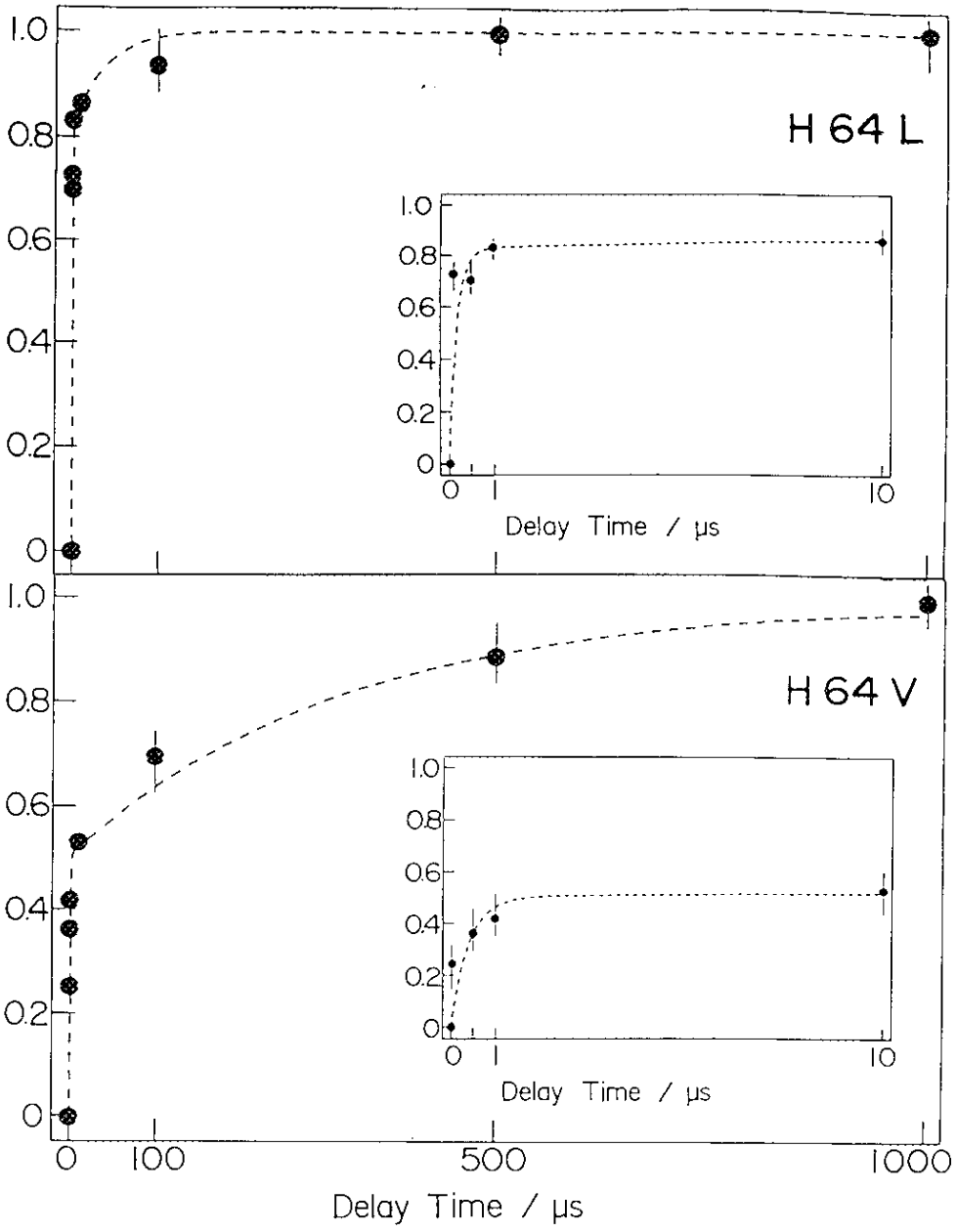

Figure IV-12B.
Recovery of CO bound form of H64L and H64V. Insertion represents the expanded Figure of the same curves for shorter Δt_d region. Otherwise as for Figure IV-11.

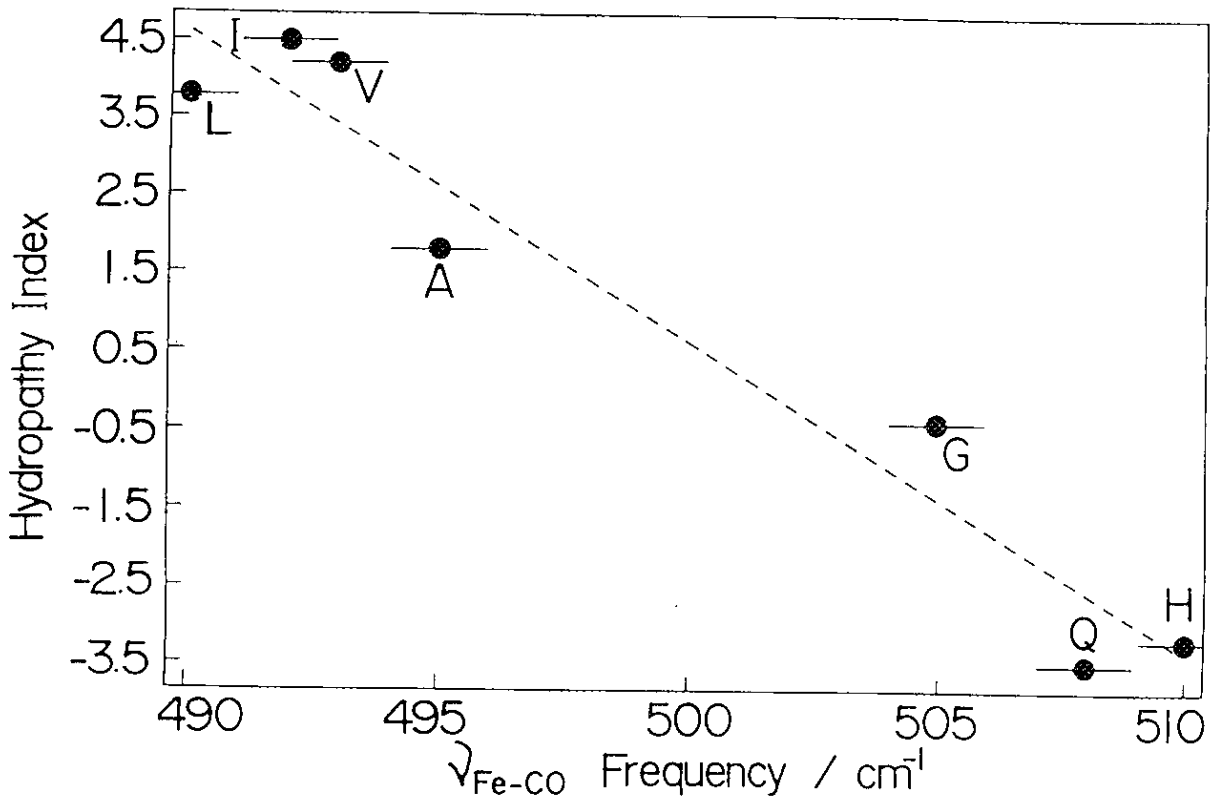

Figure IV-13.
Relation between the observed ν_{Fe-CO} frequencies and hydropathy index of the E7 residues. The values of hydropathy index for individual amino acids were taken from Ref. 40.

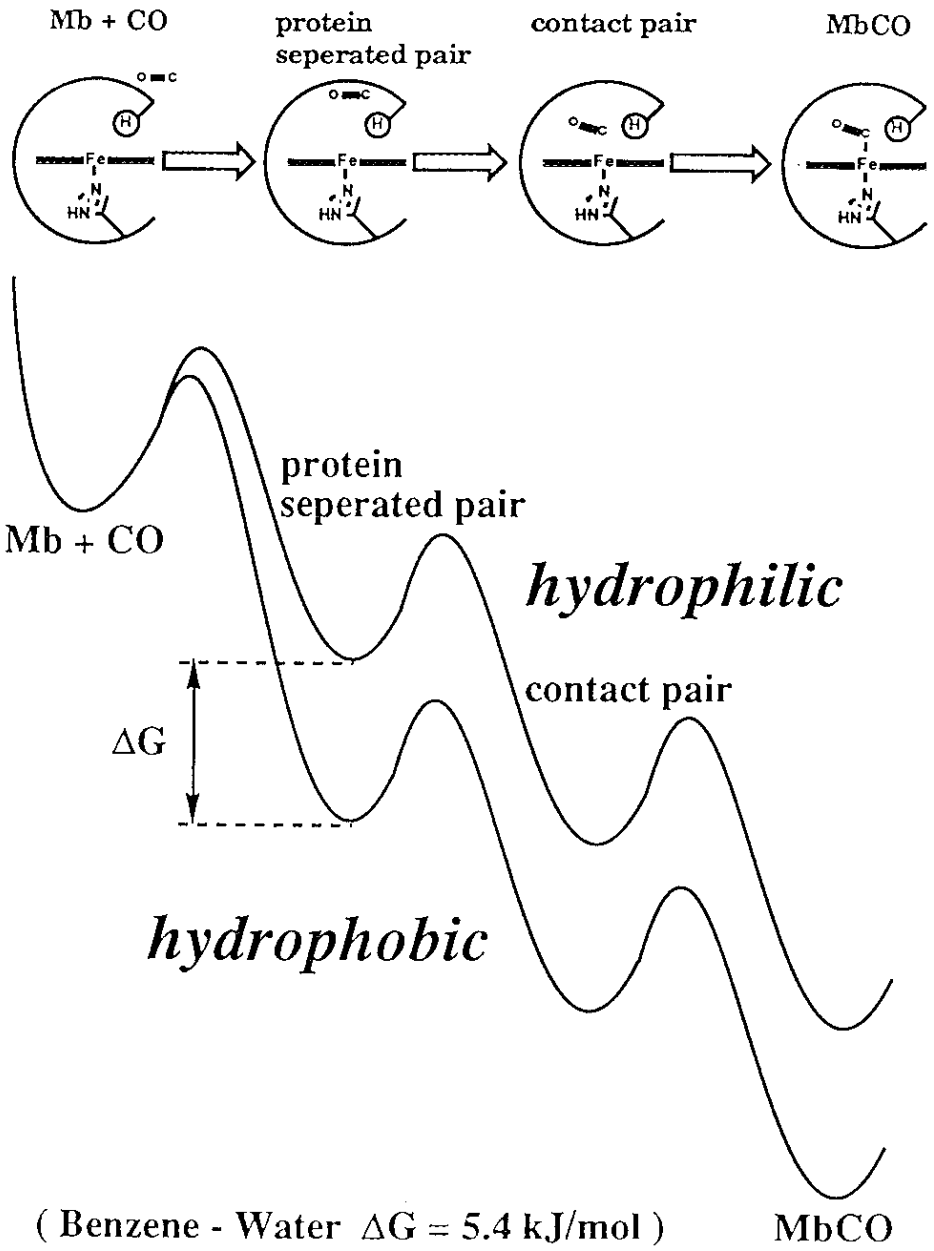

Figure IV-14.

Schematic energy diagram for binding of CO to deoxyMb. The contact pair means the state in which the Fe-CO bond is cleaved in the bound geometry of CO and the protein separated pair implies that CO is somewhere in the protein. The potential minimum for the protein separated pair is thought to be lower for a hydrophobic than hydrophilic E7 residue, although other parts are regarded to be the same in this approximation. The energy difference deduced from the solubility of CO in water and benzen is 5.4 kJ/mol, but the actual difference for MbCO between hydrophilic and hydrophobic E7 residues would be much smaller than this value.

Table IV-1.
Rebinding rate constants and amplitudes of photodissociated MbCOs*

	ν_{Fe-CO}/cm^{-1}	k_1/s^{-1}	k_2/s^{-1}	A_1	A_2
H64H	510	2.0×10^4	6.9×10^2	0.31	0.69
H64G	505	2.5×10^4	3.2×10^3	0.33	0.67
H64Q	508	1.0×10^5	1.1×10^3	0.29	0.71
H64L	490	5.5×10^6	2.5×10^4	0.83	0.17
H64V	493	2.5×10^6	3.1×10^3	0.50	0.50
H64I	492	2.0×10^5	1.2×10^4	0.17	0.83
H64A	495	3.0×10^5	3.2×10^3	0.23	0.77

(*) These values were estimated by a trial and error method for curve fitting with Eq. IV-2.

Chapter V

Determination of the Action Spectrum for MbCO Photodissociation and Energy Transfer Pathway for the Photodissociation by UV Light

Abstract

Time-resolved resonance Raman spectra in the iron-histidine stretching ($\nu_{Fe\text{-}His}$) region of ligand-photolyzed species of oxy myoglobin (MbO_2) and carbonmonoxy myoglobin (MbCO) were investigated. The action spectrum for photodissociation of MbCO was separately determined using visible absorption spectra and light illumination in the Large Spectrograph Facility of NIBB. Since the action spectrum indicated facile photodissociation upon UV illumination, the effect of the extra energy for photodissociation on the protein was examined by monitoring the $\nu_{Fe\text{-}CO}$ frequency of the photodissociated species. Unexpectedly, the $\nu_{Fe\text{-}His}$ frequency of UV photolyzed species was identical with that of the visible photolyzed species, in a time interval between 10 ns - 100 μs. Despite of the fact that the relaxation behavior of photolyzed MbO_2 is distinct from that of MbCO, the $\nu_{Fe\text{-}His}$ frequencies of photodissociated MbO_2 and MbCO were found to be the same within 10 ns after photolysis. However, the temporal behavior of intensity of the $\nu_{Fe\text{-}His}$ band exhibited some difference; MbCO gave a maximum at 50 ns after photolysis whereas MbO_2 gave a constant intensity. This may suggest that energy transfer process from an aromatic residue, provably tryptophan, to heme, which results in photodissociation of ligand, differs between MbCO and MbO_2.

V-1. Introduction

Myoglobin consists of 153 amino acid residues, containing two triptophans, three tyrosines, and six phenylalanines. Figure V-1 shows the absorption spectra of these amino acids in UV region. These aromatic amino acid residues absorb UV light around 200 - 280 nm region. Bucher and Kaspers[1] reported that the MbCO was photolyzed by 280 nm light with the quantum yield of unity. If it were true, protein dynamics would be different between the visible and the UV photolysis, because the energy of UV light must be first absorbed by aromatic amino acid residues and then transferred to the heme through the protein. It may be possible to detect the effect of extra the energy in the UV photolysis on the protein dynamics by monitoring the $\nu_{\text{Fe-His}}$ frequency, although the photodissociation process by visible light occur in the femtosecond time scale[2].

The $\nu_{\text{Fe-His}}$ RR band is sensitive to the heme structures[3]. The $\nu_{\text{Fe-His}}$ frequency reflects the Fe-N (proximal His) bond strength. If the transient species after photolysis were different from stationary deoxyMb, the $\nu_{\text{Fe-His}}$ band might appear at a frequency different from that of equilibrium deoxyMb. Accordingly, the TR[3] were measured in the nanosecond region by using Nd:YAG lasers. The measurements were extended to the time scale of microsecond region by using CW He/Cd laser excitation (441.6 nm) and high speed spinning cell (1800 rpm), since in the case of Hb, the protein dynamical reformation from R-state to T-state occur in microsecond time scale[4]. However, no differences were observed in the $\nu_{\text{Fe-His}}$ band between UV and visible photodissociated species for both MbO_2 and MbCO. It is deduced that the protein motion of Mb is much faster than that of Hb.

Recently, Sato et al.[5] pointed out some difference in transient absorption spectra in a microsecond time region between photoproducts from MbO_2 and deoxyMb. However, in the case of MbCO, no differences between photoproducts

and statical deoxyMb were observed. Sato et al., explained the different behaviors in terms of a cage effect of heme pocket. The cage effect is that the photodissociated ligand is trapped by some amino acid residues in heme pocket.

In order to confirm that it is possible to photolyze MbO_2 and MbCO by UV light, the action spectrum for photodissociation was determined by using the Okazaki Large Spectrograph Facility in NIBB. In addition, the TR[3] measurements in the nanosecond - microsecond time region were carried out for the photodissociation of MbO_2 and MbCO by using UV-pump/visible-probe technique.

V-2. Experimental Procedures

Measurement Procedure for The Photodissociation Action Spectrum[6] Figure V-2 displays the equipment system for measurements of the photodissociation action spectrum in the Okazaki Large Spectrograph of NIBB (National Institute for Basic Biology). The halogen lamp which is used as a head lamp of an automobile, was used as the light source for obtaining the absorption spectra. The white light of the lamp was introduced to the cell holder unit through the optical fiber (core diameter = 1 mm, length = ca. 3 m). The airtight optical cell was made of synthetic quartz, and the pass length was 10 mm. The airtight cell contained 10 μM MbCO solution at pH 8.0 with extremely small amount of dithionite and filled with CO gas at 1 atm. The purification of Mb was carried out as same as the Chapter 2. The light of each wavelength from the large spectrograph was irradiated at right angle from the white light. The photon density of the photodissociation light was unified by ND filter and determined with the photon density meter (5.55 - 5.75 $\times$ 10^{15} photon/cm^2.s). However, in a 250 - 300 nm region, the photodissociation light from large spectrograph source was relatively weaker (2.0 - 6.6 $\times$ 10^{14} photon/cm^2.s) than in other region therefore, the photon density was normalized

by calculation. The probe light passed through the sample was introduced to the specially designed triple polychromator which has 10 cm pass length and is equipped with three ruled gratings (500 nm blazed, 600 grooves/mm). The cooled (-20 °C) photodiode array (Hamamatsu, C2327) with the thermocontroller (Hamamatsu, C3434) and data processing unit (Hamamatsu, C2890) were used to measure the absorption intensity. This photodiode array is composed of 1024 channels, and in visible region it can cover a spectral range of about 300 nm in one time. The exposure time for each spectrum was 2 sec and 10 of such spectra were averaged. The photodissociation light from the large spectrograph was varied with 250 - 600 nm region at 10 nm step. Since the photodissociation light interfered with measurement of the absorption spectra, for the photodissociation light in the 250 - 490 nm region, the absorption spectra were measured around the α-band (580 nm) region, while the absorption spectra were obtained in the Soret band region (ca. 420 nm) for the photodissociation light in the 490 - 600 nm region. The observed spectra were transferred to the personal computer (NEC, PC-9801VX) through the GPIB interface for further calculations. The absorption spectra were calibrated by holomium glass.

The absorption spectra were calculated from equation V-1,

$$A = \log\{(I_{obs} - I_D)/(I_0 - I_D)\} \qquad \text{(V-1)}$$

where, A; intensity of absorption spectrum, I_{obs}; observed intensity, I_0; intensity of the white light without sample, and I_D; intensity of dark current of the photodiode array. The proportion of the photodissociated species was estimated by the difference spectrum between the illuminated and non-illuminated MbCO. Since the difference spectrum has the positive peaks at 584 and 420 nm and negative peaks

at 565 and 435 nm, the valley to peak height at 565 - 584 nm or 435 - 420 nm were evaluated for individual illuminated sample and its magnitude relative to the corresponding values obtained between the MbCO and deoxyMb were determined. For illumination in the 250 - 490 nm region, the difference intensities at 565 - 584 nm was used while for illumination in the 490 - 600 nm region, the difference intensities at 420 - 435 nm was used. The photodissociation action spectrum was obtained by plotting the relative proportion of the photodissociated species for normalized photon numbers against the wavelength.

Measurement Procedures of The UV-pump/visible-probe Time-Resolved Resonance Raman Spectroscopy. Figure V-3 displays the measurement system for the TR^3 spectroscopy, which is basically the same with that in the Chapter II - IV. The pump/probe TR^3 spectra were obtained by using a 442.0 nm pulse as a probe beam and a 223.1 nm pulse as a pump beam. The 442.0 nm pulse was generated with a 3rd harmonic (354.7 nm) of a Nd:YAG laser (Quanta-Ray, GCR-11, 7 ns width, 10 Hz repetition) and dye laser (Quanta-Ray, PDL-1 and TSC-1) with coumarine-440 (Exciton). The 223.1 nm pulse was obtained as the 4th anti-Stokes Raman line of H_2 gas from the 3rd harmonic of a Nd:YAG laser (Quanta-Ray, DCR-3, 7 ns width, 10 Hz repetition). The pump and probe pulses power were adjusted to 1.9 mJ/pulse and 10 mJ/pulse, respectively. With this laser power, the probe beam partially photodissociated the ligand. The delay time (Δt_d) of the probe pulse from the pump pulse was changed from -20 ns to 100 μs. Because of the much larger extinction coefficient of aromatic amino acids of the protein compared with that of heme around the Soret band, there would be a possibility that the probe beam irradiate the unpumped MbCO if the pump beam was introduced co-linearly with the probe beam as adopted in the Chapter II. In order to avoid it, the pump beam was introduced to the front of the airtight spinning cell

rotating at 25 rpm and the probe beam was introduced from the front bottom. The sample in the airtight spinning cell was maintained at 10 °C by flushing with cooled N_2 gas to avoid heating MbCO by laser illumination. The scattered light at right angle was focused onto the entrance slit of a triple polychromator (Spex, 1877). The collection lenses in Figure V-3 were made of BK-7 glass, because they were also used as UV cut-filter. The dispersed light was detected by intensified photodiode array (Princeton Applied Research, 1420B) and accumulated on the interface of OMA III (Princeton Applied Research, 1461 and 1463). The accumulation time was ca. 15 min; spectra with 8 sec exposure were accumulated by 100 times. The accumulated data was transferred to the personal computer (NEC, PC-9801VX) through the GPIB interface for further calculation. The dark current spectra of photodiode array under the same accumulation time were subtracted from the observed spectra. The resultant spectra were disturbed by strong Rayleigh scattering and thus Raman bands were too weak to identify. Accordingly, the Rayleigh wing was polynomial functions (3rd - 4th) whose coefficients were determined by least square method and subtracted from the observed spectra. The spectra obtained were calibrated by CCl_4 Raman spectrum.

V-3. Results and Discussions

Action Spectrum for the Photodissociation of MbCO The action spectra for photodissociation of MbCO are displayed in Figure V-4. The ordinate scales indicates that the relative proportion of the photodissociated species of MbCO upon illumination of the photodissociation light at each wavelength. The profile of the action spectrum was similar to that of the absorption spectrum of MbCO. Although the experimental error in the UV region was relatively larger, this demonstrates that MbCO is photolyzed by UV light with relatively higher yield. It was

hard to photolyze MbO_2 by the same light as used for MbCO, and we failed to determine the action spectra for the photodissociation of MbO_2. This fact implicates that the UV light should be absorbed by some aromatic amino acid residues first. The excited aromatic residues fluoresce in a picosecond time scale[8, 14]. As shown in Figure V-5[15], only tryptophan is expected to fluorescence around 400 nm region where the absorption maximum of the heme is located. Therefore, the absorbed UV light energy would be transferred to the heme through the tryptophan residues.

UV-Pump/Visible-Probe Time-Resolved Resonance Raman Spectra of MbCO and MbO_2 in the $\nu_{Fe\text{-}His}$ Region Figure V-6 shows the Raman spectrum of equilibrium deoxyMb obtained only with the probe beam at 442.0 nm. The band at 222 cm^{-1} is assigned to the iron-proximal His stretching vibration ($\nu_{Fe\text{-}His}$), while other bands are assigned to skeletal vibrational modes of the porphyrin ring.

The TR^3 spectra of MbO_2 are displayed in Figure V-7, where the ordinate scales are common to all spectra. Therefore, the intensities of the $\nu_{Fe\text{-}His}$ band reflects the population of photodissociated MbO_2 (deoxyMb) at each delay time. In the spectrum for Δt_d = 0 sec, the $\nu_{Fe\text{-}His}$ band is observed at 222 cm^{-1}. A part of intensity of $\nu_{Fe\text{-}His}$ might come from the photodissociation by probe beam itself. In these transient spectra observed, all bands exhibit no frequency shift. The transient $\nu_{Fe\text{-}His}$ band seems to be composed of two bands, especially at Δt_d = 100 μs. This superposed transient $\nu_{Fe\text{-}His}$ bands may indicate the presence of a new transient species, but the S/N ratio is not sufficient to conclude it from the present spectrum. Further experiments are necessary to determine it.

Figure V-8 shows the TR^3 spectra of MbCO, which are also obtained in the same way as for MbO_2. The $\nu_{Fe\text{-}His}$ bands in these transient spectra also seem to be composed of two bands, but their relative intensity does not change with the delay

time. Therefore, it is hard to assume the presence of two intermediates which have different $\nu_{Fe\text{-}His}$ frequencies.

In order to discuss temporal behavior of the $\nu_{Fe\text{-}His}$ intensity quantitatively, intensities of the $\nu_{Fe\text{-}His}$ band relative to the porphyrin skeletal mode at 370 cm^{-1} (MbO_2) and 368 cm^{-1} (MbCO) were plotted against the delay time in Figure V-9. The $\nu_{Fe\text{-}His}$ intensity of MbO_2 is scarcely altered with the delay time. In contrast, the intensities of the $\nu_{Fe\text{-}His}$ of MbCO reached the maximum at Δt_d = 50 ns, and then decreased gradually. The intensity at 1 ms was nearly equal to that at 0 sec. The visible-pumped spectra of MbCO are shown in Figure V-10. The $\nu_{Fe\text{-}His}$ band intensity at Δt_d = -20 ns was relatively weak, but after photolysis the $\nu_{Fe\text{-}His}$ bands intensities became larger than that of Δt_d = -20 ns, and the intensity after photolysis did not alter with delay time. This indicates that in contrast to the UV-pumped spectra of MbCO, the photodissociation by visible light occur within 7 ns. These facts suggest two alternative interpretations; it takes place 50 ns for MbCO to photodissociate by UV light but it is less than 10 ns for MbO_2 to photodissociate. Another interpretation is that MbO_2 is hardly photolyzed by UV light and only the probe beam photolyzed species is observed. However, measurements of the action spectrum for photodissociation demonstrated that the amount of the photodissociated species of MbO_2 was extremely small. Therefore, the latter alternative seems more likely.

The fluorescence lifetime and its depolarization of Trp in a protein were observed in the femtosecond or picosecond time scale in order to analyze the energy transfer or the protein dynamics[8, 14, 16]. The fluorescence lifetimes of tryptophan of sperm whale Mb exhibited two phases in its decay, 14 - 26 ps and 106 - 135 ps for all of met, deoxy, and CO-bound forms[8], while in the case of yellowfin tuna Mb, the fluorescence lifetime showed only one phase decay, 31 - 33 ps for

metMb[8]. The lifetimes of apoMb (it has no heme) were 627 ps and 2.68 ns for sperm whale Mb and 2.81 ns for yellowfin tuna Mb[8a]. Sperm whale Mb has two Trp residues at Trp-7 and Trp-14[10], whereas yellowfin tuna Mb has only one Trp residue at Trp-14[11]. The facts that sperm whale and yellowfin tuna Mbs have similar lifetimes but apoMb has much longer one suggest that the energy transfer from excited Trp to the heme[9] is the origin of the fluorescence decay. Furthermore, from the Förster-type energy transfer calculation[12] for X-ray crystallographic structure[13], the fluorescence with faster decay arises from Trp-14 (calculated lifetime was ca. 30 ps), and that with longer lifetime was assigned to the Trp-7 (calculated lifetime was ca. 130 ps)[8a, 14]. This difference of the lifetime between Trp-14 and Trp-7 arises from different distances from the heme. Trp-14 was separated 15Å from the heme while Trp-7 was 21.5Å separation from the heme. These suggested that the energy of UV light was absorbed by Trp residues and subsequently transferred to the heme in subnanosecond time scale. If the energy transfer directly causes photodissociation, the $\nu_{\text{Fe-His}}$ RR band should appear within 1 ns at the longest. However, as a matter of fact, the intensity maximum of $\nu_{\text{Fe-His}}$ Raman band appeared at 50 ns after UV light irradiation. Although more experiments are required, it is deduced at the present stage that some new transient species in which heme has received the energy but CO is not dissociated. However, all the Raman bands observed did not any frequency shift within 50 ns and there were no new bands, an alternative interpretation is that the energy transfer in the present protein took place around 50 ns.

References

(1) T. Bucher, J. Kaspers, Biochim. Biophys. Acta, **1**, 21 (1947).

(2) J. L. Martin, A. Migus, C. Poyart, Y. Lecarpentier, R. Astier, A. Antonetti, Proc. Natl. Acad. Sci. U.S.A., **80**, 173 (1983).

(3) (a) M. F. Perutz, Nature, **228**, 726 (1970).
(b) T. Kitagawa, K. Nagai, M. Tsubaki, FEBS Lett., **104**, 376 (1979).
(c) K. Nagai, T. Kitagawa, H. Morimoto, J. Mol. Biol., **136**, 271 (1980).
(d) M. J. Irwin, G. H. Atkinson, Nature, **293**, 317 (1981).
(e) K. Nagai, T. Kitagawa, Proc. Natl. Acad. Sci. U.S.A., **77**, 2033 (1980).
(f) R. M. Ondrias, D. L. Rousseau, T. Kitagawa, M. Ikeda-Saito, T. Inubushi, T. Yonetani, J. Biol. Chem., **257**, 8766 (1980).

(4) S. Kaminaka, T. Ogura, T. Kitagawa, J. Am. Chem. Soc., **112**, 23 (1990).

(5) F. Sato, Y. Shiro, Y. Sakaguchi, T. Suzuki, T. Iizuka, H. Hayashi, J. Biol. Chem., **265**, 2004 (1990).

(6) This study was carried out under the NIBB Cooperative Research Program for the Okazaki Large Spectrograph (90-534).

(7) Y. Sakan, T. Ogura, and T. Kitagawa, in "Time-Resolved Vibrational Spectroscopy V", ed. H. Takahashi, (Springer-Verlag, Berlin), pp. 14-15(1992).

(8) (a) R. M. Hochstrasser, D. K. Negus, Proc. Natl. Acad. Sci. U.S.A., **81**, 4399 (1984).
(b) K. J. Willis, A. G. Szabo, D. T. Krajcarski, J. Am. Chem. Soc., **113**, 2000 (1991).
(c) K. J. Willis, A. G. Szabo, M. Zuker, J. M. Ridgeway, B. Alpert, Biochemistry, **29**, 5270 (1990).

(9) G. Weber, F. W. J. Teale, Discuss. Faraday Soc., **27**, 134 (1959).

(10) A. B. Edmundson, Nature, **205**, 883 (1965).

(11) F. E. Lattman, C. E. Nockolds, R. H. Kretsinger, W. E. Love, J. Mol. Biol., **60**, 271 (1971).

(12) Th. Förster, in *Modern Quantum Chemistry*, ed. O. Sinanoglu, (Academic Press, New York), Vol. 3, pp. 93 - 137 (1965).

(13) (a) J. C. Kendrew, R. E. Dickerson, B. E. Strandberg, R. G. Hart, D. R. Davies, D. C. Phillips, V. C. Shore, Nature, **185**, 422 (1960).
(b) H. C. Watson, in *Progress in Stereochemistry*, eds. B. J. Aylett, M. M. Harris, (Butterworth, London), pp. 299 - 333 (1969).

(14) S. M. Janes, G. Holtom, P. Ascenzi, M. Brunori, R. M. Hochstrasser, Biophys. J., **51**, 653 (1987).
(15) F. W. J. Teale, G. Weber, Biochem. J., **65**, 476 (1957).
(16) (a) I. Munro, I. Pecht, L. Stryer, Proc. Natl. Acad. Sci. U.S.A., **76**, 56 (1979).
(b) T. Ichiye, M. Karplus, Biochemistry, **22**, 2884 (1983).
(c) J. R. Lakowicz, G. Weber, Biophys. J., **32**, 591 (1980).

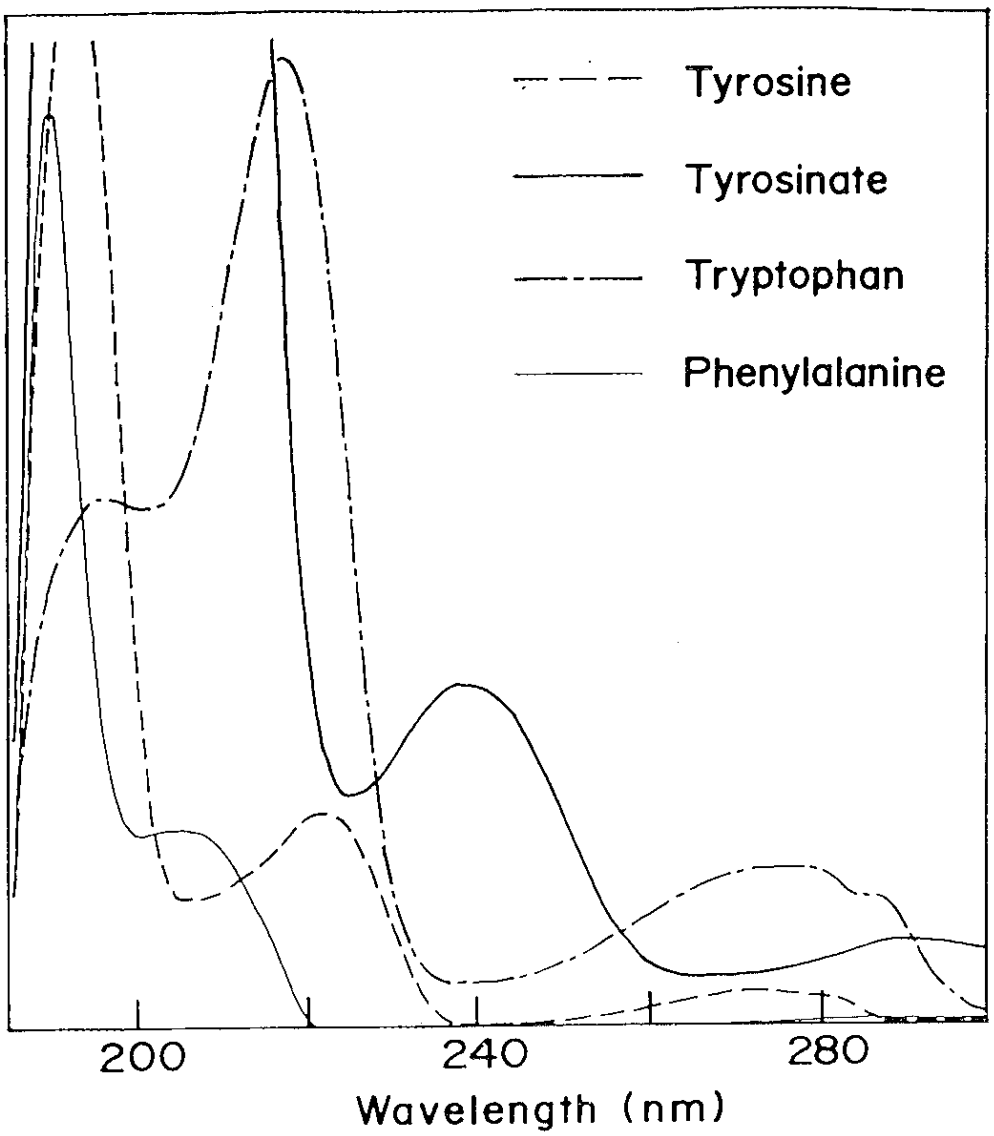

Figure V-1.
The absorption spectra of aromatic amino acids in the UV region.

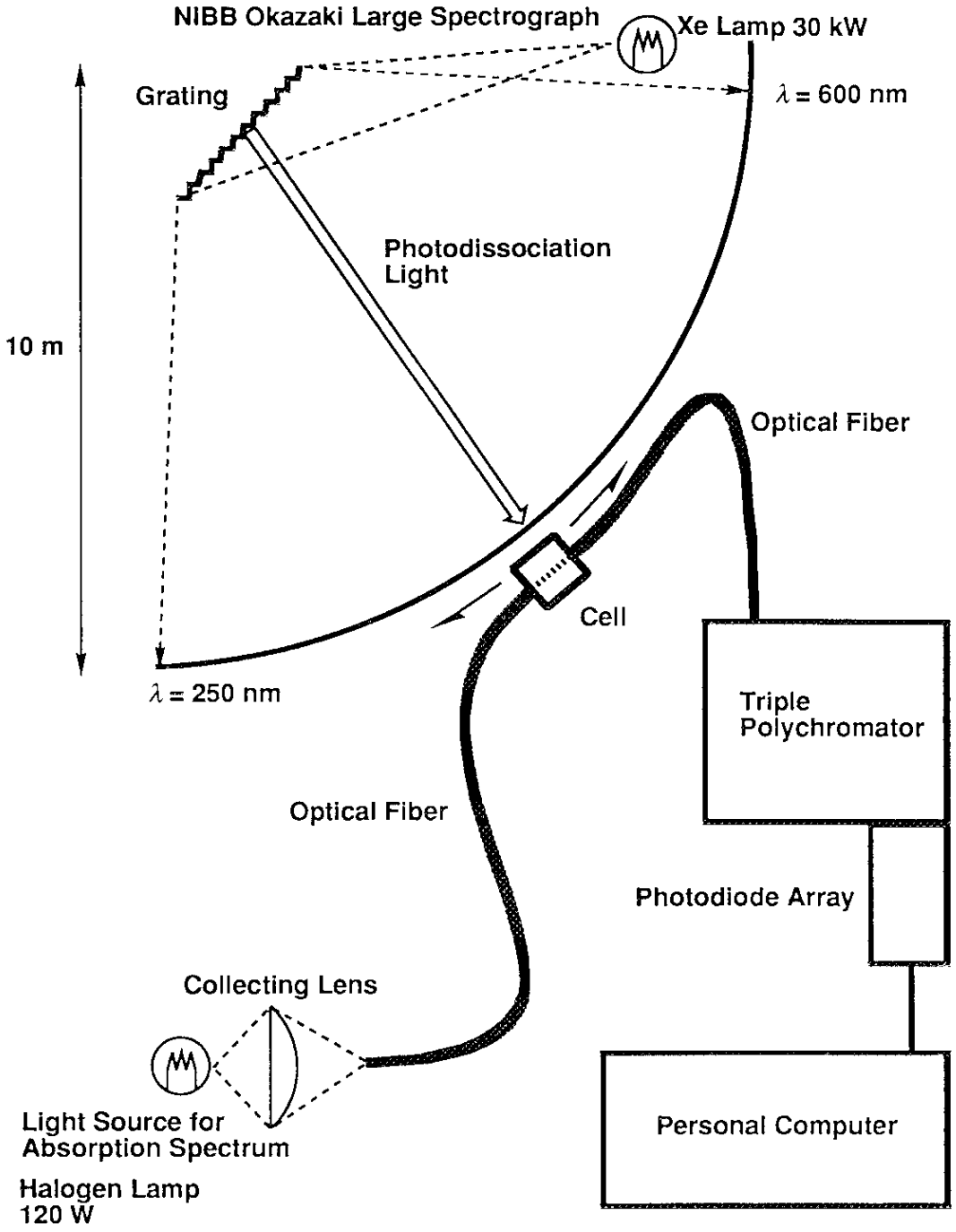

Figure V-2.
The equipments illustration for the photodissociation action spectrum measurements in the Okazaki Large Spectrograph in NIBB.

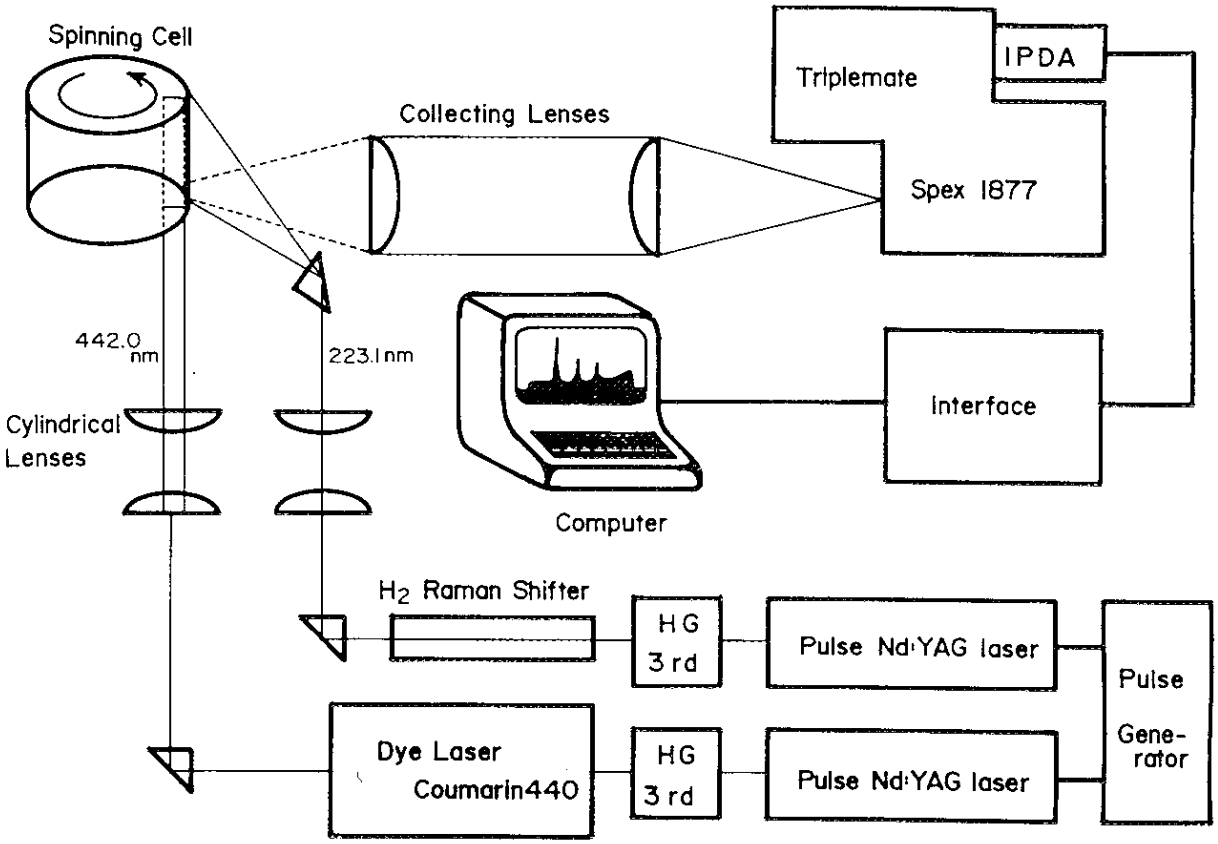

Figure V-3.
The block diagram of the measurement system for the UV-pump/visible-probe time-resolved resonance Raman spectroscopy.

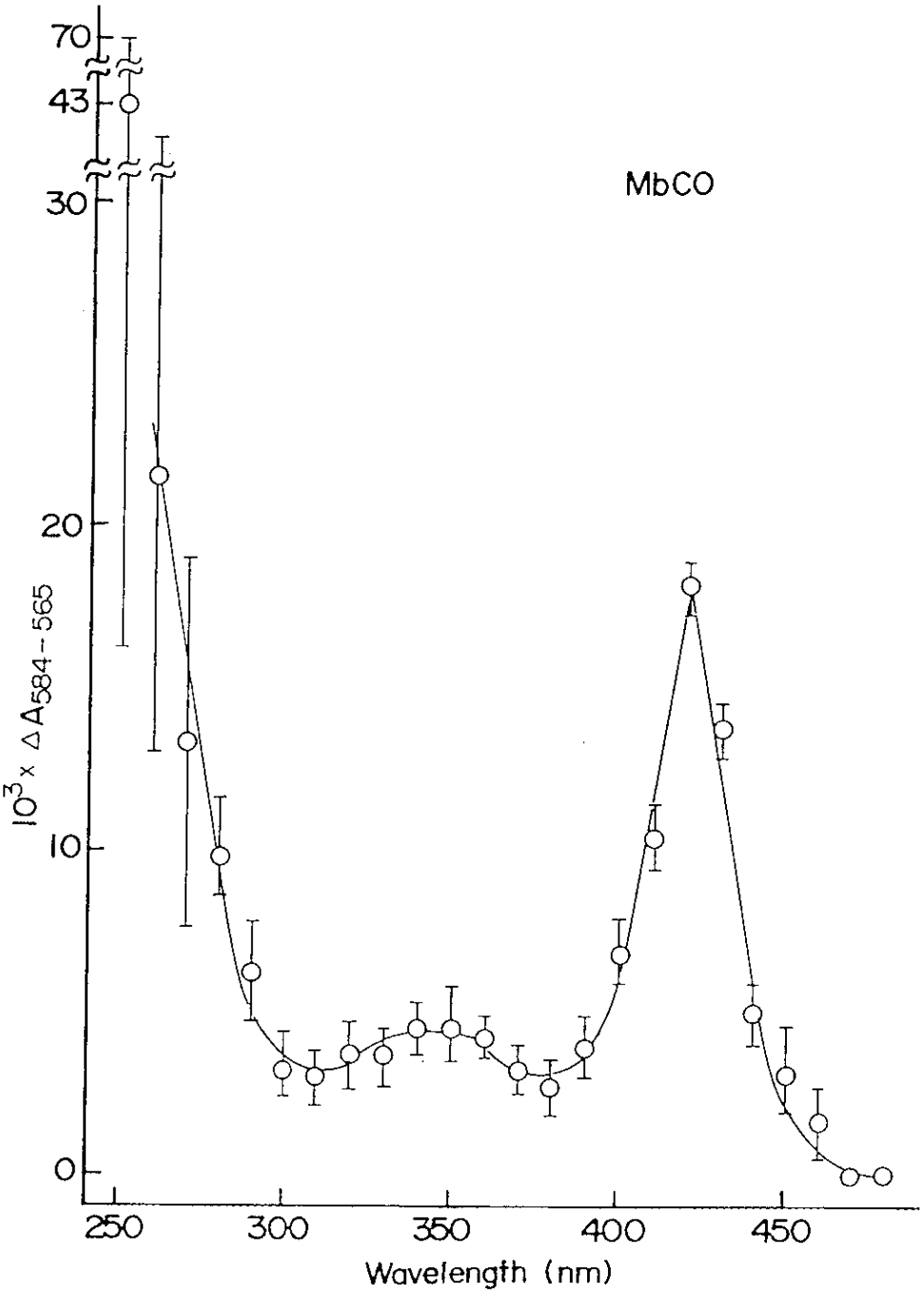

Figure V-4a.
The action spectrum for the photodissociation of MbCO in 250 - 480 nm region. The ordinate axis indicates the population of photodissociated species (deoxyMb).

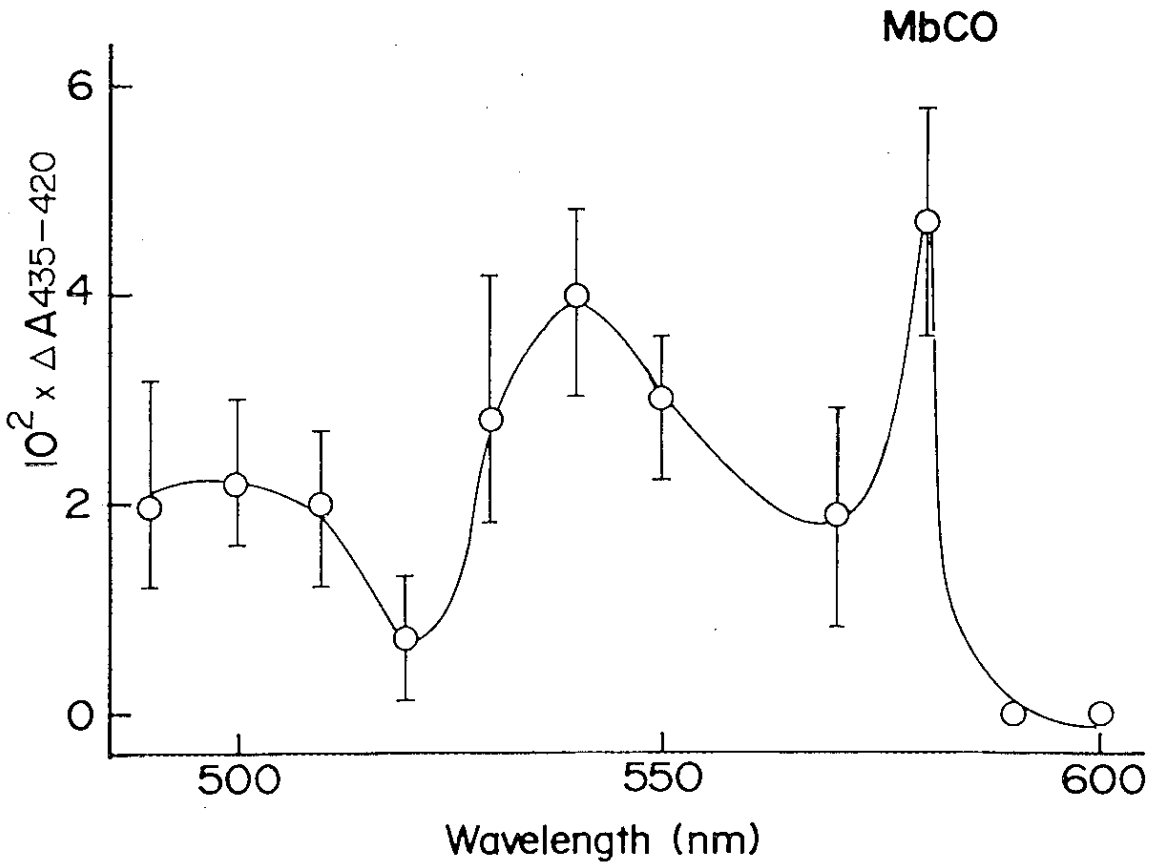

Figure V-4b.
The action spectrum for the photodissociation of MbCO in 490 - 600 nm region. The ordinate axis indicates the population of photodissociated species (deoxyMb).

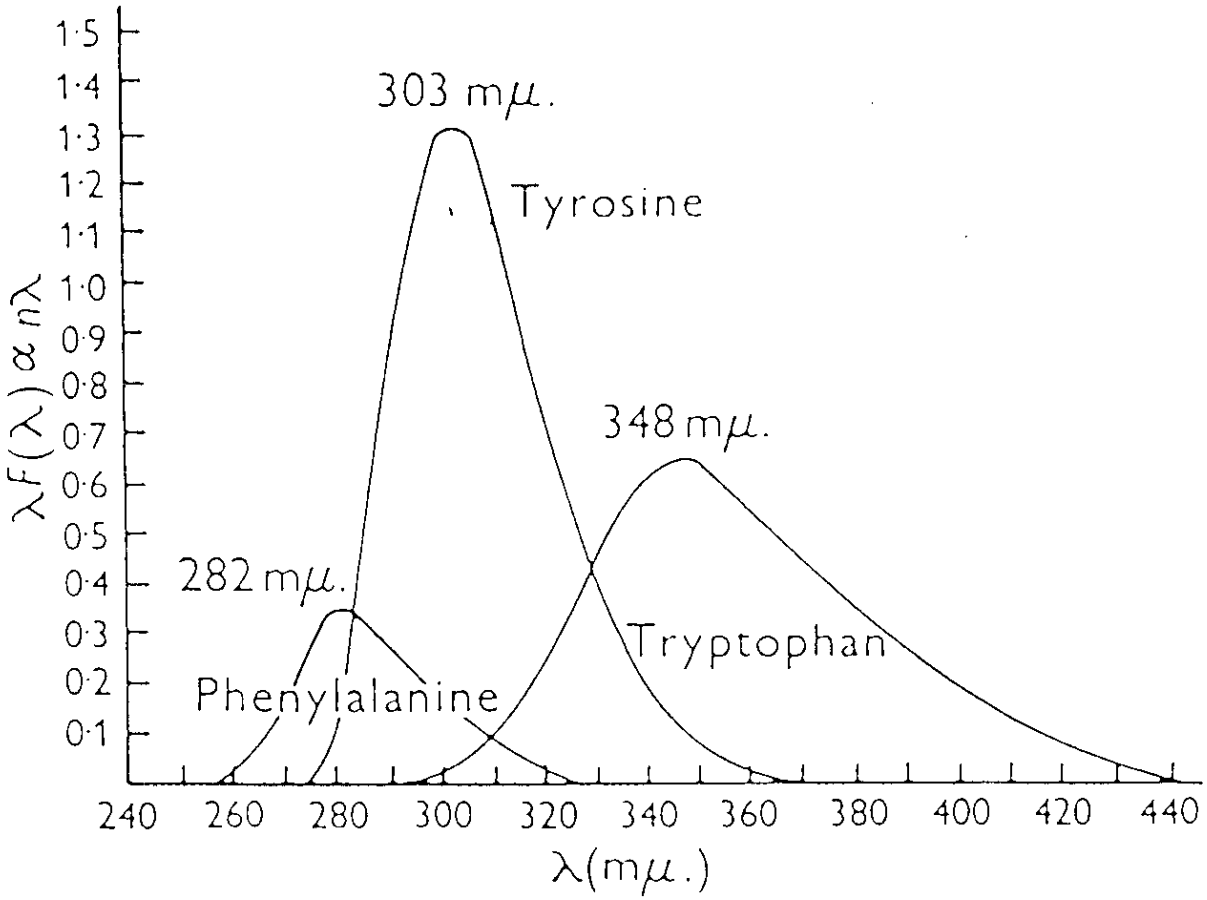

Figure V-5.
The fluorescence spectra of Phe, Tyr, and Trp on the ref. 15.

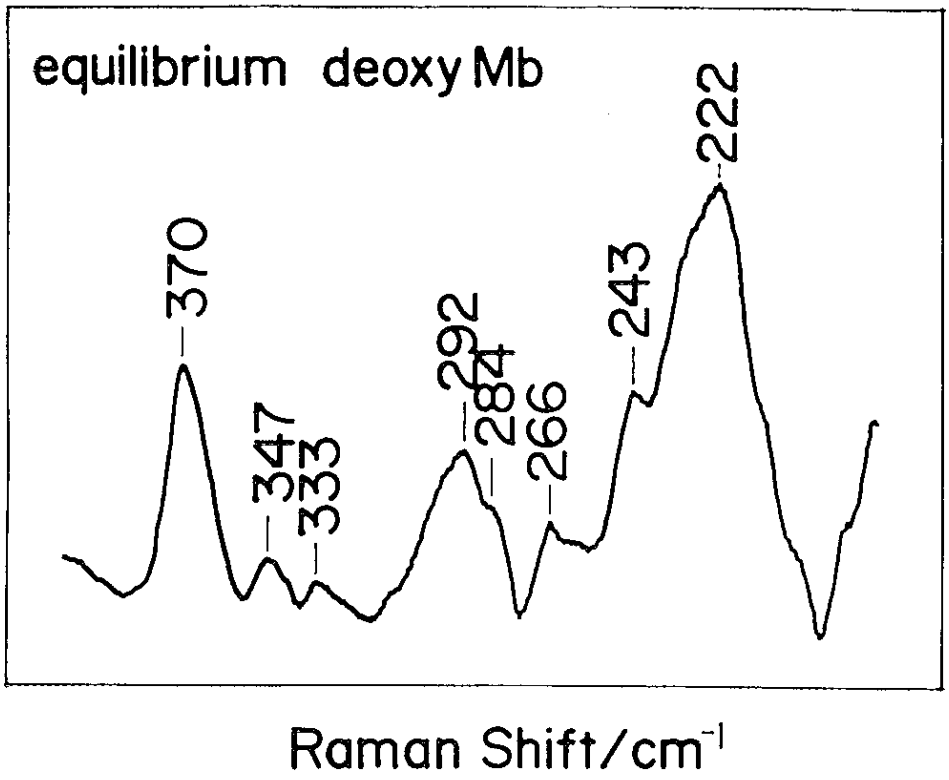

Figure V-6.
The resonance Raman spectrum of equilibrium deoxyMb in the $\nu_{\text{Fe-His}}$ region by the probe 441.6 nm pulse excitation.

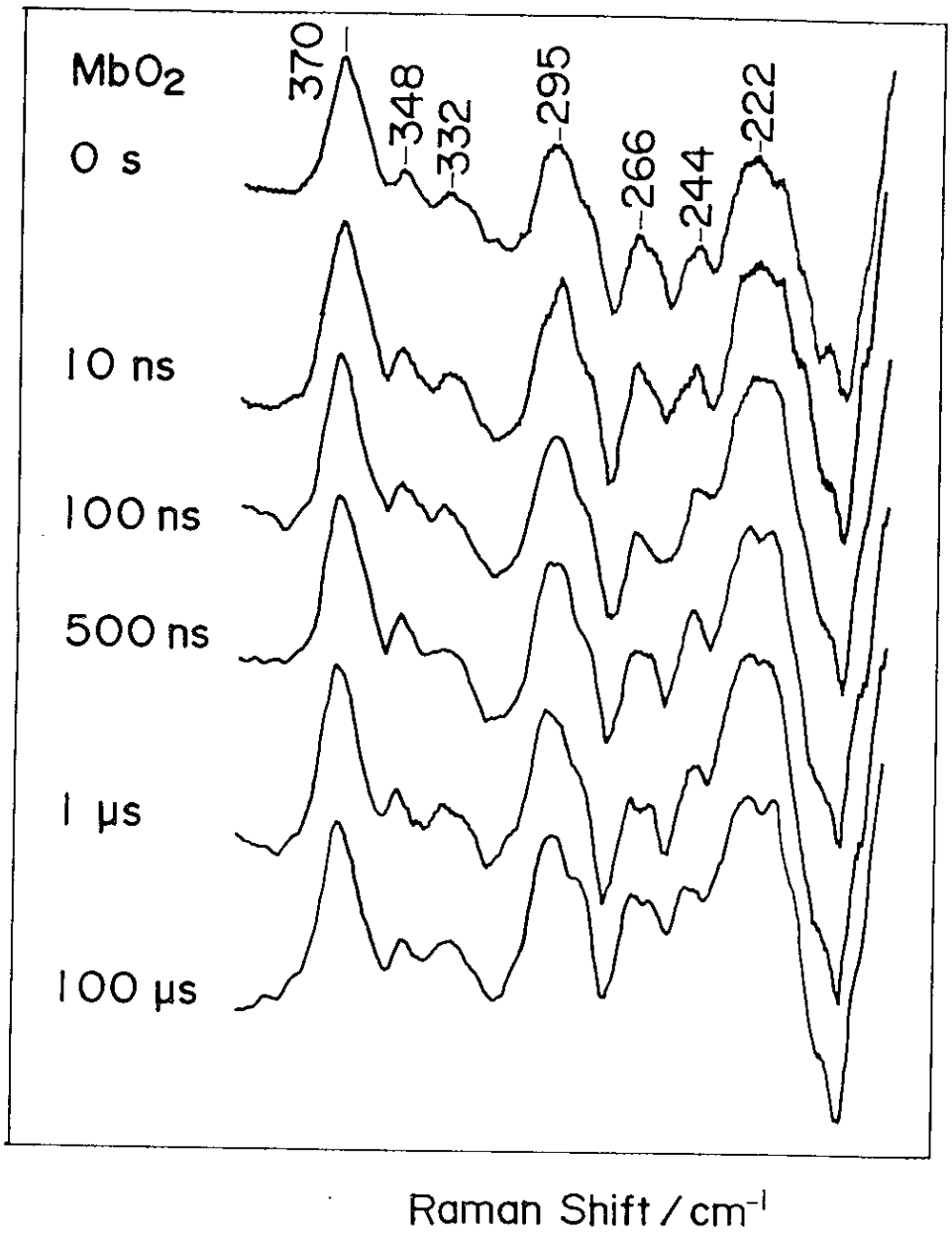

Figure V-7.
The UV-pump/visible-probe time-resolved resonance Raman spectra of MbO_2. The time in the left side indicate the delay time from the pump pulse to the probe pulse.
Pump beam: 223.1 nm, Probe beam: 442.0 nm

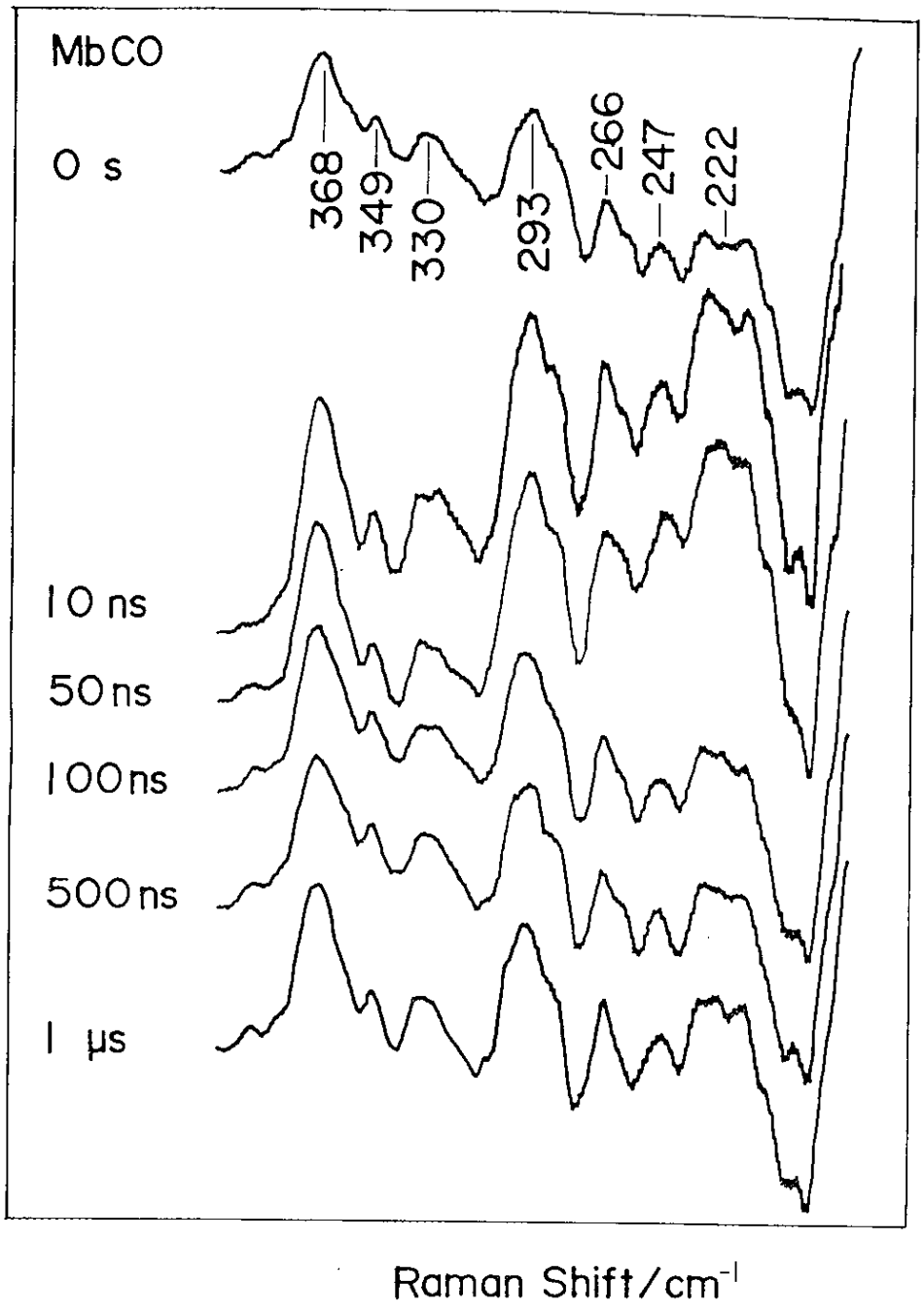

Figure V-8.
The UV-pump/visible-probe time-resolved resonance Raman spectra of MbCO. The time in the left side indicate the delay time from the pump pulse to the probe pulse.
Pump beam: 223.1 nm, Probe beam: 442.0 nm

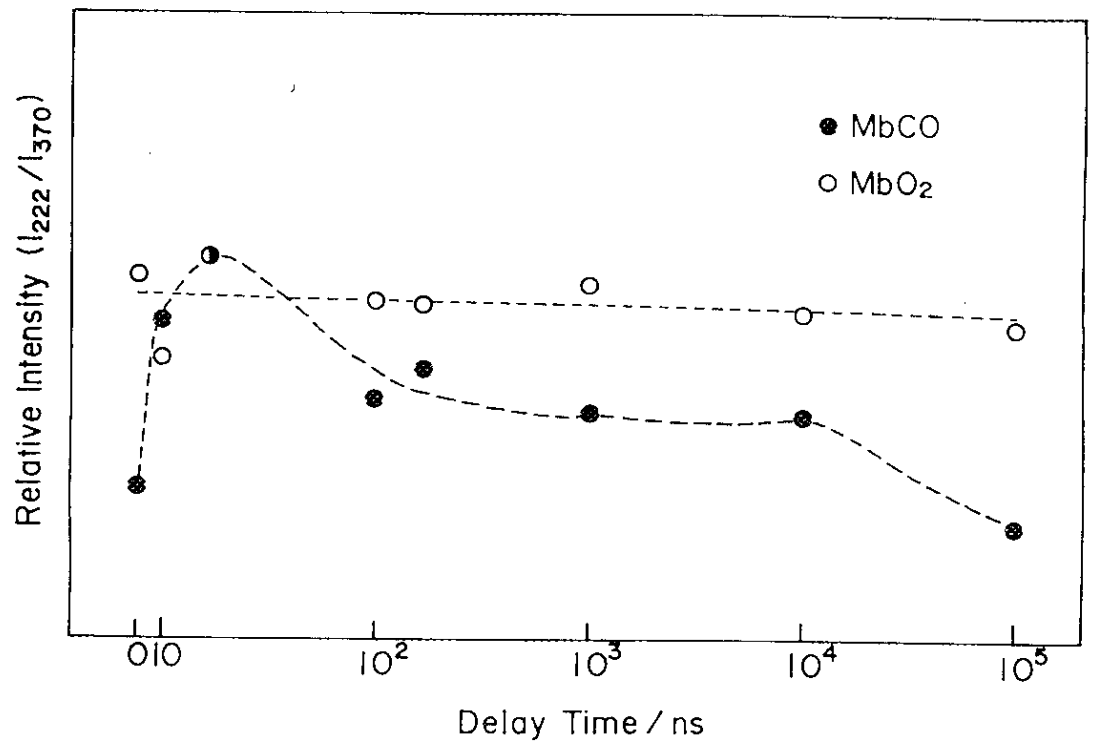

Figure V-9.
The relative intensities of the $\nu_{Fe\text{-}His}$ bands of MbO_2 and MbCO to the around 370 cm^{-1} porphyrin skeletal vibrational mode were plotted against the delay time.

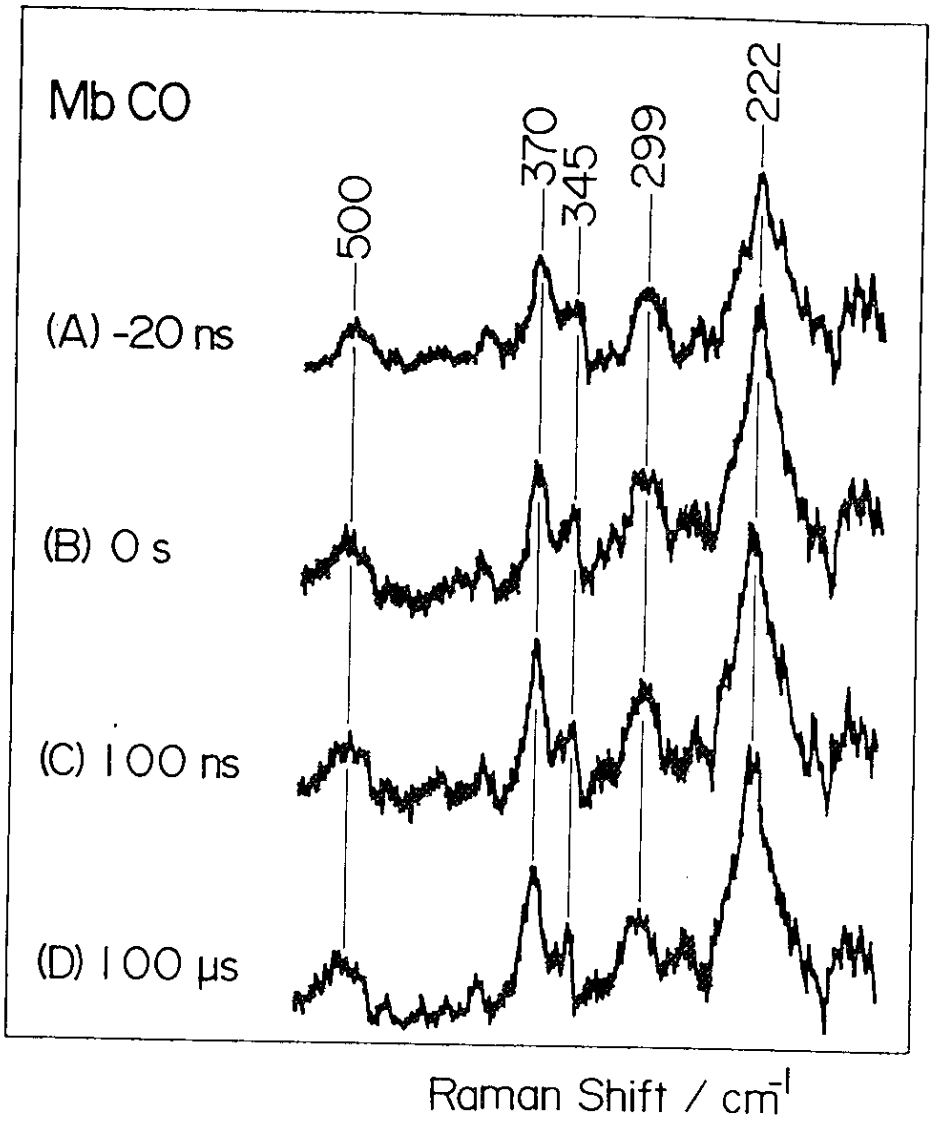

Figure V-10.
The visible-pump/visible-probe time-resolved resonance Raman spectra of MbCO. The time in the left side indicate the delay time from the pump pulse to the probe pulse.
Pump beam: 532.0 nm, Probe beam: 442.0 nm